Optics and Laser Technology 115 (2019) 404–432

Contents lists available at ScienceDirect

Optics and Laser Technology

journal homepage: www.elsevier.com/locate/optlastec

Chemically modified optical fibers in advanced technology: An overview

S.K. Shukla[a,*], Chandra Shekhar Kushwaha[a], Tugrul Guner[b], Mustafa M. Demir[b]

[a] Department of Polymer Science, Bhaskaracharya College of Applied Sciences, University of Delhi, Delhi 110075, India
[b] Department of Materials Science and Engineering, Izmir Institute of Technology, 35430 Izmir, Turkey

HIGHLIGHTS

- The significance of chemically modified optical fiber have been presented.
- These fiber bears catalytic, adsorption and optical properties.
- It advances optical based sensing, biomedical and environmental technology.

ARTICLE INFO

Keywords:
Optical fibers
Chemical modification
Sensors and biosensors
Biomedical technology
Environmental monitoring

ABSTRACT

In recent years, chemically modified optical fibers have widely used for development of several advanced chemical and biosensors, biomedical technology and environmental monitoring. The chemically modified optical fiber bears several valuable properties like energy loss, catalytic behaviour, refractive index, and mechanical strength to advance the optical fiber technology. In this article, we reviewed the chemically-modified optical fiber and their applications in different optical fiber-based technologies. The basics of optical fiber and their modification are discussed along with the adopted methodologies. The advancements in different optical fiber based technologies viz sensing, imaging, tomography, magnetic resonance imaging, photodynamic therapy, optogenics, surgery and environmental monitoring are discussed in the light of the contribution of chemically modified optical fibers. In conclusion, success and challenges for the use of chemically modified-optical fiber are presented on the basis of existing literature.

1. Introduction

Optical fiber is a hair-like, one-dimensional, flexible filament of molten glass or a suitable polymeric material. Initially, it was explored as an efficient energy transmission medium for local access computer networks [1–4]. Further, use of OF has been also demonstrated for transmission of image called flexible fiberscope [5,6]. Moreover, preservation of energy by OF has added immense boost up to improve the different technologies such as communications, defense, biomedical technology, imaging and analytical chemistry.

However, the versatility of its application was realized with limitation of functionality and surface structure. Thus, intensive efforts have been made to functionalize and modify the surface of OF for different properties and applications. In this context, chemical modification of OF has developed several attractive features to boost the existing optical fiber based technology such as sensing, biomedical laser cutting,

Abbreviations: OF, optical fiber; NA, numerical aperture; POF, polymer optical fiber; T_g, glass transition temperature; T_m, melting temperature; TSB, *trans*-4-stilbene methanol; BDK, benzyl dimethyl-ketal; VA, 9-vinylanthracene; CVD, chemical vapor deposition; PDMS, polydimethylsiloxane; SPCVD, surface plasma chemical vapor deposition; MCVD, modified chemical vapor deposition; PCVD, plasma-activated chemical vapor deposition; OVD, outside vapor deposition; VAD, vapor axial deposition; RE, rare earth; NCs, nanocrystals; NDs, nano-diamonds; HP-CVD, high-pressure chemical vapor deposition; ChG, chalcogenide; FEWS, fiber evanescent wave spectroscopy; SMF, single-mode fibers; MMF, multimode fibers; EW, evanescent wave; MTES, methyl-triethoxy-silane; FBG, fiber braggs grating; ecPOF, eccentric core polymer optical fiber; LSPR, localized surface plasmon resonance; SPR, surface plasmon resonance; SNARF-1C, seminaphthorhodamine-1carboxylate; BPA, bisphenol A; TMMF, tapered multi-mode optical fibre; MOFs, microstructured fiber sensors; OCT, optical coherence tomography; OFPS, optical fibre pressure sensor; MRI, magnetic resonance imaging; PDT, photodynamic therapy; LEF, light-emitting fabric; OFI-ALA-PDT, optical fiber imported intra-tissue photodynamic therapy; TRPA1, transient receptor potential cation channel, subfamily A, member 1; SI-MM POF, single-index multimode polymer optical fiber; PMMA, poly-methyl-methacrylate; COC, cyclic olefin copolymer; PC, polycarbonate; ADC, allyl diglycol carbonate; H-PCF, hexagonal photonic crystal fiber; LB-PCF, low birefringence photonic crystal fiber; HCPCF, hollow-core photonic crystal fibre; EMI, electro-magnetic interefrence; FBG, Fiber bragg grating

* Corresponding author.
E-mail address: sarojshukla2003@yahoo.co.in (S.K. Shukla).

https://doi.org/10.1016/j.optlastec.2019.02.025
Received 15 June 2018; Received in revised form 29 January 2019; Accepted 2 February 2019
Available online 02 March 2019
0030-3992/

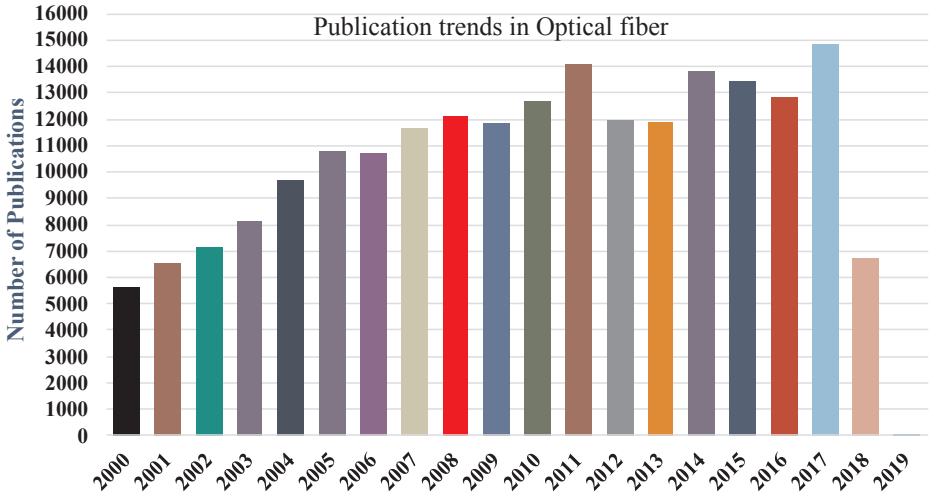

Fig. 1. Publication trends in optical fiber (www.scopus.com, term: optical fiber).

etc. The adopted functionalization modified the unclad portion of an optical fiber with different coating materials. The coating has been performed by dip-dry-fire, dip coating, evaporation and plasma processing. Generally, chemically modified OF enhances the energy conservation, efficient signal transmission, which provides a better platform to modulate interactive sites for several applications [7,8]. The number of publications is more or the less constant on a very high level, which also confirmed the importance of field [Fig. 1].

In the light of above-mentioned developments, present review summarizes the recent advances in process and application of chemically modified optical fibers along with advantageous features. Among the volcanic publication rate, it is very difficult to select original and significant contributions. However, an effort has been made to select a communication on the basis of its indigenous contribution of the fields.

2. Basic structure

The cross-section view of OF is shown in Fig. 2, which consists of two parts core and cladding. Basically, core and cladding possess different refractive indices. The refractive index (n_1) of core is slightly higher than refractive index (n_2) of the cladding. The difference between refractive indices of core and cladding facilitates the OF to guide the propagation of incident light. Due to this guiding property of light, OF is also referred as “optical waveguide.” Sometimes two or more cladding layers are also used, which are referred as secondary cladding. Secondary cladding does not participate in the propagation but provides protection to the fiber [4].

The guiding factor of light is based on Snell’s law, which consider the interface of both dielectric media having different refractive indices, $n_1 > n_2$. The incident and refracted rays satisfy the Snell's law of reflections as in Eq. (1):

$$n_1 \sin\theta_1 = n_1 \sin\theta_2 \tag{1}$$

This relation also defines angle within which the fiber can accept and propagate light and is referred to the “Numerical Aperture” (*NA*) (Eq. (2)):

$$NA = n_0 \sin\theta_{acc} = (n_1^2 - n_2^2)^{\frac{1}{2}} \tag{2}$$

Furthermore, the relation of NA can be also expressed in terms of the difference between the refractive indices of core and cladding according to Eq. (3):

$$\Delta = +\frac{n_1^2 - n_2^2}{2n_1^2} \approx \frac{n_1 - n_2}{n_1} \tag{3}$$

Thus, above equation justifies the importance of composite refractive index of core and cladding as well as its importance in light propagation. NA indicates the importance of launching and propagation of single mode of rays through OF is called single mode. However, if multiple rays having reflection angle less than that of the critical angle, all can be also transmit through OF. This type of fiber used for the simultaneous propagation of a beam of rays is called as multimode fiber. A pictorial representation of both types of OF is shown in Fig. 3.

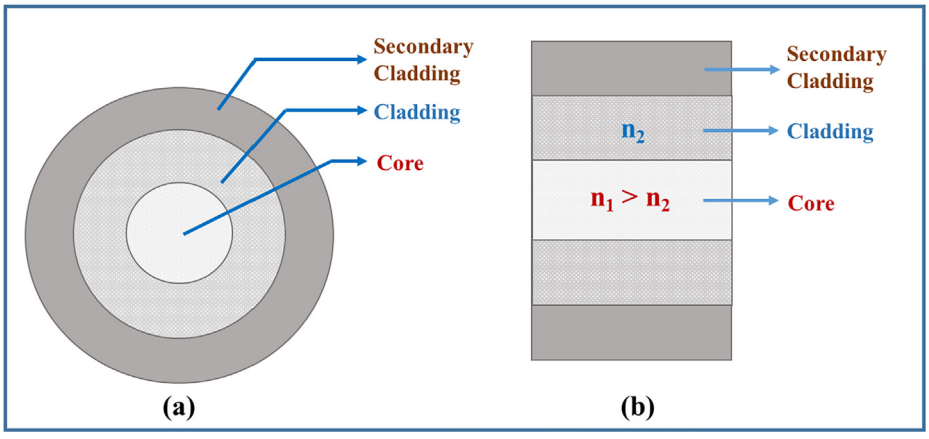

Fig. 2. Cross section representation of a typical core and cladding of optical fiber.

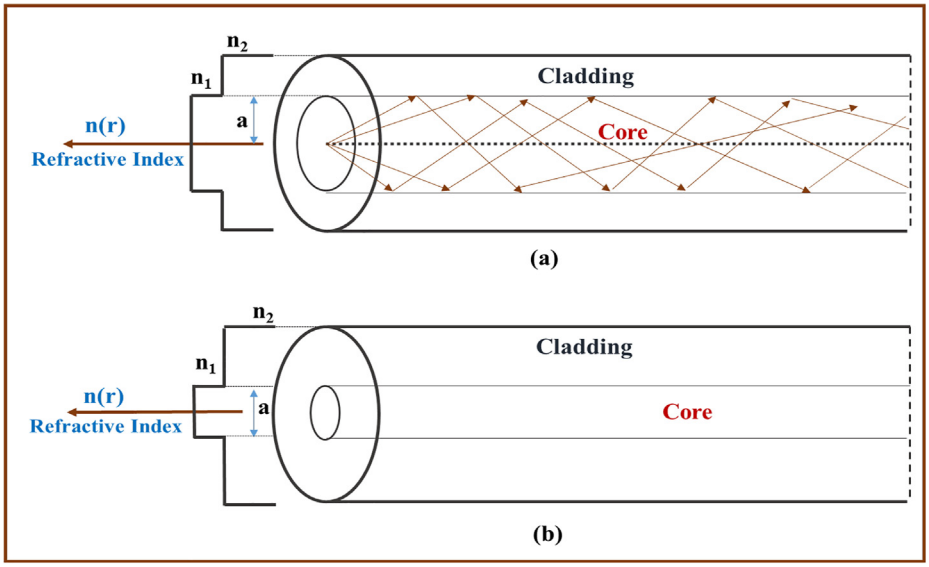

Fig. 3. a) Multimode and b) single mode optical fiber.

3. Requirements of modification

Generally, materials used in preparation of OF are inorganic glasses like vitreous silica dioxide. But they bear several limitations like energy losses, changes of refractive index, brittleness and mechanical strength. Initially, the doping with different substances are used to improve the selective properties. However, surface strength, brittleness, rigidity and functionality are still needed to be improved. In this regard, several polymers like polymethylmethacrylate (PMMA), polycarbonates (PC), polystyrene (PS), cyclic olefin copolymer and amorphous fluoropolymer are used for preparation of mechanically improved OF. These fiber are called as polymer optical fiber (POF). But, the properties like refractive index (n), photosensitivity, glass transition temperature (T_g), melting temperature (T_m), thermal expansion coefficient, thermo-optic coefficient (dn/dT), stress-optic coefficient and moisture absorption of POF are other limitations of POF [8]. Photosensitivity is another important property of POFs, which showed different light induced properties for various applications. The composition of important OFs are given in Table 1 along with properties and promising application.

In this regard, a number of groups have been improved the OF by chemical modifications [8,15,16]. Stajanca et al. has doped the cladding of commercial PMMA optical fiber using solution method. The optimisation in diffusion and dynamics of doping process make the POF as a suitable candidate for sensing applications in a simple and cost effective manner [17]. Several modifications are used for photosensitivity in OF by incorporating functional dopants like fluorescein, *trans*-4-stilbenemethanol (TSB), benzildimethyl-ketal (BDK), 9-vinylanthracene (VA), etc) [18,19]. Photosensitivity has been also improved by straining during the grating inscription or the etching of photosensitive cladding of POF [20–23].

The difference between optical properties of core and cladding has been also optimized by chemical modifications. For example, doping of silica along with other elements such as germanium, phosphorus or aluminium increases the refractive index, while addition of fluorine or boron decreases the refractive index. Sometimes rare earths or transition metal ions are also doped to generate luminescent properties. Luminescent properties of rare earth and transition metal ions strongly depend on the arrangement and the nature of the surrounding atoms. Further, silica has relatively high phonon energy, which results in the non-radiative de-excitations among energy levels of the luminescent ions [24,25]. Another limitation of OF is mechanical cracking on the surface, causing the decrease in strength, which reduces the long-time reliability of optical transmission systems. Thus, its improvement in reliable manner is necessary to make it suitable for different applications. The different methods used for modification of OF are chemical vapor deposition (CVD), dip coating, thermal annealing and plasma processing techniques [26–29]. Although, several improvements have been reported but the optimization of refractive index profile is required. A schematic presentation of different modifying methods is given in Fig. 4.

3.1. Chemical treatment

This process is performed for coating of optical fibers with chemicals having different RF and stability or a spliced area of OF. The coating is carried out by various methods like dip coating, plasma processing, evaporation techniques, etc. This modification generates funtionality, adsorption, and energy conservation. In an example, for the detection of molecules like H_2O, the chemical treatment allows the efficient absorption than virgin one. However, the etching of fibers reduces its diameter, which shortens the time requires to water molecules to reach the bragg grating sensor in POF core. Thus, combined effect is beneficial for the use of OF in humidity sensing applications.

3.1.1. Dip coating

Dip coating is an industrially popular alternative method to spin coating. It is also commonly used to coat the thin film onto flat or cylindrical shaped optical fibers. The advantage of this method is to develop films on a complex substrate in economic manner. Several reports are available for the use of this technique. A very simple dip coating was used by Shukla et al. [30,31] to design a humidity-sensing probe using nano size MgO and ZnO onto the OF. The authors have initially developed a highly stable precursor solution from metal alkoxide to develop metal oxide on surface of U shaped substrate. The modified optical fiber was found suitable for efficient monitoring of humidity inside the closed chamber. The basic design of sensing set up is shown in Fig. 5.

Similarly, a dense and defect free film of cobalt doped $NiFe_2O_4$ was deposited by dip-coating process using a solution of iron (III) nitrate dissolved in ethylene glycol and 2-methoxy ethanol [32]. The film was coated on both flat (alumina plates, fused silica, and slide glass) and curved substrates. The onset of the film's crystallization was between 450 and 500 °C and crystallinity increased as the processing temperature increases. Further, magnetization of developed films on optical fibers was reported nearly reversible to external magnetic field H_{ext} up to about 2.4 kA/m even without preceding AC demagnetization.

Table 1
Properties and applications of different type of optical fibers [9–14].

Type of OF	Materials used	Properties	Applications
Polymer-based	Polymethylmethacrylate (PMMA)	Transmittance: 92% Refractive Index (n): 1.49 Loss (dB/cm): 0.2 (at 850 nm) Yellowness: High temp & UV T_g: 105 °C NA: 0.47	LANs, industrial communications and sensing, etc.
	Cyclic olefin copolymer (COC)	Transmittance: 92% Refractive Index (n): 1.5258 Loss (dB/cm): 0.1–0.2 dB/cm Yellowness: High temp & UV T_g: 140–180 °C	Optical waveguide, sensing, etc.
	Polycarbonate (PC)	Transmittance: less than 92% Refractive Index (n): 1.58 Attenuation (dB/km): 600 (at 670 nm) Yellowness: High temp & UV T_g: 145 °C NA: 0.78	High temp. communications and sensing
	Polystyrene (PS)	Transmittance: less than 92% efractive Index (n): 1.59 Attenuation (dB/km): 330 (at 570 nm) Yellowness: High temp & UV T_g: 100 °C NA: 0.73	High temp. industrial short haul communications and sensing
Glass based	Silica glass fibers (PCF and HCS)	Refractive index: 1.458 at 850 nm Attenuation (dB/km): 5–6 (at 820 nm) NA: 0.40 Core/cladding RI: 1.492/1.417	Communication, medical, industrial and sensing
	Fluoride glass fibers (Silica mixed with ZrF, BaF, LaF, AlF and NaF)	Low transmission losses at mid IR wavelength region with the minimum loss being around 2.55 μm	Mid distance data communications, amplifiers and optical switches
	Active glass fibers (Containing RE elements)	Refractive indices of melted SAL glass – with and without Yb_2O_3: 1.60–1.74 & 1.60–1.61 Tg (°C) of with and without Yb_2O_3 glass: 861–875 & 867–884.	Photonic sensor, photonic memory, single photon sources, to microcavity lasers, as well as full-color display systems, etc.
	Chalcogenide glass fibers (S, Se, or Te)	$As_{40}S_6$ Refractive index: 2.415 Tg (°C): 197 Typical loss (dB/km): 100–200 (2.2–5.0) $Ge_{30}As_{10}Se_{30}Te_{30}$ Refractive index:2.80 Tg (°C): 265 Typical loss (dB/km): 500–1000 (6.0–9.0)	Laser power delivery, chemical sensing, imaging, scanning near field microscopy/ spectroscopy, fiber IR sources/lasers, amplifiers and optical switches

3.1.2. Electrospinning

Electrospinning has been also used for efficient coating of fiber optic cables. Typically, a potential difference in the order of ~1–2 kV/cm^{-1} is applied to a viscous polymer solution. When electrical force overcomes the surface tension of polymer solution, a charged jet whose thickness is on the order of μm is ejected from the polymer solution droplet to a ground, which can be a fiber optic cable. Evaporation of solvent leaves behind submicron diameter polymeric fibers in a form of mat with high surface area per unit volume. Boyacı et al. reported the coating of glass OF with polydimethylsiloxane using electrospinning

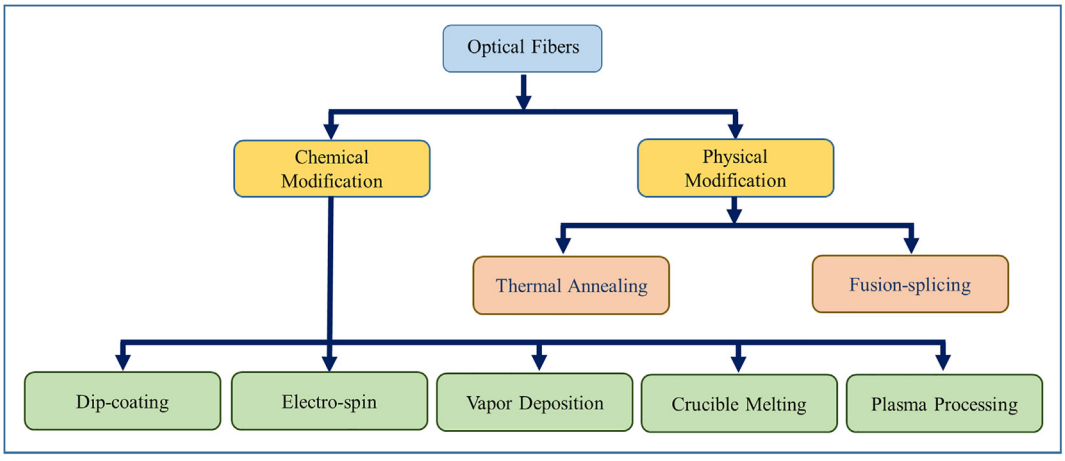

Fig. 4. Different modifying methods of optical fiber.

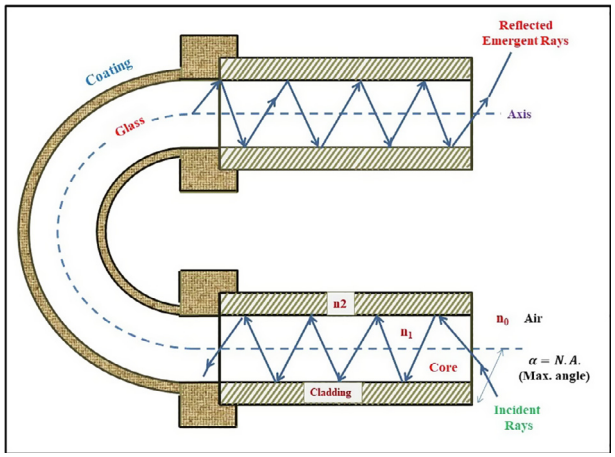

Fig. 5. Schematic of chemically modified optical fibre for humidity sensor [30].

process [33]. The homogeneously coated fiber is used for the solid phase microextraction of inorganic and organic arsenate species. The extraction performance of the electrospinning coated OF is compared with the one prepared with dip coating. It was found that the coating prepared by electrospinning shows better extraction performance. The reason behind this result was hypothesized that electrical field applied during the electrospinning process orients the functional groups through the surface of the fiber and makes these groups vulnerable towards arsenic. In another example, a composite coating of multi-walled carbon nanotubes (MWCNTs) and polyvinyl alcohol (PVA) was directly electro-spun onto the cleaved surface of a multimode optical fiber and subsequently dip-coated with polydimethylsiloxane (PDMS). The developed composite film generates an uniform nano fibrous absorbing mesh over the optical fiber end-face. The MWCNTs were aligned preferentially along individual nano fibers. Further, infiltration of PDMS through this nano fibrous mesh onto the underlying substrate was observed and the resulting composites exhibited high optical absorption (> 97%). On comparing, the electrospun ultrasound transmitters with a dip-coated reference fabricated using the same constituent materials. Five-fold increase in the generated pressure and wider bandwidth was observed. The electro-spun transmitters exhibited high optical absorption, good elastomer infiltration, and ultrasound generation capability in the range of pressures suitable for clinical pulse echo imaging [34].

3.1.3. Vapor deposition

It is a group of techniques (MCVD, PCVD, OVD, VAD, etc) for deposition of different materials on OFs. For MCVD, a burner or furnace initiates the chemical reaction; however, in PCVD, the chemical reaction is initiated by microwave plasma. But for the case of OVD and VAD processes, the layer deposited on the outside of a rotating mandrel by using the flame hydrolysis. These methods are different in terms of deposition rate, efficiency and precision of refractive index profiles [35]. Particularly, MCVD process is a most common method for passive and active modification of OFs [36]. The MCVD process is an extremely flexible technique for modifying the several OF structures and compositions. Rare-earth (RE)-doped fibers have often been fabricated using a combination of modified chemical vapor deposition (MCVD) and solution doping. In these processes, single or low-molded fibers are modified in a simple and versatile manner [37]. However, solution doping based MCVD is a multi-step procedure, which produces a doped core made of 1–10 layers. However, it limits the accuracy, flexibility of dopant concentration and refractive index profiles. Furthermore, it is difficult to deposit rare-earth (RE) ions using conventional vapor delivery system for the main glass component precursors such as $SiCl_4$, $GeCl_4$, and $POCl_3$ due to low vapor pressure of RE halide precursors at room temperature [38]. A novel approach of MCVD is in-situ doping technique/chemical-in-crucible method, which is used to deposit a number of doped layers [39]. An aluminosilicate fiber, which was in-situ doped with Yb, was successfully fabricated and exhibited a slope efficiency of 79%. In this MCVD, rare-earth precursor directly heated within the MCVD glassware, which increases versatility with maintaining high doping uniformity [40]. This deposition technique uses the phase-separating agent and directrly synthesizing nanoparticles by in situ method [41]. The technique produces nanoparticle doped silica glass in the fibers. For example, Yb-doped nano-crystalline Yttrium Aluminum Garnet (YAG) in a silica-based preform was fabricated using MCVD using solution doping followed by thermal annealing [42]. In MCVD compatible process, the synthesized Er^{3+}-doped Al_2O_3 nanoparticles produces homogenous glass with improved performances in terms of erbium homogeneity and standard doping levels [43]. A new development in MCVD for the preparation of doped glasses based on a powder sintering method has been developed [44]. In this technique, a tube containing silica is fused to create the core, called Reactive Powder Sintering of Silica (REPUSIL). The process is based on powder sintering method [45]. The powders are dried, purified and sintered into homogeneous bubble-free RE-doped silica rods. Using this technique, single-mode optical fibers have been successfully processed in cost effective manner due to the replacement of the thick and expensive cladding of OF by synthetic pure silica powder. This technique was used for the development of homogeneously doped active OF core with background attenuation of 20 dB/km and slope efficiency of 80% [46,47].

3.1.4. Crucible melting technology

This method has significant advantages like implementation of high dopant contents in melted glass, easy volume scaling along with good glass quality due to high melting homogeneity. The glasses are processed to form fibers, tubes, rods and plates by applying specific melting and casting techniques. The melted glass is used in combination of different glasses e.g., highly doped silicate glass as a light-guiding core material with an ultra-pure fused silica cladding [48–50]. These glass materials combined with SiO_2 cladding shows refractive index difference between the core and the cladding is 0.1 along with numerical apertures of 0.55 [51]. Lanthanum and aluminium are the codopants in this case, however, high fraction of aluminium (e.g., 20 mol% Al_2O_3) enables a very good solubility for rare earth (RE) ions. The substitution of lanthanum with other elements allows a great variability in glass properties [51,52]. The SiO_2-Al_2O_3-La_2O_3 glasses were fabricated by using high-quality raw oxide materials (SiO_2, La_2O_3, Yb_2O_3, CeO_2) and hydroxide [$Al(OH)_3$] after several hours of melting. The liquid glass was poured into a stainless steel mold to form glass blocks (Fig. 6A). The blocks were slowly cooled down from T_g to room temperature at 100 K/h. Following this controlled cooling procedure, the homogeneous bubble-free blocks were prepared, grinded and polished into a cylindrical shape as shown in Fig. 6B and C. These are used as pre-forms for fibers and as rods.

3.1.5. Plasma processing

In the continuation of different techniques, plasma based chemical vapor deposition is capable of producing a coating on OF with low loss (less than10 dB/km) and high deposition rates [53]. The plasma is generated with use of a RF argon-oxygen operating system at pressure of 1 atmosphere. It provides the potential for higher deposition rates as well as increased efficiency. In this technique, the plasma temperature is in the range of 10,000–20,000 K, which produces an intensive reaction region for highly ionized species. Under these conditions, reaction between ionized species deposit a film in similar manner to the MCVD. The significant improvements in efficiency of deposition rate was achieved by this method due to the gas phase reaction occurs in a highly ionic environment. Geittner et al. reported another approach for the preparation of low-loss optical fibers is called as plasma activation method [54]. The method exploits the use of non-isothermal plasma to

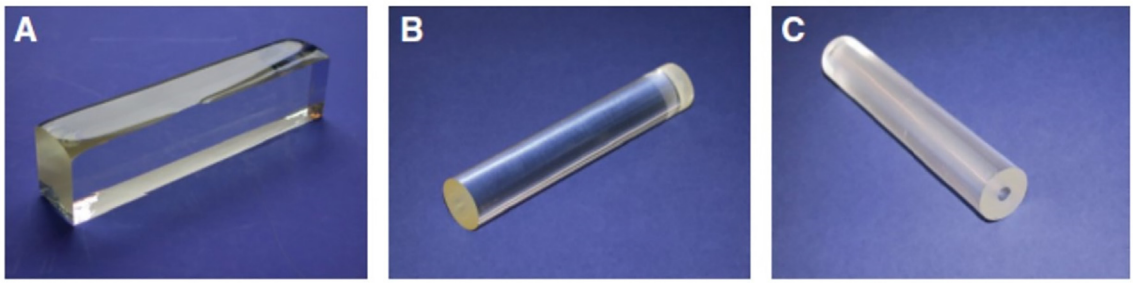

Fig. 6. SAL glass block after fine cooling (A), grinded and polished SAL preform (B), and SAL tube (C) [47].

stimulate the reactions. The other alternative method to conventional methods for silica fiber preform fabrication is the surface plasma chemical vapor deposition (SPCVD). In SPCVD, the halide precursor is converted to oxide at reduced pressure and lower temperature due to microwave induced plasma. This technique was initially used for the fabrication of preforms with an Er-doped silica core and fluorine-doped silica cladding [55,56]. Savel'eV et al. reported the preparation of two and three-layer light-guiding structures using SPCVD of doped SiO_2 [57].

3.2. Physical methods

The physical treatments like thermal annealing are also used to improve the performance of OF after creating some change in OF [58]. It may be because the change in shrinking properties of anisotropically drawn polymer fiber after heating above the β-transition temperature. The shrinkage induces a permanent blue shift of the Bragg's wavelength. Thus, device multiplexing is feasible by using only one phase mask to record multiple Bragg gratings. It was also demonstrated that annealing OF can developed several advantageous features for the use of OF in strain [59] and humidity sensor [60]. The sensitivity of sensor is enhanced along with a higher operational range for temperature monitoring. In another effort, optical-fiber was modified by fusion-splicing method. It produces different functional properties like low attenuation in specific wavelength ranges, the variation of refractive index, highly nonlinear coefficient, or specific structural properties of OF [61].

4. Classification

OFs are classified on the basis of composition, modes and profile. A pictorial representation for classification of OF is shown in Fig. 7.

Among the different classification methods, classification on the basis of materials composition has significant impact on application of OFs. The different classes of OFs like glass/glass, plastic/plasic and plastic/glass have been used after optimised transmission, tunable physical and mechanical properties. The important classes of OFs are discussed below.

4.1. Fluorescent particle-doped optical fiber

The incorporation of fluorescent nanocrystals (NCs) in OF has significant applications in photonics [62]. Incorporation of NCs into optical fibers ensures efficient and robust excitation and collection of fluorescence from NCs in a device. The most exclusive approach is to integrate luminescent NCs into glass matrix by in-situ growth method. In this method, NCs may be formed by the ions in diffusion process through out the glass during heating [63–66]. A wide range of oxides, fluorides, chalcogenides and metal-based NCs are prepared using this technique [67,68]. The continued growth of in-situ-grown NCs could occur during a post-annealing or during a reheating process [69]. The continued growth of NCs increases the light scattering and so the optical loss in the resulting glass/fiber. The other advancing synthetic techniques of NCs are wet chemistry [70–72], laser ablation [73], ball milling [74] and detonation [75]. These methods have shown exceptional control over emitting center concentration, crystallite phase, size, shape, composition and nanostructure.

An alternative approach is direct doping of NCs into tellurite-based glass melts at different temperatures [76–78]. Initially, materials without NCs is melted at a higher temperature to obtain a clear, homogenized glass melt. After lowering this temperature to a point where the glass melt has an optimum viscosity to disperse NCs as well as to be cast into a mold. The direct doping approach was also used to embed the nitrogen-vacancy (NV) center containing nano-diamonds (NDs) in tellurite glass using a batch melting temperature of 900 °C. A doping temperature of 700 °C the doping concentration of 9 and 280 ppm ND by weight is reported [76]. Fibers were fabricated from these glasses by fabricating preforms using billet extrusion at 350 °C followed by fiber drawing at ~400 °C. NDs were used as a chemical reducing agent, which reduces higher valence species in the melt phase, such as tellurium (IV) ions, and gold ions. The presence of oxygen also results in the formation of lower valence species such as gold

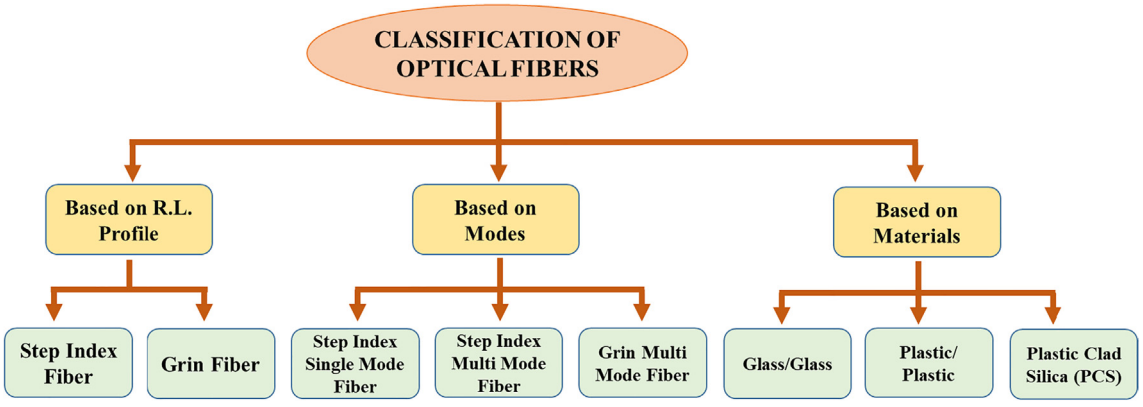

Fig. 7. Basic classification of OFs.

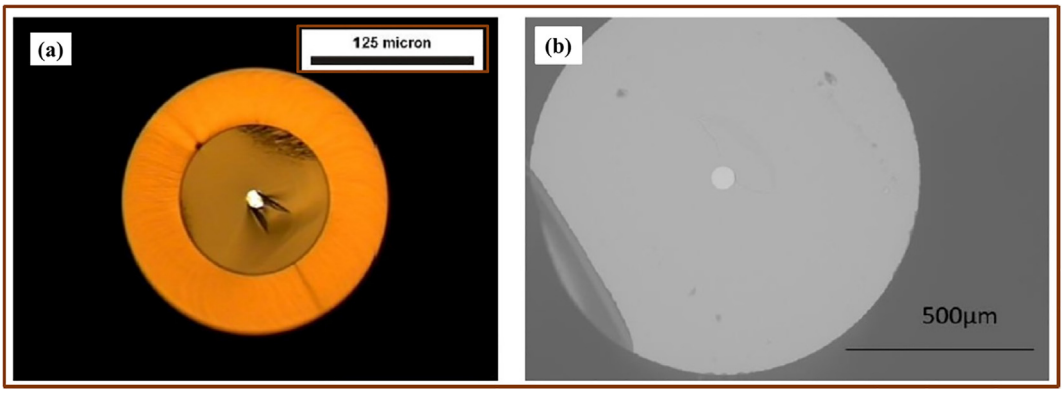

Fig. 8. (a) Optical micrograph of a polymer-coated glass-clad germanium (Ge) core optical fiber and (b) an electron micrograph of an uncoated glass-clad silicon core optical [83].

nanoparticles (GNPs) and reduced tellurium species [77,78].

4.2. Semiconducting optical fiber

This class of optical fibers offers a potential advances in the fields of nonlinear fiber optics and infrared power delivery. A number of reports have been published for the development, optimization and utilization of semiconductor optical fibers. Crystalline silicon (Si) optical fibers were prepared by the micro-pull-down method in 1996 [79]. These fibers have not received significant attention until high-pressure chemical vapor deposition (HP-CVD) was employed to develop crystal engineering in photonic crystal of fibers [80]. The advantage of HP-CVD approach is that both amorphous and crystalline silicon fibers are possible to be fabricated. The molten core method was also employed to prepare long glass-clad silicon optical fibers [81]. A number of unitary and binary systems were developed to fabricate glass-clad semiconductor core including doped-silicon, germanium (amorphous and crystalline), selenium, tellurium, silicon-germanium alloys, selenium tellurium alloys, indium antimonide, and zinc selenide [82–90]. Some glass-clad based crystalline semiconductor core optical fibers are shown in Fig. 8. Fig. 8a is polymer-coated, borosilicate glass-clad germanium (Ge) core fibers and Fig. 8b is electron micrograph of an uncoated silica glass-clad silicon (Si) core fiber. The ZnSe and Si are also excellent materials for the preparation of semiconducting OFs [91–93].

The glass-clad semiconductor core optical fibers are generally used for planar waveguide analogs in terms of optical attenuation with losses in the order of dB/cm. In planar waveguides, the loss is often dominantly controlled by surface roughness. Generally, there is a excedding smooth interface in glass-clad semiconductor core based optical fibers [94].

The scattering of light from impurities or defects that aggregate at the grain boundaries can lead to loss in isotropic cubic materials e.g., silicon, germanium, indium antimonide. The wide range of core materials and cladding compositions have been reported along with science of the crystal formation with optimized crystallinity. The first in-depth analysis of the longitudinal single crystallinity in these fibers has been investigated to refine or recrystallize the crystalline semiconductor core by thermal annealing, core geometry, core size, tapering, and laser recrystallization [95–98]. The semiconductor fibers have also been used for the production of microspheres [99]. Such microspheres are useful in variety of high-Q resonators [100] including tunable ones based on thermal and Kerr-related nonlinearities [101,102]. These fiber-based devices have potential advantage of electronic transport and junction effects in doped semiconductors. In these devices, fiber geometry, core size for light absorption and efficient charge transport without concern for the relatively high optical attenuations are reported. To date, such devices i.e. p-i-n and p-n [103,104] in-fiber junctions can operate at GHz band widths as well as series of microwire radial solar cells [105,106].

4.3. Chalcogenide glass based optical fiber

The chalcogenide (ChG) based optical fibers contain at least one chalcogenide element, e.g. S, Se and Te, which are used in the mid-infrared region between 2 and 20 µm electromagnetic spectral range. Numerous research activities are reported for the development of chalcogenide-based mid-IR optical fibers [107]. ChG fibers can be transparent but depends on the composition like 1 µm–6.5 µm for an As-S glass fiber [108] and 1.5–10 µm for an As-Se fiber [109]. A common geometry and morphology of the chalcogenide fibers are given in Fig. 9a.

Two methods: a) the rod-in-tube technique, and b) the double crucible method are used to fabricate such fibers [110,111]. The double crucible method is adapted to yield a high quality core-clad interface. It

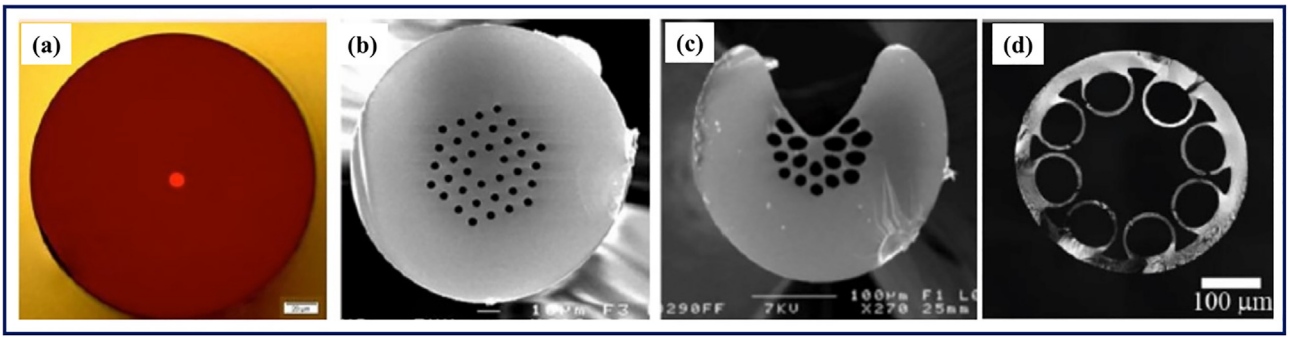

Fig. 9. Chalcogenide-based fiber designs: (a) step index fiber (courtesy of IRflex); (b) single-mode microstructured fiber (courtesy of SelenOptics); (c) exposed core fiber [119 copyright with Elsevier]; (d) hollow core fiber, reproduced with permission from [119], copyright with OSA.

is used for the fabrication of commercial step index chalcogenide fibers [112]. The rod-in-tube technique permits the realization of step index fibers [113]. In this case, a small rod of the core is placed into a clad tube and drawn together while applying a small negative pressure between the core and the clad to collapse any gap between the two glasses. In this method, it is easier to control the size of the fiber-core and the core-clad ratio. The minimum of attenuation obtained with the double crucible technique is 12 dB/km, where the minimum of attenuation obtained with the rod in tube technique is more than 5 dB/m [114]. Furthermore, in order to improve the quality of interface between the cores and clad, chalcogenide preforms are obtained by extrusion, which reduces the scattering loss to around 1–2 dB/m [115]. However, the optical loss is still higher than the one obtained by the double crucible method. The researchers paid great interest to combine the properties of microstructured fibers with those of chalcogenide glasses (mid-infrared transmission and high nonlinear properties) [116,117]. Fig. 9b, c and d show the morphology of chalcogenide glass. The fiber illustrated in Fig. 9b is an example of the three rings of a hole fiber with a d/L ratio lower than 0.42 exhibiting an endlessly single-mode behavior. The fiber presented in Fig. 9c is an exposed core fiber, which is very sensitive to the environment and can be used as an infrared sensor [118]. The last fiber presented in Fig. 9d is a hollow core fiber. This design permits light to propagate in the air core of the fiber such that the mid-infrared wavelength can be carried at wavelengths that are beyond the multi-phonon cutting edge of a classical solid core fiber [119].

The other methods are stack and draw method [120], drilling, in this method the preform is obtained by drilling several holes in a glass rod, or the molding. The chalcogenide glass is flown down in a silica mold, which permits to produce monolithic preforms for producing microstructured optical fibers [121,122]. Due to their mid-IR optical transparency, chalcogenide glasses are good candidates for the development of optical sensors and fiber evanescent wave spectroscopy (FEWS) [123]. The tellurium-based chalcogenide fibers were developed to detect IR signatures beyond 12 μm. The Mid-IR fluorescence can be obtained by doping/codoping a chalcogenide glass with luminescent rare-earth (RE) ions such as Er^{3+}, Pr^{3+}, Nd^{3+},Tb^{3+}, Dy^{3+} and Ho^{3+} [124–127]. Among different RE ions, the most studied ions are Dy^{3+} and Pr^{3+}. The Dy^{3+} ion exhibits two mid-IR emissions centered at 2.9 μm and 4.3 μm [128]. In the presence of Pr^{3+} ions, broad IR emissions from 3.5 μm to 5 μm were achieved. Due to the presence of the broad fluorescence signal from 3.5 μm to 4.7 μm of Dy^{3+}, the chalcogenide-doped fibers have been used for detection of CO_2 gas, which has a strong absorption band at 4.26 μm. The developed mid-IR fluorescence source permits to detect the concentration of CO_2 down to the concentration of 500 ppm [128].

5. Applications

The guided, conserved and efficient flow of light has made the OF valuable for wide range of technological applications. Generally, OFs are used as active and passive form in diverse branches of science and engineering [129]. The overall applications of optical fibers are given in Fig. 10. The passive form of application is mainly used in transmission and chemical composition play main role. However, the chemical modified OF are significantly improves the application of OF in active form, which are mainly described here.

5.1. Chemical sensing

Today, OFs have found significant use in the field of sensors due to their inherited advantages over the conventional sensors. The advantages of these sensors are portability, immunity to electromagnetic interference, and large dynamic range of optical spectrum. The integration of OF into a wide variety of materials including composite materials offer immunity to harsh conditions, high sensitivity, multiplexing capability for sensing networks for different chemicals. These sensors have widely used to monitor environmental parameters such as position, vibration, strain, temperature, humidity, viscosity, chemicals, pressure, current, radiation, electric field and several other environmental factors [130–132]. In this section, we present a brief discussion on chemical sensor.

The general structure of an optical fiber sensor is shown in Fig. 11. It consists of an optical source (laser, LED, laser diode, etc), optical fiber, sensing or modulator element (which transduces the measurand to an optical signal), an optical detector and processing electronics (oscilloscope, optical spectrum analyzer, etc).

Fiber optic sensors can be classified under three categories as (i) the sensing location, (ii) the operating principle, and (iii) the application. Based on the sensing location, a fiber optic sensor can be classified as extrinsic or intrinsic. In an extrinsic fiber optic sensor (Fig. 12), the fiber is simply used to carry the light from a source to an optical detecting device. In these cases, usually single-mode (single-mode fibers, SMF) or multiple modes (multimode fibers, MMF) OF are employed to transport light from the source to the detector (Fig. 12a).

In an intrinsic fiber optic sensor, one or more physical properties of the fiber undergo a change in properties of light (Fig. 12b). Perturbations act on the fiber and the fiber in turn changes the characteristics of the light inside the fiber [133]. For such types of sensors, light–analyte interaction occurs inside or on the fiber, but depending on the structure, the sensing principle may vary. The basic priniciple of sensor catagorise the sensor like inensity, phase, frequency, or polarisation. However, on the basis of application it can be physical or chemicals.

5.1.1. Intrinsic-reflection sensors

This is a conventional type of fiber optic sensors, which employed an indicator like a doped film based reflection [134]. This type of fiber optic sensors has been mostly used for humidity, pH, and ammonia sensing. A disposable pH sensor based on an organic-inorganic hybrid matrix–ORMOSILs (organically modified silicates) with pH sensitive dye has been developed [135]. Polyethylene oxide (PO) was used as the organic fraction of the matrix, which allows good adhesion between the POF and the porous matrix. The inorganic fraction of the matrix was silica glass, which enhances the ductility and permeability of the matrix. Schryy et al adopted a similar strategy using TEOS and methyltriethoxysilane (MTES) to prepare an organic-inorganic matrix that supports bromophenol blue (BB) to monitor pH in biological fluids [136]. The sensor showed good sensitivity in the range of pH 5–8 and temperature resistance in the range from 20 to 25 °C. The low cost and fast detection of nitro aromatic explosives such as trinitrotoluene (TNT) and trinitrophenol (TNP) are possible by this fiber optic sensor technique. The discovery of fluorescein conjugated-poly(2-methoxy-(2-ethylhexloxy)-p-phenylene-vinylene) (MEH-PPV) enables fast identification of these explosives due to its fluorescence quenching effect, when it contacts with nitro aromatic compounds [137]. Chu et al. reported a TNT polymer optical fiber sensor by dip coating MEH-PPV on a coil-shaped PMMA fiber [138]. The lowest detection limit (1–15 ng-mL^{-1}) was extrapolated from the sensor's response curve and also verified by experimental tests.

The graphene films exhibit characteristics of ultra-low thickness, high permeability, good optical transparency as well as chemical inertness as an ideal carrier for binding of transducer reagents integrating to chemical transducer fiber optic systems [139,140]. The application of graphene in FOSs has been mostly focused as graphene OFs but a limited number of POF based FOSs has been reported [141,142]. Kulkarni et al. reported a simple strategy to transfer large area graphene films onto the distal end surface of PMMA fibers by direct deposition of preformed graphene films synthesized via a chemical vapor deposition (CVD) technique [143]. Later, sensing of volatile organic compounds (VOCs) was explored by monitoring the intensity of light reflected from the deposited thin film due to absorption of VOCs present in surrounding atmosphere [144].

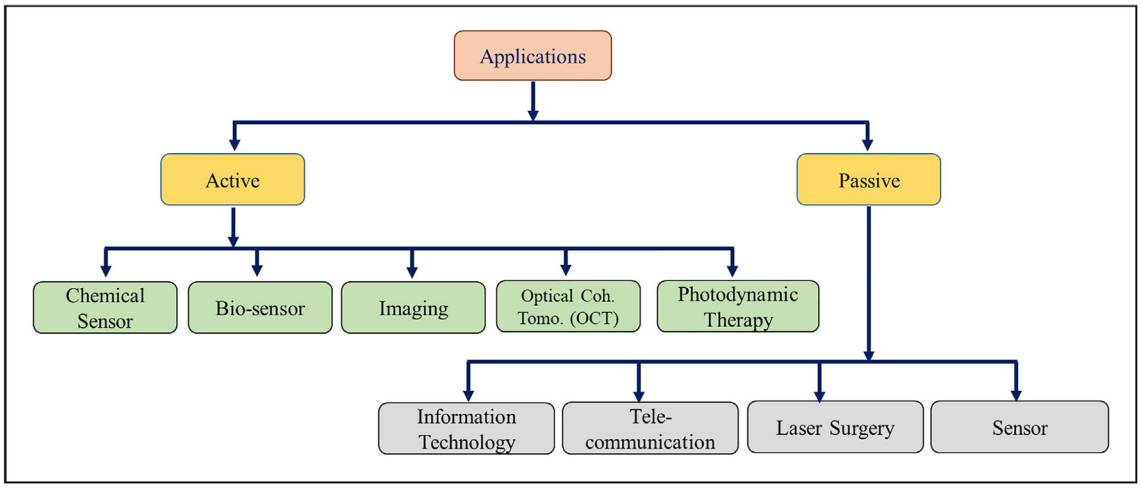

Fig. 10. Applications of optical fibers.

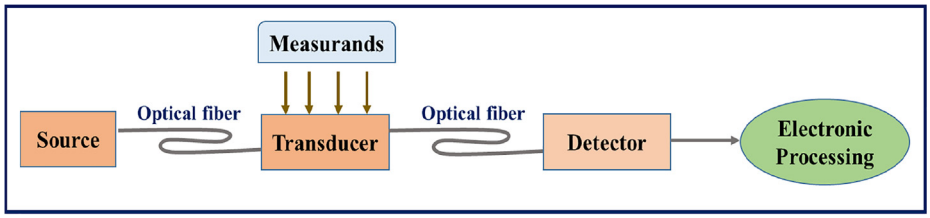

Fig. 11. Basic components of an optical fiber sensor system [133].

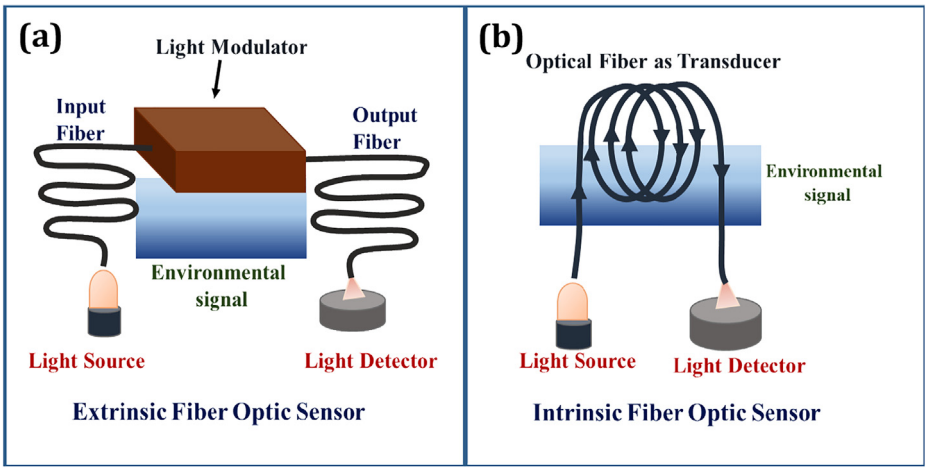

Fig. 12. (a) Extrinsic types of fiber optic sensors, and (b) intrinsic types of fiber optic sensors [133].

5.1.2. Intrinsic-transmission sensor

This detection mechanism is based on evanescent wave absorption and localized surface plasmon resonance. This class sensor is attracting great attention in medical applications for sensing of biomolecules [145,146]. In this type of sensor, when light is transmitted through the fiber, it undergoes total internal reflection on the inner surface of the fiber core. It gives rise to the standing evanescent wave at the interface along the axis of the fiber due to the interference between incident and reflected beams. The evanescent wave (EW) interacts with analytes in the vicinity of fiber surface via absorption of EW at certain wavelengths or emission of light after EW luminescence (Fig. 13) [147].

By analyzing the output light spectrum, the compostition of gases present around the surface can be identified. Sometimes the EW was excited by immobilized nanoparticles on the surface like localized surface plasmon resonance (LSPR). It exhibits ultrahigh sensitivity towards the variation of refractive index in the vicinity of the particle surface [148,149]. Pulido et al. reported an EW type oxygen sensor based on the fluorescence-quenching effect of oxygen with cationic ruthenium complexes [150]. Tris-(2,2′-bipyridyl) dichlororuthenium (II) hexahydrate was first dissolved in the solvent of acetone and water, followed by immersing the tapered section of PMMA based optical in the solution for a short period of time. This sensor showed linear responses to oxygen concentration from 0 to 100 vol% both in terms of fluorescence intensity and fluorescence lifetime. A sol-gel technique was also employed to anchor ruthenium complexes onto a U-shape polymer fiber for the fabrication of a dissolved oxygen sensor [151]. Ruthenium (II) chloride was incorporated into a sol-gel prepared from TEOS and MTEOS and then dip-coated onto a U-shape de-cladded PMMA fiber. The non-linear response was observed for both fluorescence intensities and lifetimes against oxygen concentrations.

5.1.3. Wavelength modulated sensors

These sensors explore the changes in the wavelength of light for detection purpose in medical applications, chemical sensing and

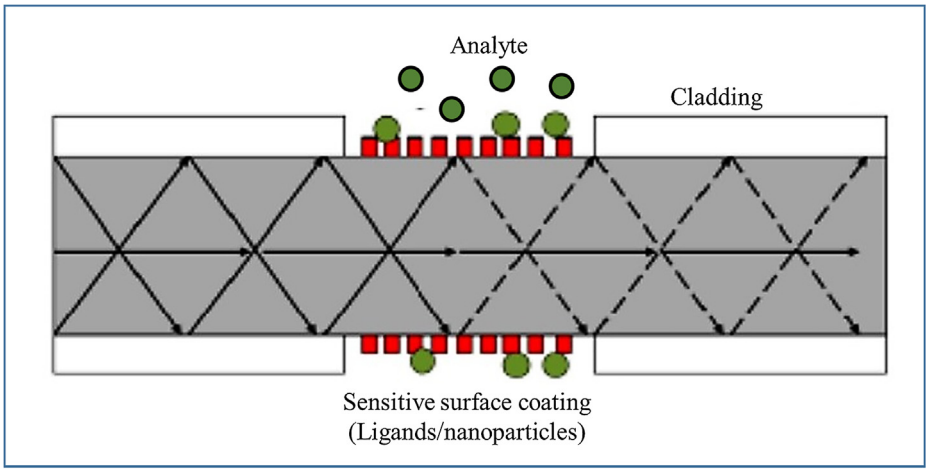

Fig. 13. EWA luminescence [147].

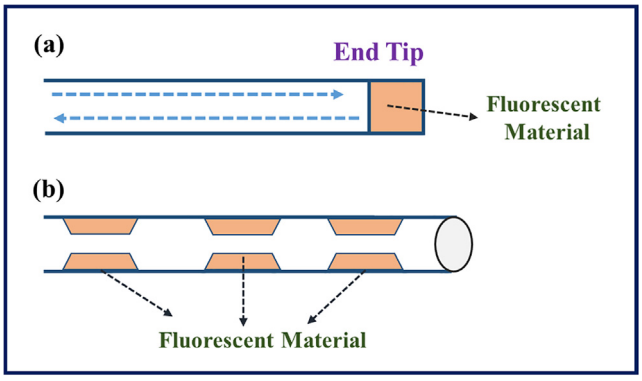

Fig. 14. Fluorescent fiber optic sensor probe [152].

physical parameter such as temperature, viscosity, and humidity. Mostly these sensors are fluorescence sensors, black body sensors, and fiber bragg grating sensors. A representative fluorescent-based optical fiber sensor is shown in the Fig. 14a and b, in which the light propagates down the fiber to a probe of fluorescent material [152].

The simplest model of blackbody wavelength-based sensor is shown in the Fig. 15. In this sensor, a blackbody cavity is placed at the end of an optical fiber. This type of sensor has been successfully commercialized and has been used to measure temperature to within a few degrees centigrade under intense RF fields.

Other wavelength based sensor is called bragg grating, which is formed by constructing periodic changes in index of refraction in the core of a single mode optical fiber. This type of sensor directly transforms the sensed parameters into shifts of optical wavelengths, which has the advantage of minimal influence caused by extraneous optical power variations [153]. The operating principle of FBG sensor is shown in Fig. 16, which indicates that a broadband light source (LED), whose center wavelength is close to the bragg wavelength is launched into the fiber. The light propagates through the grating and part of the signal is reflected at the braggs wavelength [154]. Generally, FBG sensors are governed by the Eq. (4) [153].

$$\lambda_B = 2n_e\Lambda \tag{4}$$

Where, 'n_e' is the effective refractive index of the grating in the fiber core, λ_B is the bragg wavelength and 'Λ' is the grating period. The sensing capabilities of FBG sensors are determined by n_e and λ_B.

The extension of sensing capability of FBG sensors to detect biological agents has been reported by modifying the fiber-grating surface, which induces binding of biological analytes. Once analytes bind onto the fiber-grating surface, they change the surface strain of the fiber and result in a shift of the braggs wavelengths [155]. The advantages of this sensor are lower young's modulus that leads to a higher failure strain, improved sensitivity and detection range. Xiong et al. [156] fabricated FBG from a single mode-PMMA (SM-PMMA) polymer optical fiber using a pulse laser beam operating at 248 nm. Attention has been drawn to inscribe bragg gratings into microstructured polymer optical fibers (mPOFs) due to their superior properties [157,158]. Luo et al. [159] fabricated a polymer FBG to measure stress and strain. They inscribed gratings into a SI-MM POF with the core doped with benzyl dimethylketal (BDK) to enhance the photosensitivity. A 355 nm frequency-tripled Nd: YAG laser was used to inscribe gratings into POFs with bragg wavelength of 1570 nm. The maximum sensitivity of axial stress was determined to be 472 pm MPa^{-1} under 9.59 MPa stresses, while the sensitivity of axial strain was comparable to GOF based FBG sensors (1.18 pm $\mu\varepsilon^{-1}$). Gu et al. has demonstrated a high strain sensitivity polymer micro/nanofiber bragg gratings (MNFBGs) using a low cost nano imprinting approach [160]. The axial strain sensitivity of the

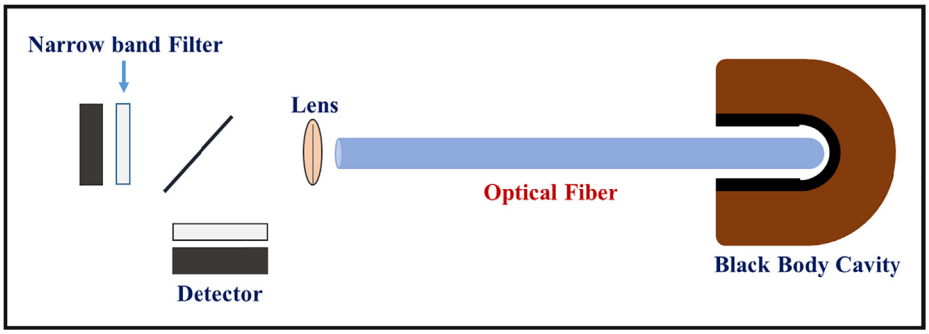

Fig. 15. Blackbody fiber optic sensor [152].

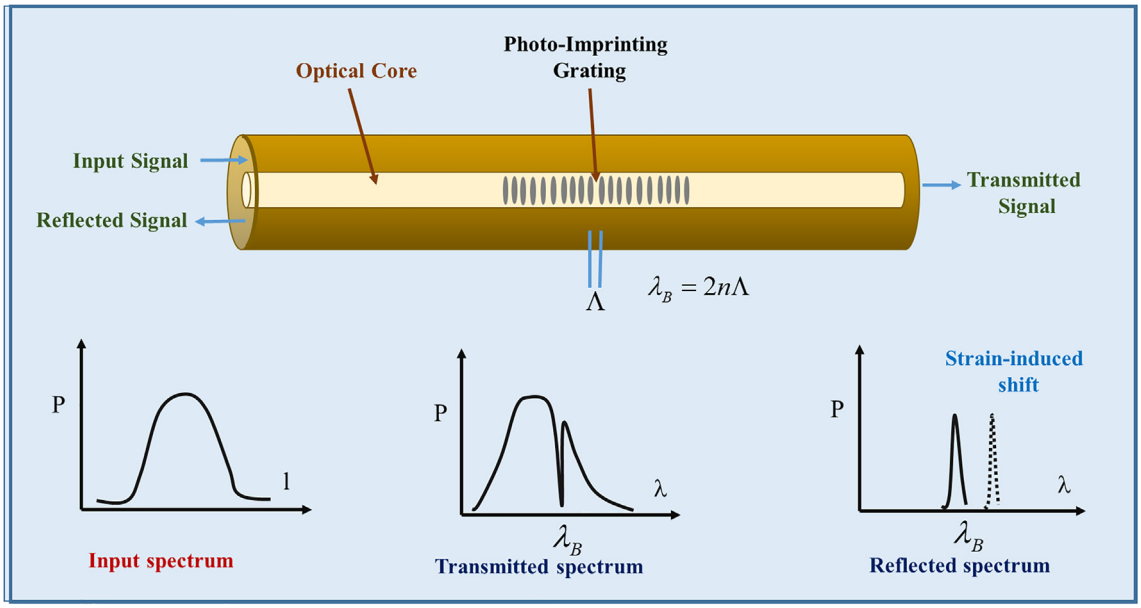

Fig. 16. Principle of FBG sensor [133].

fabricated FBG sensor was determined to be $-2.5\,\mathrm{pm}\,\mu\varepsilon^{-1}$ which is almost doubled when compared to common polymer FBG strain sensors [159]. It is proposed that this contradiction results from a large photo-elastic effect when applying strain, while the red shifts from conventional FBG sensors were originated from the elongation of the fibers. The realization of multiplex sensing in FBG sensors, especially in measuring physical parameters is much easier than other FOSs. Bragg gratings were registered into an eccentric core polymer optical fiber (ecPOF) to fabricate a strain, bend and temperature sensor [161].

5.1.4. Microstructured fiber sensors

MOFs are also known as photonic crystal fibers (PCFs). It is an emerging type of waveguide that can direct light through hollow cores running longitudinally along the fiber and has significant application in sensors. MOFs are different in terms of their geometries and light guiding mechanisms. It includes photonic band gap fiber, holey fiber, hole assisted fiber, and bragg fiber [162]. These sensors bear advantages like high sensing areas and stronger interactions with the transmitted light waves than conventional fibers. Further, microstructured polymer optical fibers (mPOFs) offer additional benefits over their glass counterparts due to ease and versatility of fabrication techniques of the polymers [163]. Li et al. reported a mPOF sensor using Rhodamine-6G (Rh 6G) as the indicator for the detection of hydrogen peroxide and nitrites [164]. The acidic solution containing tetrabutyl titanate, ethanol and Rh 6G was drawn into the hollow holes to form a three-dimensional network of titanium dioxide with entrapped Rh 6G. It was discovered that resulting sensor responded to hydrogen peroxide in an acidic solution containing certain concentrations of potassium iodide. A linear response over a range of $1.6 \times 10^{-7}\,\mathrm{mol\text{-}L^{-1}}$ to $9.6 \times 10^{-5}\,\mathrm{mol\text{-}L^{-1}}$ was reported with limited interference caused by the inorganic ions.

The mPOFs were also used to fabricate gas sensors with a considerable increase in sensitivities than to conventional FOSs. Wang et al. reported a carbon dioxide gas sensor composed of hollow channels, which were coated with porous ethyl cellulose layers doped with phenol red [165]. Yang et al. employed a sol-gel technique for the fabrication of a mPOF oxygen sensor with ruthenium (II) chloride as indicator [166,167]. The ruthenium compound was coated on the exterior surface of a conventional PMMA fiber for the detection of oxygen. The fabricated sensor exhibited a linear response to oxygen from 0 to 100 v/v% with a 50 ms response time. Peng et al. [168] developed a novel fluorescent ammonia gas probe based on microstructured optical fiber (mOF), which was modified with eosin-doped cellulose acetate film. The sensors response range can be tailored through a hexadecyltrimethyl ammonium bromide (CTAB) co-entrapment process and limit of detection was found to be 50 ppm in such cases.

5.1.5. Surface plasmon resonance based sensors

This sensor is an importnat OFs based sensing technique, which exploits the generation of electromagnetic waves (plasmons) for label-free and real-time analysis with high sensitivity and specificity. A specific class of SPR is local surface plasmon resonance based sensors (LSPR), which play significant role in analytical chemistry. It is a photo-driven coherent oscillation of free electrons on the surface of a metal substrate surrounded by a dielectric medium [169]. Compared to SPR, LSPR is more sensitive to the local dielectric environment variations within a much shorter range from the metal surface (40–50 times less than SPR), which makes it an ideal candidate for the detection of ultra-low concentrations of bio-analytes [170]. The sensitivity (S) of a LSPR sensor is based on the shift of the plasmon peaks (nm) with respect to the change of the medium refractive index, which can be defined as Eq. (5):

$$S = \frac{\delta\lambda}{\delta n_m}[nm - RIU^{-1}] \tag{5}$$

Where, n_m is refractive index, and λ corresponds to the plasmon wavelength of the particle.

For a LSPR POF biosensor, the sensitivity can also be defined as Eq. (6):

$$S = \frac{\delta\lambda}{\delta c}[\mathrm{nm} - \mathrm{L}- \mathrm{mol}^{-1}] \tag{6}$$

where 'c' stands for the concentration of the biological analytes. This LSPR peak shift and absorption variations with respect to the medium's refractive index have been employed for the fabrication of LSPR-POF sensors. Chen et al. [171] developed a LSPR POF sensor to detect the concentration of hydrofluoric acid (HF). In this sensor, a thin layer of silicon dioxide bearing amine moieties was first attached onto the surface of a PMMA POF using a typical sol-gel technique. Further, gold nano particles (AuNPs) were immobilized onto the silicon layer via electrostatic adsorption. The HF detection mechanism is based on the intensity variations of the output light, when AuNPs are exposed HF

etching. Cennamo et al. [172] reported a LSPR POF sensor for the detection of TNT using molecularly imprinted polymers (MIP) as the sensing layer. Five-branched gold nanostars (AuNSs) were dispersed in a pre-polymeric mixture that contained TNT as the template molecule and then the mixture was dropped onto a side polished PMMA POF where the polymerization was carried out at elevated temperatures. The sensor sensitivity was determined to be 8.3×105 nm-mol^{-1} for a tapered POF, which is thirty times more sensitive as compared to the TNT sensors reported previously. Jin et al. [173] had incorporated thiol and amine functionalities onto the surface of PMMA POFs through direct surface chemical modifications, with adsorption of colloidal AuNPs by means of covalent or electrostatic adsorption. They found that the sensitivity of LSPR POF sensor was substantially affected by the chemistries employed for the AuNPs immobilization. AuNPs immobilized on both thiolated PMMA POFs showed higher sensitivities compared to aminated PMMA POFs.

Similar to LSPR POF sensors, POFs have been successfully employed in the fabrication of surface plasmon resonance (SPR) optical sensors. Several experimental and theoretical works have been reported on SPR sensors with great potentials [174–176]. Cennamo et al. [177] reported an innovative SPR POF sensor. The fabricated sensors are tested in two types of configurations of optical sensor systems at the interface of a liquid sample and sandwiched structures. In the first, a layer of 40 *nm* thick gold films was sputtered coated onto cladding stripped PMMA POF. In the second configuration, microposit S1813 photoresist was dip coated onto the fiber before gold sputter coating. The experimental test results showed with the photoresist buffer layer. The proposed sensor has a greater linear response to range of refractive index ranging from 1.332 to 1.352. The resolution and signal to noise ratio (SNR) were found also higher for the sensor with the buffer layer. In the refractive index medium of 1.354, resolution was found to be 0.00059 RIU and sensitivity was determined to be 2533 nm-RIU^{-1}. Lu et al. [178] reported the performance of a SPR-photonic crystal fiber (PCF) sensor by using finite element method using large-mode-area PCF coated with a thin layer of silver outside. The spectral and intensity resolution were found in the range of 8.3×10^{-5} and 9.4×10^{-5} RIU. Similarly, Wang et al. also reported a SPR sensor based on a side-hole mPOF, about the same time [179,180]. The SPR frequencies were observed at 560 nm and 620 nm and sensor was tested in the fluids of refractive indices of 1.38 and 1.41, respectively along with sensitivity $\sim$2000 nm-RIU^{-1} [181,182].

5.1.6. pH sensor

The fiber optic pH sensors offer certain advantages such as low cost and high accuracy over other types of pH sensors. Most fiber optic pH sensor designs are based on the immobilization of pH-sensitive dye molecules onto the tip or sides of an optical fiber. To immobilize dye molecules onto tip of optical fiber, the covalent chemical linking or simple physical encapsulation techniques have been used [183]. Surface modification of the optical fibers or substrate is required for covalent attachment of dye molecules. The covalent attachment results in excellent immobilization of the pH-sensitive dye. However, these methods are often more difficult to implement and may lead to loss of dye sensitivity or result in poor fluorescence properties [184].

A new type of sol–gel based fiber optic pH sensors have been developed for in vivo measurements. The constituents and pH of sol–gel solution have optimized to achieve the desired porosity. Grant et al. [185] developed a sol–gel based fiber optic sensor for blood pH measurements. The sensor uses the self referencing dye, seminaphthorhodamine-1carboxylate (SNARF-1C), encapsulated within a sol–gel matrix. Linear and reproducible responses were obtained in human blood in the pH range 6.8–8.0, which encompasses the clinically relevant range. SPR based FOs for pH was prepared by coating an unclad core of an optical fiber with three consecutive layers of silver, silicon, and a pH-sensitive hydrogel [186]. The pH change in the fluid causes the swelling or shrinkage of the hydrogel layer, and this volumetric change varies the refractive index. The sensor is capable of measuring wide range pH values between 3 and 12. The sensitivity (ΔS/pH) at neutral pH values is relatively small, and the device can resolve pH values of not more than $\pm$ 0.1 units at best, but this is adequate when measuring pH under harsh conditions. A fiber-optic pH sensor coated with a pH-sensitive material [poly-(vinyl alcohol) and poly-(acrylic acid); PVA–PAA] has been prepared to detect pH's in the range of 3–6 with a resolution of 0.02 pH units [187]. An adsorption-based evanescent wave FOs was constructed by immobilizing the pH sensitive indicator bromophenol blue in an ormosil hybrid material [188]. The sensor can reversibly determine pH's in the range from 3 to 9, but with a poor precision (0.2 pH units). The combination of indicators is also used in order to measure a wider range of pH's. The indicators such as phenol red, cresol red, and phenolphthalein were incorporated into a mesoporous sol-gel host material, which then was placed on an uncladed plastic optical fiber to measure pH in the range from 3 to 11 [189,190]. A fluorescence based optical fiber sensor was constructed by covalent attachment of a fluorescein derivative onto a highly porous poly (ethyleneglycol diacrylate) support and then attached to the distal end of an optical fiber [191]. Fluorescence was read out by both time-correlated single photon counting and stroboscopic detection with very good resolution of the sensor is 0.02 pH. Another fluorescein-based pH sensor was developed by coating a tapered spherical probe head with an ormosil film covalently doped with the indicator dye [192]. The sensor beras high stability, good sensing ability and a resolution of 0.05 pH units in the biologically meaningful pH range of 6.

5.2. Bio sensor

The development of efficient biosensor is essential for medical diagnostics, pharmaceutical, environmental, defense, bio-processing and food processing. Generally, biological system such as tissues, microorganisms, enzymes, antibodies, nucleic acids are combined with a physico-chemical transducer via optical, electrochemical, thermometric and piezoelectric to develop a biosensor [193]. In recent years, OFs have become important constituents of biosensor technology. The excellent light delivery, long interaction length, low cost, ability of OF to excite the target molecules and capture the emitted light from the targets are the main points for its use in biosensors [194]. The basics of fiber optic biosensor is shown in Fig. 17, which comprise of a bio-recognition sensing element integrated and optical transducer. It works on the basis of transmission of light along optical fiber to the site of analysis, which produces a signal proportionate to the concentration of a measured substance (analyte). The optical biosensor can sense various biological materials including enzymes, antibodies, antigens, receptors, nucleic acids, whole cells and tissues as bio recognition elements [195].

Optical fiber biosensors can be also used in combination with different types of spectroscopic techniques, e.g. absorption, fluorescence, phosphorescence, surface plasmon resonance (SPR), etc. The surface plasmon resonance (SPR), evanescent wave fluorescence and optical waveguide interferometry utilize the evanescent field in close proximity to the biosensor surface to detect the interaction of the bio-recognition element with the analyte. Riedel et al. [196] introduced a SPR biosensor assay for the diagnosis of different stages of Epstein–Barr virus infection in clinical serum samples by the simultaneous detection of the antibodies against three different antigens present in the virus. The rapid screening method employing SPR portable biosensors have great potential in food monitoring. The sensitive on-site analysis of antibiotics in milk samples were realized by a portable six-channel SPR biosensor [197]. Pennacchio et al. [198] detected the mycotoxin patulin by an immuno-chemical SPR biosensor with a detection limit of 0.1 nM. Patulin is a toxic secondary metabolite of a number of fungal species belonging to the genera penicillium and aspergillus. Another important aspect of patulin toxicity in vivo is an injury of the gastrointestinal tract including ulceration and inflammation of the stomach and intestine. Patulin has been shown to be genotoxic causing oxidative

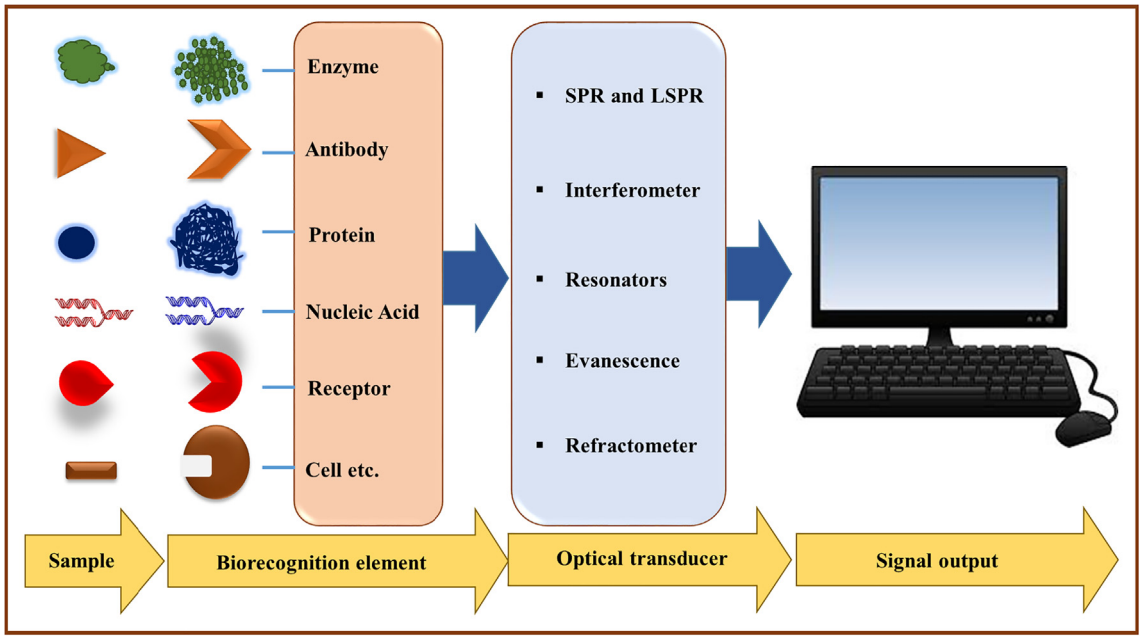

Fig. 17. Principle of optical fiber biosensors [195].

damage to the DNA, and oxidative DNA base modifications have been considered to play a role in mutagenesis and cancer initiation.

The biosensing event based on LSPR spectral shifts, often referred to as 'wavelength-shift sensing, which is caused by the surrounding dielectric environmental change. The LSPR multiarray biosensor was used for screening antigen–antibody interactions including immunoglobulins, C-reactive protein and fibrinogen with detection limits of 100 ng l^{-1} [199]. In clinical diagnostics of ovarian cancer, based on the detection of HE4 by the anti-HE4 antibody as a probe assembled on to the LSPR nanochip surface, a broad linear range (10–10000 pM) was achieved with a detection limit of 4 pM [200]. A highly sensitive label-free immune-sensor for the detection of HIV-1 was developed using localized surface plasmon resonance (LSPR) method [201]. The surface of Au nanopattern was modified with HIV-1 neutralizing gp120 monoclonal antibody fragments. The modified substrate was employed to measure various concentrations of HIV-1 particles quantitatively based on the shift of longitudinal wavelength in the UV–Vis spectrum, which results from the changes of local refractive index induced by specific antigen-antibody recognition events. The detection limit of the HIV-1 particles was estimated to be 200 fg/mL.

In evanescent wave fluorescence biosensors, the biological recognition and the consequent binding event occur within the confined evanescent wave. The evanescent wave arises from the manner in which light behaves when confined in an optical waveguide or fibers. A profuse variety of biosensors were developed on this principle with a wide array of applications ranging from clinical diagnostics to bio defence to food testing [202]. The performance of this platform was assessed using > 200 clinical samples from subjects comprising healthy individuals and those positive for HIV, syphilis and hepatitis-C [203]. The evanescent wave aptamer-based fluorescence biosensor was used for the rapid, sensitive and highly selective detection of 17β-oestradiol, anendocrine-disrupting compound frequently detected in environmental water samples. This biosensor was constructed as a portable system with the detection limit of 2.1 nM [204]. Bioluminescent optical fiber biosensors use recombinant bioluminescent cells and the bioluminescent signals transferred from the analyte. An *Escherichia coli* strain, genetically modified to make emission of a luminescent signal in the presence of genotoxic agents, was immobilized on to a fibre optic. The optrode response to the genotoxin atrazine achieved a detection limit of 10 pg l^{-1} [205]. A live cell array biosensor was fabricated by immobilizing bacterial cells on the optical fibres containing a high-density array of microwells [206]. A genetically modified Escherichia coli strain, containing the lacZ reporter gene fused to the heavy metal-responsive gene promoter zntA, was used to fabricate a mercury biosensor. A plasmid carrying the gene coding for the enhanced cyan fluorescent protein (ECFP) was also introduced into this sensing strain to identify the cell locations in the array. Single cell lacZ expression was measured when the array was exposed to mercury and a response to 100 nM Hg^{2+} could be detected after a 1 h incubation time.

5.2.1. *Blood constituents and metabolites*

Many scientists reported that the blood constituents like glucose concentrations can be directly quantified with fiberoptic systems like attenuated total reflection (ATR) [207]. Such sensors are exploiting the typical absorption of glucose in the infrared region. The absorbance at the five wavelengths correlates well with glucose concentration in the range from 500 mg/L to 5 g/L with 38 mg/L limit of detection. Sensitivity can be enhanced by using a U-shaped fiber-optic ATR sensor coated with nanoparticles like silver [208]. A glucose sensor was developed by replacing the cladding of the optic fiber with a layer of gold nanoparticle and an overcoating of a borate-functionalized polyacrylamide [209]. The binding of glucose to the borate polymer changes the surface RI of the sensor, and signal was readout by measuring the SPR absorbance. Glucose concentration in the range of 1–300 mg/dL can be accurately determined, and the sensor shows high sensitivity at low concentration of glucose. The opto-chemical glucose sensor has been developed over cupric ion doped polyaniline (Cu^{+2}/PANI) hybrid polymer matrix coated glass rod based optode [210]. The developed optode has been explored for direct oxidization of glucose on Cu^{+2}/PANI hybrid matrix for non-enzymatic glucose sensing employing O-dianisidine indicator system. The proposed glucose sensor works well in range of 50 mg/dL–200 mg/dL with response time of 15 s in artificial as well as in biological samples along with 40 days of life-span.

Enzymatic reactions proceed with high efficiency and specificity at temperatures below 50 °C. These reactions are also exploed for sensing of different biomolecules like glucose, urea, etc. using OF approach. An SPR-based fiber-optic enzymatic biosensor for glucose was fabricated by coating a fiber core with a sensing film composed of a silver layer, a silicon layer, and a gel layer containing immobilized glucose oxidase

[211]. The SPR spectrum undergoes a blue shift in resonance wavelength with increasing concentration of glucose in samples. The sensor operates in the 0–2.6 g/L concentration range and also works in whole blood. An enzymatic SPR-based FOs was developed for urea in liquid solution by Singh et al. [212] after coating uncladded OFs by layers of silver, silicon and finally a gel layer contain urease. Urease catalyzes the hydrolysis of urea to produces ammonium ion and hydrogen carbonate. The sensor works in the 0–160 mM urea concentration range. An SPR-based FOCS for clinically significant triacylglycerides sensing was described [213]. The enzyme lipase hydrolyzes triacylglycerides to form glycerol and fatty acids. Response is linear in the concentration range of 0.5–7.0 mM. Mitsubayashi and coworkers [214] developed a fluorescence-based enzymatic fiber-optic biosensor for measuring acetone concentration in exhaled breath. Sample breath gas was passed through a flow cell containing a sensor membrane incorporating NADH and alcohol dehydrogenase (which also metabolizes acetone). The detection limit was the 20–5300 ppb (v/v) concentration range of acetone.

The amine histamine is a natural endogenous compound of intracellular part of human system. It ingested unusually in high quantity from mishandled fish and fish products causes histamine poisoning [216]. Hence, ascertaining histamine levels in the aforementioned serves as a chemical index for spoilage. Usman et al. [215] has used a continuous biconical tapered multi-mode optical fibre (TMMF) as a solid support to immobilize the enzyme diamine oxidase (DAO) on chitosan and cross-linked with glutaraldehyde (GA) through enzyme multilayer assembly (layer by layer assembly) technique. The ordered multilayer DAO film was immobilized by a cross-linking agents on the surface. A spectrophotometric signal results at 450 nm from horseradish peroxidase catalyzed reduction of H_2O_2, a secondary product of the oxidative deamination of histamine. The developed biosensor has a good potential for use in the quantitative determination of histamine in sea food.

5.2.2. Nucleic acid-based biosensors

Nucleic acid is a biomacromolecule and responsible for transmission of genetic inheritance. In biosensing, it is used as an analytes as well as sensing platform in different types of sensor. The SPR based FOCs were designed for the detection of single nucleotide polymorphism (SNP) for smallest possible type of genetic variability [217]. A short chain of single-strand DNA (ssDNA) was immobilized on the surface of a fiber, and another short chain of ssDNA was immobilized on gold nanoparticles (AuNPs). Once the target (analyte) long-chain ssDNA is present in solution, it will hybridize with the short chain ssDNA, and a monolayer of AuNPs will assemble on the fiber surface. By slowly heating the sample, the surface-bound DNA will melt and the AuNPs will detach from the sensor surface, causing a shift in SPR wavelength. The aptamers were readily immobilized on fiber surfaces to fabricate aptasensors for targeting biomolecules [218]. An SPR-based sensor for thrombin protein was fabricated by coating the cladding of a tilted FBG with a 30–50 nm thick AuNP coating. The surface of the AuNPs was self-assembled with a monolayer of thrombin-binding aptamers via the established thiol–gold interaction. Binding of thrombin to aptamer shifts the resonance wavelength is around 1550 nm, and this effect can be used to detect the protein. The sensor has an excellent selectivity for thrombin, while other proteins do not interfere. Another aptasensor was also designed in order to detect the outer membrane proteins of Escherichia coli (EcOMPs) [219]. The recognition and binding of the EcOMPs by the aptamers alters the RI of the coating and causes a resonance wavelength shift of the evanescent wave. The EcOMPs can be detected in the concentration range between 0.1 and 10 nM, and the sensor can be regenerated by treatment with acid.

5.2.3. Immunosensors

OFs have significant impact on progress of application of immunosensor for pathogens, microbes, virus, etc. A highly sensitive and selective optofluidics-based fluorescent immunosensor was developed for bisphenol A (BPA) [220]. The capture molecular BPA–bovine serum albumin was covalently immobilized on the surface of the optical fiber. A mixture of different concentrations of BPA and a certain concentration of fluorescently labeled anti-BPA monoclonal antibodies after prereaction were introduced to the optofluidic cell. A higher concentration of BPA reduced the fluorescently labeled antibodies bound to the fiber surface, and the fluorescence signal was diminished. The sensor exhibits high sensitivity and selectivity to measure BPA in the range of 0.5–100 μg/L with a detection limit of 0.06 μg/L. The label-free immunosensor was described for detection of Escherichia coli B (*E. coli* B) [221]. In this sensor, a long period grating (LPG) was used with coating of T4 bacteriophage adhesion protein (gp37). The adhesive phage protein was bound on the nickel ions immobilized on the LPG surface, and the protein could irreversibly bind to the *E. coli* B by recognizing its bacterial lipopolysaccharide. Another immunosensor based on localized SPR for detecting dengue fever is reported. It uses a standard multimode fiber whose distal end was coated with a layer of AuNPs onto which an antibody against the Dengue NS1 antigen was physically immobilized [222]. The sensor detected NS1 antigen in the range of 0–1 μg/mL with a detection limit of 74 ng/mL. It may be used for dengue fever diagnosis in the acute phase of the infection. Another LSPR immunosensor was reported for sensing of γ-interferon, and marking tumor prostate-specific antigen (PSA) [223]. The antibody against γ-interferon was physically adsorbed on the AuNPs, which was then placed at the distal end of the optical fiber. The analytical range is from 2 to 500 pg/mL of PSA with limit of detection is 1 pg/mL. Further, gold nanorods (AuNRs) based respective sensor was also designed for label-free detection of orchid viruses [224]. The AuNRs were immobilized on the surface of an unclad fiber core and then functionalized with antibodies against cymbidium mosaic virus or odontoglossum ringspot virus. The detection limits for these two viruses in leaf saps were 48 and 42 pg/mL, respectively. The improvement in sensitivity was achieved by replacing the gold nanospheres by hollow gold nanostructures (HAuNS). A localized SPR-based immunosensor was developed using HAuNS labeled with human immunoglobulin-G (HIgG) coated on the surface of unclad fiber core [225]. Goat-anti-HIgG protein can be detected in the 1 ng/mL to 10 μg/mL concentration range, which is almost 1.5 times better than in the case of a sensor using gold nanospheres. The fiber-optic immunosensor for detection of crimean-congo hemorrhagic fever (CCHF) IgG antibodies used the CCHF virus protein that was covalently immobilized on the unclad core of an optical fiber to form the sensor probe [226]. By dipping the sensor probe into a patient's serum, the CCHF IgG antibody present in serum will bind to the sensor surface. The peroxidase on the sensor surface can catalytically convert substrate and emit chemiluminescence (CL). An optical waveguide carrying immobilized streptavidin was reacted with biotinylated polyclonal antibodies to immobilize the respective antibodies on the fiber surface [227]. The biofunctionalized FOCs was exposed to the food pathogens such as listeria monocytogenes, Escherichia coli O157:H7, or salmonella enterica, then these bacteria were attached to the fiber surface. They could be detected after reaction with fluorescently labeled monoclonal secondary antibodies. These biosensors could detect each pathogen individually or in a mixture with very small cross-reactivity in meat samples. The detection limit was as low as $\sim 10^3$ cfu/mL for all three pathogens.

Hu et al. [228] designed an optical fiber biosensor for rapid detection of human immunoglobulin G (HIgG) with the average detection time about 20 min. A thin core optical fiber with a length of 2 cm was fused between two segments of single mode optical fibers. The outside surface of the thin core optical fiber was coated with the antibody using the method of layer-by-layer electrostatic self-assembly, and then become able to detect the antigen in solution. The best sensitivity was achieved to be 16.92 nm/(mg/mL) and limit of detection (LOD) as ~0.59 mg/L.

Table 2
OFs based various biomedical technologies.

S. No.	Analytes	Sensing principle	Applications	Ref.
1	Pressure and temperature Sensor	Based on the detection of optical reflection intensity changes from a diaphragm located in front of an optical fiber	Application of the pressure micro-sensor to actual balloon catheters 1.5 mm in outer diameter	[229]
		The pressure deflects the diaphragm that alters the cavity depth and thus the optical cavity reflectance at a given wavelength	Fabry–Perot cavity at the fibre tip pressure sensor. It is glass cube having a partially etched face, covered by a pressure sensitive silicon diaphragm	[230]
		The light intensity modulation of the reflected light caused by the pressure induced position of the diaphragm	Fiberoptic micro-tip pressure transducer for several clinical applications	[231,232]
		The first developed fibre optic thermometer based on UV light guided by the fibre is used to excite phosphors fixed at the fibre end and fluorescence decay-time is measured, which results temperature modulated and intrinsically down-lead insensitive as well	Fibre-optic thermometers involve tissue-heating control during MW or RF hyperthermia therapy for cancer treatment	[233,234]
2	Ultrasound imaging	Photoacoustic principle is an optical ultrasound generation mechanism, which involves optical energy absorption and conversion	This technology has been used in medical diagnosis and structural health monitoring	[235]
3	Optical coherence tomography	OCT forms truly depth-resolved tomographic cross-sectional images, with a depth resolution in the 1–20 μm range. An OCT interferometer typically consists of a single mode optical fiber terminated with a focusing element and beam deflecting element for a side-viewing sensors	OCT imaging systems used to generate impressive subsurface images of the superficial layers of the gastro-intestinal and broncho-pulmanory tracts, as well as intravascular images of atherosclerotic plaques in coronary arteries	[236,237]
4	Magnetic resonance imaging	MRI work on different principles like fiber bragg grating (FBG) technology, intensity-based and interferometry based fiber optic sensors	MRI compatible FOS, focusing on the sensors employed for measuring physical parameters in medicine i.e., temperature, force, torque, strain, and position. FBG-based sensors for monitoring temperature in MRI. Intensity-based sensor for force sensor in cardiac ablation, etc.	[238–241]
5	Photodynamic therapy	PDT is based on the activation of light sensitive molecules (photosensitizers) to cause cell death by producing cytotoxic oxygen radicals	Photodynamic therapy (PDT) is an alternative treatment option for tumours of the head and neck. There are different techniques to illuminate the tumour, respectively, to activate the photosensitizer like superficial PDT, interstitial PDT, intra-operative PDT and intracavity PDT	[242,243]
6	In optogenetics	In optogenetics, light intensity (strictly time-averaged irradiance; power per unit area) measured in $mW\,mm^{-2}$ is the recommended notation for reporting light requirements	Optogenetics is used to understand the mechanisms of functioning of the brain and peripheral neural system	[244,245]
7	Tissue characterization	Fibre optic raman probes and infrared probe based upon the phenomenon of inelastic scattering of laser light by molecules in the sample volume. The molecular information obtained can be used for the discrimination of cell and tissue types, and diseased versus healthy tissues	Fiber optic raman probes can be utilized as clinical tools able to provide rapid, non-invasive, real-time molecular analysis of disease specific changes in tissues. Infrared fibre-optic probes used for label-free tissue classification	[246,247]

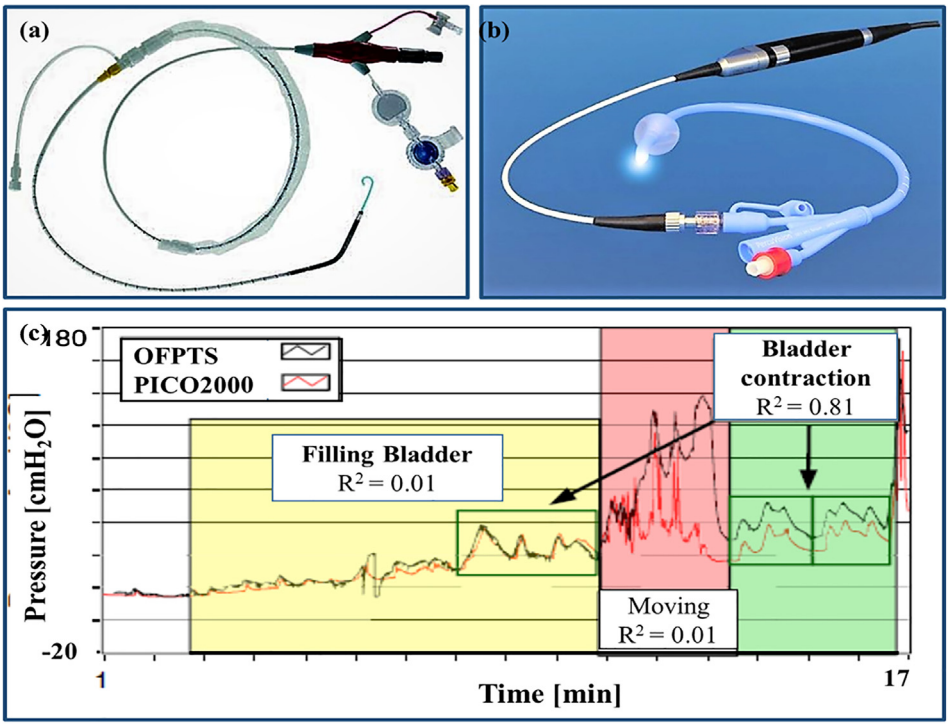

Fig. 18. (a) Abdominal balloon catheter; (b) bladder catheter; (c) urodynamic measurement [263,264].

5.3. Biomedical technology

The ever-growing rate of population and quest for longer life is demanding good medical and healthcare facilities. In this regards, advanced biomedical instrumentation is utmost requirement for more efficient diagnosis, monitoring, and treatments. Impact of OF on the development of various biomedical technologies are given in Table 2.

These applications revealed that OF added a great opportunity in the medical fields, for instance, the use of bundle of OF endoscopy for illumination and imaging. The OFs were also used in cavitational laser surgery and therapy, because they provide the most flexible, and a low-attenuation delivery system inside the ancillary channel of endoscopes inside the natural channels of the human body as well [248]. Generally, the use of OF in biomedical technology can be categorized into three types: (a) monitoring of physical parameter, (b) imaging and (c) surgical operation [249]. The monitoring of physical parameters refers to body temperature, blood pressure, and muscle displacement. The process encompasses both endoscopic devices for internal observation and imaging, as well as more advanced techniques such as optical coherence tomography (OCT) and photoacoustic imaging where internal scans and visualization can be made nonintrusively. The improvement in an accurate and efficient surgery is outcome of advanced optical fiber technology.

Another way to classify the use OF in biomedical is in vivo or in vitro. In vivo refers to application on a whole, living organism such as a human patient and in vitro refers to testing outside the body such as laboratory blood tests and urine test. From the perspective of how it is applied to a patient or biological system, it can be further classified as noninvasive, contacting (skin surface), minimally invasive (indwelling), or invasive (implantable). It can be used in clinical, veterinary, or other living organisms, depending on the intended use for diagnostic, therapeutic, or intensive care used in clinical applications, research and preclinical development or laboratory testing. OFs are also widely used in monitoring of physical parameters of medical interest such as blood flow, cataract onset, radiation dose and biting force, etc.

5.3.1. Pressure sensor

The pressure in a living human body is influenced by internal (e.g., muscles, fluids) and as well as external (e.g., gravity and atmospheric) force. Clausen and Glott [250] categorized the body pressures into three domains: (a) low pressure regions (e.g., capillaries and brain); (b) medium pressure regions (e.g., heart and lung); and (c) high pressure regions/states (e.g., joints and pressure changes during ablation techniques). The most popular pressure sensors are electro-mechanical pressure sensors like catheters and guidewires. Air-charged catheters are low-cost and popular, particularly for urology applications [251]. Fluid-filled catheters are relatively more stable and responsive sensors for urology and cardiovascular applications [252–254]. An alternative to these electro-mechanical pressure sensors is optical fibre pressure sensor (OFPS). Yang et al. [255] tested OFPS based pressure sensors for 12 weeks and demonstrated their biocompatibility and usability for in vivo human applications. Woldbaek et al. [256] described the use of an OFPS for pressure recording in the cardiology setting. They used this optical sensor for pressure measurements in mice. They tested the sensors (o. d. 0.42 mm) in vitro with a drift of < 60 Pa/h (< 0.45 mmHg/h) and a temperature sensitivity of only 9 Pa/k (0.07 mmHg/k) in the range of 22–37 °C. The frequency response is 0–200 Hz, which fulfils the technical specification.

Wu et al. [257] developed an optical sensor in conjunction with a fractional flow reserve (FFR) technique to monitor blood presuure in a swine model [258–260]. Rodriguez et al. [261] used an OFPS for simultaneous measurement of pressure and volume. Chavko et al. [262] demonstrated an intra-cranial pressure measurement in generated blast waves using OFPS. The sensors were placed in third cerebral ventricle of anaesthetized male rats. The pressure recorded were as high as 40 kPa and measured for several milliseconds. Poeggel et al. [263] used it in vivo bladder and abdom of patients, which allowed the simultaneous measurement of urodynamic pressure in a 1.6-mm (5 Fr) catheter, as well as abdominal pressure (Fig. 18a, and b). The authors used sensing technique with integrated FBG for measuring pressure and temperature as optical fibre pressure as well as temperature sensor (OFPTS) (Fig. 18c) [264]. The sensor was inserted into a silicon probe that measured radial muscle pressure and to estimate the axial load.

The intra-abdominal pressure (IAP) of the glenohumeral joint was monitored by Inokuchi et al. [265]. The intra-muscular pressure (IMP) in rats was measured in the legs of four female and three male humans [266,267]. Roritz et al. [268] measured the pressure in the intervertebral disc pressure (IDP) of an anaesthetized sheep. The ex-vivo measurements of heart rate were recorded using optical fiber macro bending sensors on foot artery or mounted around the arm. The sensors for needle tip force sensing were tested on a medical skin phantom [269–271].

5.3.2. Ultrasound imaging

A variety of fiber optics based imaging techniques such as ultrasound, x-ray and magnetic resonance were developed to observe and investigate microscopic objects along with their internal structures. Through use of imaging techniques within the clinical diagnostic field, these techniques have played an important role in improving the quality of human life. Zou et al. [272] developed a broadband miniature fiber optic ultrasound generator based on photoacoustic (PA) ultrasound generation principle for biomedical ultrasound imaging. The fiber optic ultrasound generator was fabricated by coating the gold nanocomposite on the tip of the optical fiber. The efficiency of the PA generation using gold nanocomposite was increased 10^5 compared to using aluminum thin film and 10^3 compared to using graphite mixed within epoxy. The amplitude of the generated ultrasound signal was as high as 0.64 MPa and the bandwidth was more than 20 MHz. They also explored its capability for ultrasound imaging of a slice of pork tissue specimen. The first ultrasound image of a tissue specimen was obtained with the resolution of 200 μm. Kochergin et al. replaced the cladding of an optical fiber with graphite/epoxy mixture to generate ultrasound from the sidewall of optical fibers [273]. Tian et al. successfully used ghost mode of tilted fiber bragg gratings to generate ultrasound from the sidewall [274]. The ghost-mode generated by tilted fiber bragg gratings expands the optical energy from the core to the cladding and a graphite/epoxy mixture was used to absorb the optical energy at the cladding. The advantage of using tilted fiber bragg gratings is to implent multiplexing. Wu et al. [235] reported in their review that traditional ultrasound transmitters are challenged by modern applications, which require transmitters featuring a broad bandwidth and a compact size. In order to fill the requirements, several researchers have developed novel ultrasound transmitters using photoacoustic principle and optical fibers.

5.3.3. Optical coherence tomography

OCT has presently emerged as a novel non-invasive imaging tool in biomedical application with superior properties than ultrasound, x-ray, and magnetic resonance imaging (MRI) [275]. Although ultrasound, x-ray and magnetic resonance imaging methods offer deep imaging throughout the whole body, but they do not have good enough resolutions for tissue level imaging and they also need long data acquisition and processing time. Compared to other conventional medical imaging techniques, OCTs visualize the internal structure of scattering or turbid samples including human tissues or live organs with a high three dimensional (3D) resolution as well as it is free from radioactive hazard. The recent OCT systems have been applied for clinical or biomedical fields as well as it also extended in industrial applications such as non-destructive testing [276], sensing [277] with high precision inspection or measurements [278]. The use of OCT, especially for endoscopic applications, is necessary to miniaturize the system configuration for more convenient handling, improved stability and cost-effectiveness. Most of these demands could be satisfied by introducing fiber-optics. Robust optical fibers with flexible nature were reported for use in endoscopic laser applications in mid-infrared region. Either endoscope or catheter is used for minimally invasive treatments of tumors and other diseased tissue. The chemically modifed fibers are enough to be inserted into the working channel of endoscopes to be used as laser with a bending radius of around 15 mm for necessary applications [278]. Eom et al. [279] presented an optical fiber combined-imaging system, which integrates non-contact photoacoustic tomography (NPAT) and optical coherence tomography (OCT) to simultaneously provide photoacoustic (PA) and OCT images. The PA signal was generated by a large core multimode optical fiber illuminated a bulk type Nd:YAG laser at the sample. The fiber-based OCT operating at a center wavelength of 1310 nm is combined with the fiber-based PAT system by sharing the same optical fiber probe. The two lights from the fiber laser and the OCT source are guided into the probe through each port of a 2 by 2 optical fiber coupler. The back-reflected lights from the sample are guided to respective imaging systems by the same coupler. Chong et al. [280] developed a multi-functional fiber-optic OCT system for human retinal imaging with < 2.5 μm resolution. The proposed fiber-optic OCT system has higher repetition rate, lower noise, and found to be enable a sensitivity of 87 dB with 0.1 mW incident power at the cornea and a 98 micro second exposure time. In vivo anatomical, doppler, and spectroscopic imaging of the human retina was investigated. It is reported that high-resolution visible light OCT has potential for depth-resolved functional imaging of the eye. Lee at al. [281] also demonstrated a fiber-optic-based parallel optical coherence tomography (OCT) using spectrally encoded extended illumination with a common-path handheld probe. The flexibility and robustness of the system were significantly important in the clinical environment. The parallel OCT based on fiber optics including a fiber coupler with a sensitivity of 94 dB was comparable to that of point-scanning OCT. For this homemade common-path handheld probe based on a Mirau interferometer, phase stability was obtained as 32 times better than that of the two-arm OCT. The axial resolution of the common-path OCT was measured as 5.1 ± 0.3 μm.

5.3.4. Magnetic resonance imaging

Taffoni et al. [282] reported in their review that high elasticity and small size allow designing miniaturized fiber optic sensors (FOS) with metrological characteristics such as accuracy, sensitivity, zero drift, and frequency response for medical applications. The immunity from electromagnetic interferences along with its good metrological characteristics, make FOS attractive for several applications in magnetic resonance scanner. In magnetic resonance (MR)-compatible devices, FOS can be useful for both improving surgical procedure outcomes and patient monitoring. FOS based MR-compatible devices were used to measure the temperature of patients undergoing MRI-guided hyperthermic procedures [283], assessment of deflection and force on needles during MRI-guided procedures [284] along with estimation of other physiological parameters (e.g., heart rate and respiratory monitoring) [285]. The concept of photonic sensing system combines the advantages of fiber bragg grating (FBG) based sensors. This photonic integrated circuit based optical interrogator was developed for patient condition monitoring during MRI diagnostics [286]. The proposed system is dedicated to remote, all-optical monitoring of condition of a patient during magnetic resonance imaging. The proposed system (Fig. 19) consists of three substantial components: (a) a set of FBG sensors imprinted on optical fiber/fibres inserted into MRI bed overlay, (b) interrogator unit exploiting photonic integrated circuit and (c) control unit composed of a computer with a dedicated software. All optical sensors located within MRI chamber are connected with the interrogating unit via single fiber-optic link, thus eliminating any need of electrical or wireless connection with the sensors.

The important feature of FBGs with respect to the vital signs detection is their highly sensitive and linear strain and temperature response, the best of reported values are in the order of 1 pm/με and 10 pm/°C at 1550 nm. Bützer et al. [287] designed a low-cost, 3D-printed, inherently MRI-compatible grip force sensor based on a commercial intensity-based fiber-optic sensor. A compliant monobloc structure with flexible hinges transduces grip force to a linear displacement captured by the fiber-optic sensor. The structure can easily be adapted for different force ranges by changing the hinge thickness.

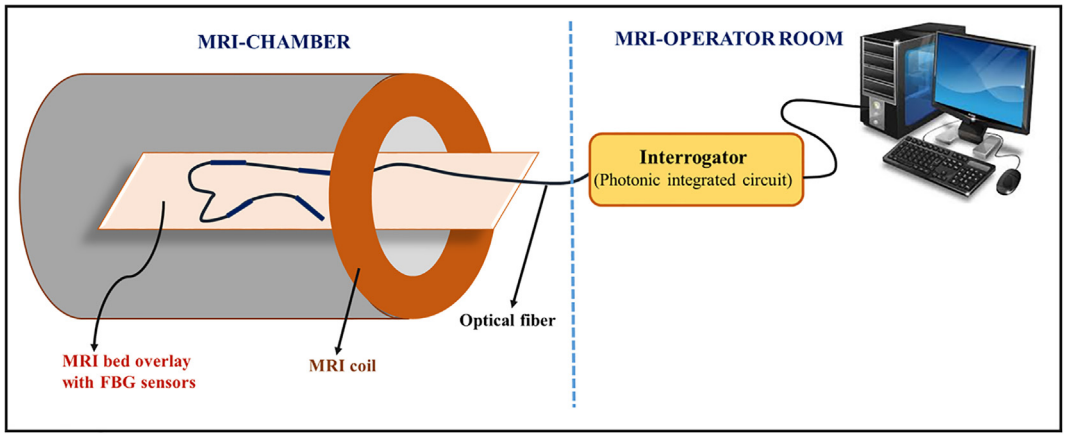

Fig. 19. Photonic sensing system for patient condition monitoring during MRI diagnostics [286].

5.3.5. Surgical applications

Shephard et al. [288] reported the challenges of integrating next generation laser systems into manufacturing processes inorder to expand the use of lasers in medicine and surgery. The fundamental requirement of having a truly flexible fiber delivery system has until now been a significant restriction to the development of these technologies. The emergence of hollow core fiber designs extend both the power handing capability and operating wavelength regime of fibers by reducing the interaction of the light with the glass material. The development of novel hollow core Negative Curvature Fibers (NCF) provides very promising solutions. It has been demonstrated to flexible delivery for both picosecond (ps) and nanosecond (ns) pulses from commercial micro machining lasers whilst preserving the beam quality and the pulse parameters necessary for practical applications. The processed materials show no reduction in quality due to the delivery of fiber [289]. This is to avoid ingress of debris and liquids (e.g., blood or tissue fragments) into the core. The approach was adopted to mount the solids sapphire end tip onto the OF output end [290]. The NCF has also been proven to be a realistic delivery system for the Er:YAG (2.94 μm) laser. In NCF design, all silica fibers were operated well above the transmission cut-of for conventional silica fibers (around 2 μm) with low guidance demonstrated up to around 4.5 μm. Using such a fiber to deliver 225 μs pulses at 2.94 μm practical ablation of both soft and hard tissue have been demonstrated. A practical solution for end-capping NCF at these mid-infrared wavelengths has also been proposed utilizing a sapphire window. Thus, the NCF has significant potential for exploitation in new minimally invasive medical procedures. Similarly, an optic sleeve was also developed with integrating phacoemulsification system for cataract surgery. The sleeve is comprising of surgical hand pieces and bundle of fiber optic bundles to transmit the visible light for enhancement intraocular illumination [US Patent:patent/US5651783A/en].

5.3.6. Photodynamic therapy

The fiber optics used in successful photodynamic therapy treatment of hyper proliferative tissue diseases, for instance dysplasia. The previously developed PDT is administered to patients with light-emitting diode (LED) panels. These panels deliver a non-uniform light distribution on the human body parts, as the complex human anatomy is not a flat surface (head vertex, hand, shoulder, etc.). Thus, for an efficient PDT, a light-emitting fabric (LEF) was woven from plastic optical fibers (POF) aiming at the treatment of dermatologic diseases such as actinic keratosis (AK), severe acne vulgaris, etc. Wang et al. [291] developed an optical fiber imported intra-tissue photodynamic therapy (OFI-ALA-PDT) to treat moderate to severe acne vulgaris. Acne vulgaris is a common skin disease of great cosmetic concern to young people. PDT is based on the activation of light-sensitive molecules (photosensitizers) to cause cell death by producing cytotoxic oxygen radicals. 5-aminolevulinic acid (ALA) is frequently used in topical PDT because it is converted into protoporphyrin (PpIX), an extremely active photosensitizer, upon irradiation with red light [292]. Recent studies have suggested that ALA-PDT is also effective in treatment of acne vulgaris [293]. In the OFI-ALA-PDT therapy, the red light was directly imported into the target lesion with optical fiber used intra-tissue irradiation for 5 min (Fig. 20). Each irradiation was given to patient after interval of 7–10 days. After the 4th irradiation, about 90.0% of significantly different effective rates were observed which was better than previous traditional ALA-PDT.

Another dermatology disease is actinic keratosis (AK), which is a pre-cancerous condition due to chronic UV light exposure that may develop into non-melanoma skin cancer [294]. Photodynamic therapy (PDT) is particularly used to treat pre-cancerous or cancerous lesions with the combination of a photosensitizer and a subitable lighting source. In order to maximize the comfort of the PDT the light-emitting woven gabric (LEF) composed of PMMA optical fibers (POF) was developed [295,296]. The portwine stain (PWS) birthmarks are congenital vascular malformations of the skin that affect 0.3% of newborns. PWS appears on the face and neck area and require medical intervention. Pulsed-dye laser (PDL)-mediated photo thermolysis is the current standard treatment. However, studies have indicated that vascular-targeted photodynamic therapy (PDT) is an alternative of pulsed-dye laser (PDL) treatment. A typical optic fiber coupled lasers was used with the maximal diameter of the light spot on the skin surface is set at 7–10 cm and the duration of irradiation 20–25 min/spot to maintain the fluence levels of 80–100 mW/cm^2 in order to achieve desired clinical

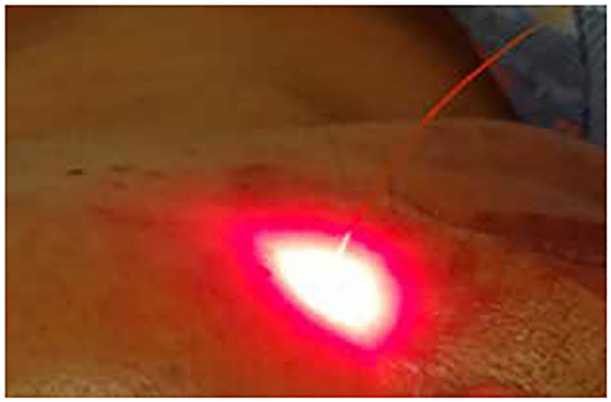

Fig. 20. Illustration of intra-tissue OFI-ALA-PDT. The red light was imported directly into the target lesion with optical fiber [291]. (For interpretation of the references to color in this figure legend, the reader is referred to the web version of this article.)

outcomes [297]. Currently, several prototype LED devices emitting a narrow band of 532 nm are tested. Preliminary results suggest that the fiber-free LED panel can generate uniform light field that covers at least twice size of the laser at the same fluence with comparable clinical outcomes to PDL. Ongoing trials demonstrate that with a good assurance of uniform light distribution and adequate light fluence, in conjunction with real-time monitoring of light fluence, high power LEDs might offer an ultimate solution for treating larger PWS lesion. Costa et al. [298] evaluated the effect of photosensitizers used in photodynamic therapy (PDT) on tooth color change in combination with conventional endodontic treatment. The samples were irradiatiated by means of an optical fiber cable with 330 µm in diameter at a power density of 40 mW for 120 s. The fiber cable was introduced inside the root canal to reach the working length (WL), at a distance of 1 mm from the radiographic apex. Helical movement was performed from the apical to the cervical region in order to ensure a uniform distribution of light within the canal [299].

5.3.7. Optogenetics

The optogenetics is a powerful tool, which combines optics with genetic engineering to probe neural circuits inorder to investigate their underlying functions [244]. Most recent optogenetics studies have largely focused on in vivo optical manipulation of brain cells and circuits through a stereotactic insertion of an optical fiber to specific regions in the brain [300]. Shin et al. [301] proposed a Monte Carlo (MC) method for fiber-optics-based optogenetic neural stimulations. It provides an accurate and direct solution for light intensity distributions in brain regions with different optical properties. The flexibility of optogenetics is unique in further enabling causal tests over a broad range of spatial and temporal timescales to meet the unique challenges of neuroscience. The modern optogenetics now includes naturalistic behavioral paradigms with fast quantitative readouts and even closed-loop feedback based on changes in the physiology or actions of the experimental system, which enables an unprecedented level of hypothesis testing precision [302]. This technique requires an exchange of light with nervous system through implanting a small fiber optic probe into the brain. It is typically interfaced with a lightweight fiber-optic patch cord coupled to a laser diode or to a light-emitting diode (LED) light source for input and to a fast camera or photomultiplier for readout [303–306]. Thermogenetics is other promising innovative neuro stimulation technique, which enables robust activation of neurons using thermosensitive transient receptor potential (TRP) cation channels. Broader application of this approach in neuroscience is activation of TRP channels by ambient temperature variations or chemical agonists. Ermakova et al. [307] demonstrated the rapid, robust and reproducible repeated activation of snake TRPA1 channels heterologously expressed in non-neuronal cells, mouse neurons and zebrafish neurons in vivo by infrared (IR) laser radiation. A fiber-optic probe that integrated a nitrogen-vacancy (NV) diamond quantum sensor with optical and microwave waveguide delivery enables thermometry with single-cell resolution, allowing neurons to be activated by exceptionally mild heating, thus preventing the damaging effects of excessive heat. The neuronal responses to the activation by IR laser radiation are fully characterized using Ca^{2+} imaging and electrophysiology, providing, for the first time, a complete framework for a thermogenetic manipulation of individual neurons using IR light.

5.3.8. Tissue characterization

Several recent approaches regarding fibre-optic probes for tissue characterization with single spot measurements or for mapping larger tissue areas have been manifested, with a technique also termed as evanescent wave spectroscopy [308]. Such studies were performed on skin [309], bladder and human colon carcinoma tissue [310]. Further advances into applications of fiber-coupled ATR-spectroscopy have been used for dyes and hyperplasia detection in colonoscopy obtained human biopsy samples [311] and areas detection of colonic inflammation in a mouse model [312]. Dong et al. [313] developed a system to differentiate normal and cancer tissue regions from macroscopic human colorectal tissue samples of radical resections, which revealed that fiber-optic spectroscopic colonoscopy could be advanced into the operating room. In the light of this development, Ollesch et al. [314] designed the infrared fiber-optic probes for the discrimination of colorectal cancer tissues and cancer grades. The researcher presented a compromise approach with regard to the reduction of the data volume and measurement/processing time. It is gaining a far greater instrumental flexibility by a reduced spatial resolution using ATR-probes with a 4–6 mm^2-size sensing area. They set the two standard-sized fiber-coupled ATR probes on fresh colorectal tumour resectates within the clinical environment. The sampling protocols were optimized to meet clinical demands. Thus, a rapid spectral characterization of freshly resected and unfixed colorectal tissues, similar to tissue as presented during colonoscopy, was achieved. The prediction of tumour regions was validated using a second independent dataset. Thus, two discriminative spectral feature sets and three classifiers obtained from the calibration data, which could assess under real-life conditions. The work flow from surgical tissue resection to Monte Carlo leave-one-third-out cross-validated classification is schematically illustrated in Fig. 21.

Subsequently, first and second derivative spectra were obtained and concatenated to form a representative conjunct spectral vector of the biochemical tissue status. Finally, the class assignment obtained by the medical gold standard of histopathology was used for feature selection, classification and validation [314]. The measurements were performed at room temperature with two sealed spectrometers with externally attached fibre-optic probes. First, a DiProbe/Upgrade with a 6 mm diameter shaft, provided by infrared fiber sensors was coupled to a Tensor 27 spectrometer using an external pigtailed MCT-detector. The ATR-probe head consisted of a diamond micro-prism for sampling with two reflections (Fig. 22). A second ATR-probe was coupled to a Matrix MF spectrometer, which is equipped with a high-sensitivity MCT detector. All detectors were cooled in liquid N_2.

The performance was assessed of infrared spectral analysis of colorectal tissue with millimeter spatial resolution for cancer lesion identification and grading within a surgical setting. Colorectal tissue was removed during routine therapeutic surgery. The spectral discrimination of tumour versus normal tissue under the cross-validation scheme was achieved with an accuracy of 90 ± 5% (sensitivity of 89 ± 7%, specificity of 90 ± 7%), where as respective test-set validation led to an accuracy of 80% (sensitivity of 83% and specificity of 78%). Low versus high tumour grading was assessed under cross-validation with an accuracy of 81 ± 8% (sensitivity of 80 ± 16%, and specificity of

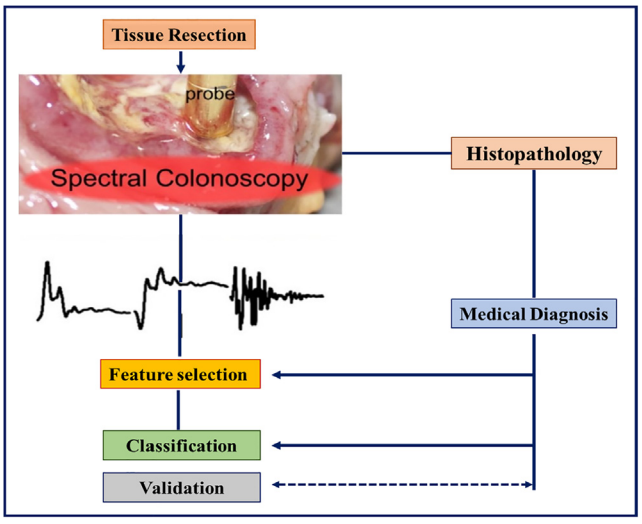

Fig. 21. Scheme for the analysis of colorectal resectates [314].

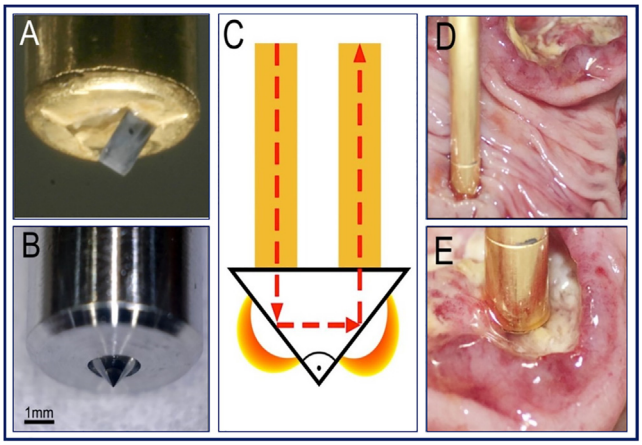

Fig. 22. Two probe heads (A), A cone-shaped diamond tip (B). In both fibre-optic probes withcladded silver halide (C). The probe head (D) Tumour lesion and (E). Grading information [314].

81 ± 14%). Thus, fibre-optic infrared spectroscopic tissue analysis has the potential of supporting clinical decisions by providing immediate tissue and grading information during surgery.

5.4. Environmental monitoring

Today's researchers have a great interest for smart environmental monitoring to protect the public and environment from toxic contaminants and pathogens, which are released from varrious sources such as air, soil, and water [315]. The outdoor and indoor environments includes air pollutants such as sulfur dioxide, carbon monoxide, nitrogen dioxide, and volatile organic compounds, which originate from vehicle emissions, power plants, refineries, and industrial and laboratory processes, etc. Some of soil and water have contaminants such as microbiological (e.g., coliform), radioactive (e.g. tritium), inorganic (e.g. arsenic), synthetic organic (e.g. pesticides), and volatile organic compounds (e.g. benzene). Pesticide and herbicides are applied directly to plants and soil. The incidental releases of other contaminants are from spills, leaking pipes, underground storage tanks, waste dumps and waste repositories. Some of these contaminants can persist for many years and migrate through large regions of soil until they reach water resources, where they may cause an ecological or human-health threat. For this purpose, optical fiber based sensors and imaging technologies are widely useful to monitor various contaminants present in the air, soil, and water.

5.4.1. Monitoring of air quality

Generally, environmental monitoring has been classified into indoor and outdoor monitoring. The majority of the studies have been concentrated on indoors environment and they are daily in contact with household products such as paints and paint strippers, solvents, sprays, preservatives, disinfection products, repellents and air fresheners containing volatile organic compounds (VOCs). Consequently, indoor air quality (IAQ) are directly influenced by a mixture of physical, chemical and biological factors [316]. The temperature, relative humidity (RH) and volatile organic compounds (VOCs) are the key factors of interest of sensing and monitoring. Fiber optic sensors are promising probes to solve problems of IAQ monitoring. The fiber-optic sensing platform based on long period gratings (LPGs) with functional coatings has been used to measure various measurands, including RH [317], ammonia [318], and VOCs [319]. Shukla et al. [30] has developed an efficient humidity sensor for closed chamber by using metal oxide coated oxides (MgO and ZnO) of wide range humidity from 5 to 95% RH (Fig. 23).

The authors discussed the sensing mechanism on the basis of change in numerical aperture of optical fibers after adsorption of water molecules. It is indicated that modulation in numerical aperture leads to change in output power of light through the optical fiber. A single mode optical fiber containing a long period grating (LPG) was modified with a mesoporous thin film that was infused with calixarene molecules that acted as the functional compound for VOCs detection [320–322]. Calixarene molecules contain a number of phenol or resorcinol aromatic rings connected to gether to a larger ring and the whole molecule seems to be a bowl. The sensing mechanism is based on the measurement of the refractive index (RI) change induced by a complex of the VOCs with calixarene. The LPG, modified with a coating of 5 cycles of (SiO_2 NPs/PAH) and infused with CA [318]. Further, it was exposed to the vapor of chloroform, benzene, toluene and acetone [322]. The functionalized LPGs have been achieved a limit of detection lower than of 100 s of ppm and response of the sensor was observed in less than 30 s, and sensor exhibited different responses to individual VOCs and mixtures.

The problem of global warming is very acute problem due to various types of toxic gases including C_2H_2, CH_4, NO_2, SO_2, NH_3, H_2S, CO_2, and CO. These combustible and explosive gases are emitted from industries and vehicles. Cordeiro et al. [323] proposed a microstructure of photonic crystal fiber (PCF) that increased the energy of gas filling air holes. Hoo et al. [324] reported an all-fiber gas sensor with relative sensitivity of 10.15% at the 1.4 μm wavelength. Morshed et al [325] developed PCF with improved relative sensitivity of 16.88% and reduced confinement loss of 1.765×10^{-8} dB/m. Olyaee et al. [326] proposed a micro structured PCF with enhanced the sensitivity of 32.99% as well as minimizing the leakage loss of 2.59×10^{-5} dB/m at the 1.33-μm wavelengths. A hexagonal photonic crystal fiber (H-PCF) has been developed with five layer hexagonal cladding and single layer circular core territories by circular air holes [327]. The proposed H-PCF was explored as a gas sensor that improves the relative sensitivity of 56.65% and reduces the confinement loss of 2.31×10^{-5} dB/m at $\lambda = 1.33$ μm. In addition, the effective area and nonlinearity of 6.44 μm^2 and 22.73 W^{-1}-km^{-1} respectively were gained at the same wavelength. Olyaee et al. [328] reported a novel gas sensor based on the index-guiding photonic crystal fiber. The sensing properties such as relative sensitivity and confinement losses on the fiber structural parameters and working wavelength were investigated for three types of index-guiding photonic crystal fibers with hollow high-index GeO_2–SiO_2 ring defected core. The higher sensitivity and lower confinement loss has been achieved simultaneously. To obtain much more sensitivity, they introduced the hexagonal holes instead of circular holes in the innermost ring. In the proposed fiber with optimized parameters, the relative sensitivity at wavelength of $\lambda = 1.33$ μm, the methane absorption line enhanced to value of 13.23% (previous index guiding PCF was 3.25%). Also the confinement loss reduced to 3.77×10^{-6} that was about 1×10^{-3} in the previous index guiding PCF.

5.4.2. Temperature sensing

The thermal sensitivity of fiber-optic platforms based on LPGs arises from a combination of the thermo-optic effect and thermal expansion of fiber. The sensitivity of the LPGs can be increased by appropriate choice of grating period and composition of the optical fibre [329]. The shift of the central wavelength of resonance bands caused by a temperature change is generally linear from ambient temperatures to up to 150 °C. An ultrahigh sensitive point temperature sensor was prepared by inserting a section of low birefringence photonic crystal fiber (LB-PCF) inside the fiber loop mirror structure [330]. The sensor head was configured by applying a mechanical lateral force on the LB-PCF, whose birefringence is sensitive to environmental temperature change due to stress optic effect. This sensor has been used as a point temperature sensor because only the small sensor head is sensitive to environmental temperature change. They showed a linear response to the temperature change with an ultrahigh temperature sensitivity of 30.33 nm/°C.

Another technique called distributed temperature sensing (DTS),

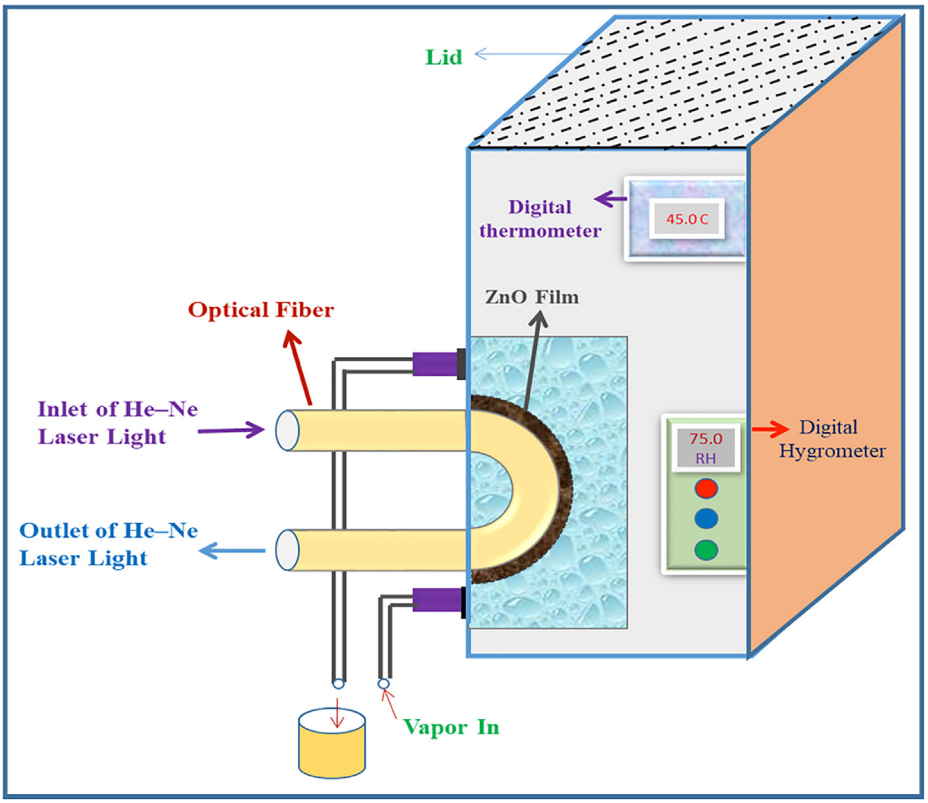

Fig. 23. Opto chemical humidity set up [30–32].

which is also used for measurement of temperature using optical fibers. Laser pulses are shot into the fiber, and backscatter from within the fiber is analyzed. Analysis of the Raman spectrum of the backscatter allows for the calculation of the temperature at the place where the backscatter originated. The DTS technique can be used for temperatures measurement continuously at sub-meter intervals along cables of more than 5 km, with laboratory accuracies up to 0.01 °C and typical field accuracies of 0.08 °C [331]. The applications of this technique has been used for evaluation and variation of temperature profiling of the subsurface such as borehole observations [332], soils [333,334], temperature profiling of estuaries water [335], surface/groundwater [336], solar ponds [337], streams [338], lakes [339], rocks, ice caves [340,341], some infrastructures like dam surveillance [342], sewers [343], electric transmission cables [344] and gas pipelines [345], etc. These atmospheric temperature profile is hindered by solar heating in distributed temperature sensing (DTS), which may lead to significant deviations from the true air temperature. A group of researchers under leadership of Jong et al. [346] showed that it was possible to correct for solar heating and found a good estimation for the air temperature, by using cables with different diameters. The corrected temperatures matched the temperature measurements of the reference with a root mean square error of 0.38 °C.

5.4.3. Monitoring of water pollutant

The demand of clean and suitable water attracts researcher and scientists to developed new devices to monitor and balance the water pollutants and contaminants. It becomes useful for the environmental ecosystem, human health and industrial developments. One of the major steps toward controlling water quality is to develop optical fiber based sensor to monitor harsh environmental conditions. Several commercial sensors are available in the market to rapidly detect oil and chemicals present in water. These sensors are based on different technologies such as colorimetry, laser-induced UV fluorescence, focused ultrasonic acoustics or optical fiber sensors. However, these sensors can be used only in laboratory of a fixed place and they bear several limitations in field applications [347]. There are few commercial devices based on optical fiber technology are developed with good characteristics and variety of fields of application, especially its capability to work in difficult environments with water, electricity or extreme temperatures [348]. MacLean et al. [349] described a fiber optic sensor capable of distributed detection of multiple hydrocarbon fuel and solvent spills. The sensor incorporated liquid-swelling polymers that convert the swelling into a micro-bend force on an optical fiber. The device provided the potential of locating target hydrocarbon fuel and solvent spills at many separate positions along the sensor length. The sensor response time after exposure to the fuel is 30 s. Another OF technique is reported to detect some specific pollutants e.g. Zn, Cu, cyclohexane and xylene in a very low concentration [350,351]. These type of optical fiber chemical sensors are coated with an organic cladding, which changes its refractive index (RI) after adsorption of hydrocarbon [352,353]. Kuramitz et al. [354] presented a novel fiber optic sensor for real-time sensing of silica scale formation in geothermal power plants. Silica formation called silicate scaling has been observed in almost all water-based systems such that creates a costly problem. The sensor is fabricated by removing the cladding of a multimode fiber to expose the core to detectthe scale-formation-induced refractive index change. This sensor is a promising tool not only for geothermal and petroleum fields but also in cold water systems.

Another type of tapered optical fiber sensor has been widely employed during the last decades for the sensing of pollutants [355,356]. In this detection method, the intensity variations produced by an index change of the taper surroundings is measured with a single diode detector or a power meter. The three different types of tapered optical fiber sensors, all of them made with standard SMF-28 optical fibers, were employed to detect the presence of large spills of hydrocarbons in sea water [341]. Three different types of optical fiber tapers have been made using the well-known technique of travelling-burner. Fig. 24 shows a scheme of the different parts of a tapered optical fiber sensor.

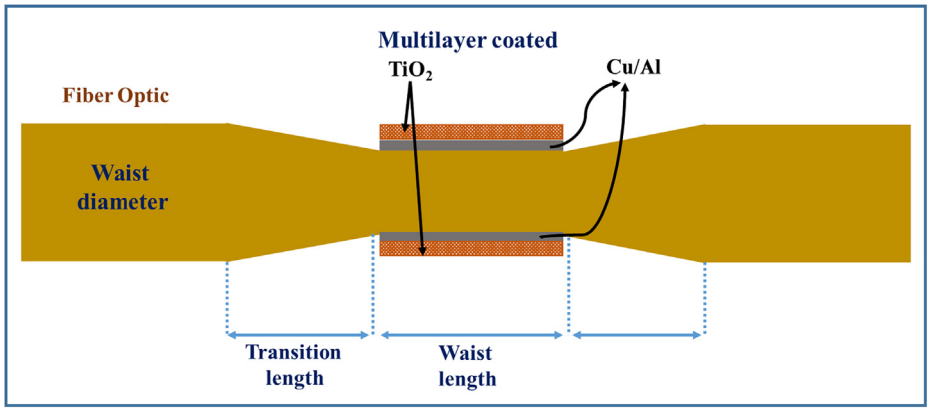

Fig. 24. Scheme of an optical fiber taper [357].

Irigoyen et al. [357] employed the three tapered silica optical fibers, uncoated and coated with metallic (Al or Cu) and dielectric layers (TiO_2), to determine the presence of oil, hazardous and noxious substances in water, by means of the measurement of their spectral transmittance. Using the three tapers, it is possible to detect all the substances lying in range of refractive indices from 1.329 to 1.501. It is reported that a 5% concentration by volume was enough for detection, except for products with high solubility in water that need higher concentrations. Kim et al. [358] reported a remote photocatalysis system using modified plastic optical fiber fabrics. They successfully deposited TiO_2 onto a modified plastic optical fiber fabric using the dip-coating method. The TiO_2 coated woven plastic optical fiber fabric was applied to the photocatalytic degradation of methylene blue (MB) and the simultaneous oxidation of 4-chlorophenol (4-CP) and reduction of Cr (VI) present in polluted water. They reported that plastic optical fiber fabrics together with photocatalysts were suitable for remote (in situ) advanced oxidation process useful for the remediation of contaminated soil or groundwater. The heavy metal pollution (for example, Pb, Cu, As, Zn, Cd) in natural water environment is another major problem for both human health and ecosystem. Many techniques have been developed to detect heavy metal pollution in natural water quantitatively. However, all current systems available in the market for detecting heavy metal ions have common drawbacks such as bulky size, expensive set-up and costly maintenance. An optical microfiber sensors functionalized with chelating agents have investigated to detect low concentrations of specific heavy metal ions in water samples [359]. The chelating agents such as EDTA and DPA successfully coated onto the microfiber surface, which had a very thin diameter of only 3.9 μm. The sensitivity or detection limit for all types of metal ions tested in the experiments was below 10 ppb.

5.4.4. Soil pollution monitoring

García et al. [360] proposed an optical fiber sensor to monitor the presence of volatile organic compounds (VOCs) in soil. The sensor consists of a single mode fiber 1 cm long, coated with a composite of prussian blue and an acrylic polymeric emulsion, inserted between two multimode fibers. The sensor's working mechanism is based on attenuation changes of the optical fiber evanescent wave. The hetero core fibers are fabricated by joining standard telecommunications fibers of different core sizes, by inserting a small section (in mm) of single mode fiber (SMF) between two sections of multimode fiber (MMF) [361–363] (Fig. 25).

The developed sensor was used for detection of VOCs such as acetone, isopropyl alcohol and chloroform. This sensor was used to monitor VOCs gases during the treatments to remove hydrocarbons (HC) in polluted soil by electrokinetic treatment (EKT). This is a promising technique, which uses electrokinetic transport mechanisms (electroosmosis, electrophoresis, and electromigration) under an applied DC electric field between two electrodes inserted into the polluted soil [364,365]. This process can remove pollutants, both inorganic and organic, from the solid matrix, even from soils with low hydraulic conductivity such as clays [366,367].

5.4.5. Moisture sensor

The measurement of environmental moisture and relative humidity (RH) becomes great need in various industries such as food process and storage, agriculture, pharmaceutical, biomedical, chemical, SHM, ecological, and atmospheric weather conditions monitoring, etc. Alwis et al. [368] reported in their review that fiber-optic techniques play important role for the measurement of humidity/moisture and the calibration of humidity/moisture for sensing applications. They highlighted that the use of fiber-optics in different areas such as structural health monitoring (SHM); food processing and storage, medicine, ecology, agriculture, mineral processing, fuel quality control, aerospace and human comfort. The fiber optics humidity sensor like fibre grating sensors, evanescent wave sensors, interferometric sensors and hybrid sensors (fiber gratings + interferometric) were used.

The use of an optical fiber LPG as a soil moisture sensor was also reported [369]. The device revealed sensitivity to moisture levels in the range of 10–50% in both clay and sandy soils. Woyessa et al. [370] reported a polycarbonate (PC) microstructured polymer optical fiber (mPOF) bragg grating (FBG) humidity sensor that can operate beyond 100 °C. The fiber loss was reduced by a factor of two compared to the latest reported PC mPOF, holding the low loss record in polycarbonate (PC) based fibers. A relative humidity (RH) sensitivity of 7.31 ± 0.13 pm/% RH in the range 10–90% RH at 100 °C along with a temperature sensitivity of 25.86 ± 0.63 pm/°C in the range 20–100 °C at 90% RH were measured. The measurements of the rate of corrosion in concrete sewers need to take into consideration the humidity in the environment and thus, its accurate measurement becomes critically important. Alwis et al. [371] introduced a novel tailored fiber bragg grating (FBG)-based humidity sensors to examine their durability, time response and stability when used in measurements over an extended period of time under the aggressive gaseous environment of a gravity sewer, experienced high levels of both humidity and hydrogen sulfide gas. Hernandez et al. [372] described an optical fiber sensor for simultaneous temperature and humidity measurements. The sensor consists of one fiber bragg grating (FBG) to measure temperature and a mesoporous film of bilayers of poly(allylamine hydrochloride)(PAH) and silica (SiO_2) nanoparticles deposited onto the tip of the same fiber to measure humidity. The temperature sensitivity of the FBG was 10 pm/°C while the sensitivity to humidity was (-1.4×10^{-12} W/% RH) using 23 bilayers. This developed sensor was useful in the mechanical ventilator and temperature. The humidity of the delivered artificial air can also be measured by this sensor.

Liu et al. [373] proposed an optical fibre fabry–perot interferometer

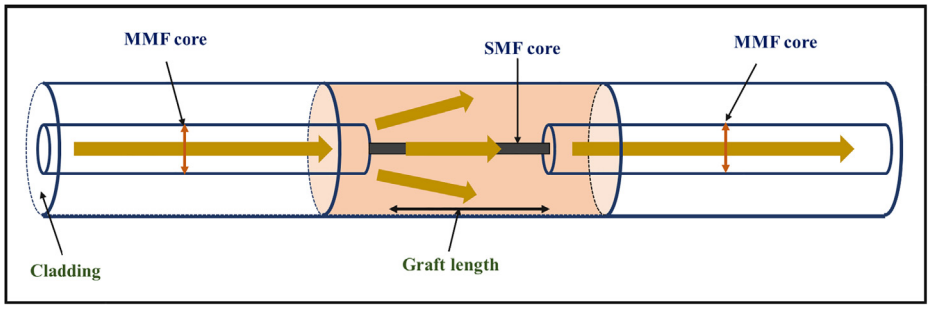

Fig. 25. Diagram of a heterocore optical fiber [360].

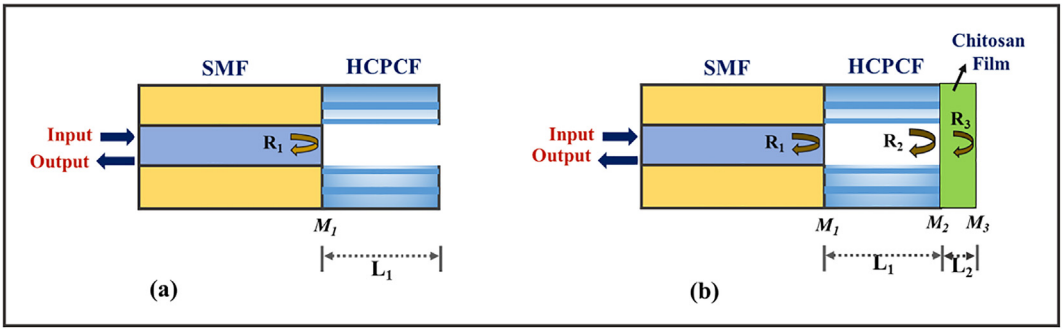

Fig. 26. Structures of the proposed sensor (a) before coating film; (b) coated with chitosan film [373].

(FPI) sensor for RH measurement. The FPI was formed by splicing a short section of hollow-core photonic crystal fibre (HCPCF) to single mode fibre and covering a chitosan film at the end of HCPCF (Fig. 26).

The refractive index of chitosan and film thickness will change with ambient RH, leading to the change in the reflected interference spectrum of FPI. This sensor showed a nonlinear response to RH values from 35 to 95%RH. The interference fringe shifted to shorter wavelength as RH increases with a maximum sensitivity of 0.28 nm/%RH at high RH level. The fringe contrast also decreases as RH increases with an available maximum sensitivity of 0.5 dB/%RH. The sensor showed good stability and fast response time less than 1 min. Thomas et al. [374] developed a 64 m long distributed relative humidity sensor with excellant spatial resolution. The distributed sensor was strongly humidity sensitive if polyimide coated fiber was used and weakly sensitive when acrylate coating was used. The polyimide coated fiber based sensor showed a near linear response across the entire range of relative humidity tested covering 15–92%, with a sensitivity ~1.3 με/%RH and showing low hysteresis. The sensor was able to resolve relative humidity changes ~0.1%. The response time of the sensor was found to be strongly dependent on temperature in the range tested, covering 30–50 °C. In another example, Açıkgöz et al. reported the usage of fiber optics as humidity sensor in range from 10 to 95% relative humidity [375]. The cladding part is scratched and coated with polyethylene glycol. This coating swells under various levels of humidity such that the refractive indice changes upon swelling. In situ measurement of the refractive index hints about the relative level of humidity.

6. Conclusion

Chemically-modified optical fibers have added several advantageous features in existing active and passive OF based technology. Various methods are used for chemical modifications of OFs to improve energy conservation, refractive index, mechanical, and transfer properties. The applications of these OFs in different applications such sensors, biosensor, biomedical technology and environmental monitoring are described on the basis of available literature. Although this field of research is relatively recent, but becomes promising for new areas in the near future investigations. In particular, the exploitation of the chemically modified OFs provide various sensors with the ultimate detection limit along with improvement in other related technologies such as biomedical technology and environmental monitoring systems.

References

[1] L.A. Ketron, Fiber optics: the ultimate communications media, Am. Ceram. Soc. Bull. 66 (11) (1987) 1571–1578.
[2] T. Nakahara, M. Hoshikawa, S. Tanaka, H. Yokota, Fiber optics, Ullmann's Encyclopedia of Industrial Chemistry, (Ed.). 2000.
[3] L. Alwis, T. Sun, K.T.V. Grattan, Developments in optical fiber sensors for industrial applications, Opt. Laser Technol. 78 (2016) 62–66.
[4] R. Jenny, S. Kittelberger, A.G. Volpi, N.Y. Auburn, Fundamentals of optics–an introduction for beginners, J. Comp. Vision 40 (2) (2000) 142–167.
[5] H.H. Hopkins, N.S. Kapany, A flexible fibrescope, using static scanning, Nature 173 (1954) 39–41.
[6] S.-F. Cheng, L.-K. Chau, Colloidal gold-modified optical fiber for chemical and biochemical sensing, Anal. Chem. 75 (2003) 16–21.
[7] S. Rizzolo, J. Périsse, A. Boukenter, Y. Ouerdane, E. Marin, J.-R. Macé, M. Cannas, S. Girard, Real time monitoring of water leveland temperature in storage fuel pools through optical fibre sensors, Sci. Rep. 7 (2017) 8766.
[8] Y. Luo, B. Yan, Q. Zhang, G.-D. Peng, J. Wen, J. Zhang, Fabrication of Polymer Optical Fibre (POF) Gratings, Sensors 17 (2017) 511.
[9] J. Zubia, J. Arrue, Plastic optical fibers: An introduction to their technological processes and applications, Opt. Fiber Technol. 7 (2001) 101–140.
[10] J.S. Sanghera, I.D. Aggarwal, Active and passive chalcogenide glass optical fibers for IR applications: a review, J. Non-Crystal. Solids 256 & 257 (1999) 6–16.
[11] K. Nielsen, H.K. Rasmussen, A.J.L. Adam, P.C.M. Planken, O. Bang, P.U. Jepsen, Bendable, low-loss topas fibers for the terahertz frequency range, Opt. Express 17 (10) (2009) 8592–8601.
[12] G. Khanarian, H. Celanese, Optical properties of cyclic olefin copolymers, Opt. Eng. 40 (6) (2001) 1024–1029.
[13] S. Iftekhar, J. Grins, M. Eden, Composition-property relationships of the La_2O_3-Al_2O_3-SiO_2 glass system, J. Non-Cryst. Solids 356 (2010) 1043–1048.
[14] M. Rajesh, V.P.N. Nampoori, Fabrication and characterisation of polymer optical fibers for smart sensing and optical amplification, Doctoral dissertation Cochin University of Science & Technology, 2006.
[15] D.J. Webb, Fibre Bragg grating sensors in polymer optica fibres, Meas. Sci. Technol. 26 (2015) 092004.
[16] H.Y. Liu, H.B. Liu, G.D. Peng, P.L. Chu, Observation of type I and type II gratings behavior in polymer optical fiber, Opt. Commun. 220 (2003) 337–343.
[17] P. Stajanca, I. Topolniak, S. Pötschke, K. Krebber, Solution-mediated cladding doping of commercial polymer optical fibers, Opt. Fiber Technol. 41 (2018) 227–234.
[18] Y. Luo, Q. Zhang, H. Liu, G. Peng, Grating fabrication in benzildimethylketal doped photosensitive polymer fibers using 355 nm nanosecond pulsed laser, Opt.

Lett. 35 (2010) 751–753.
[19] T. Wang, Q. Wang, Y. Luo, W. Qiu, G.D. Peng, B. Zhu, Z. Hu, G. Zou, Q. Zhang, Enhancing photosensitivity in near UV/vis band by doping 9-vinylanthracene in polymer optical fiber, Opt. Commun. 307 (2013) 5–8.
[20] D.R. Tyler, Mechanistic aspects of the effects of stress on the rates of photochemical degradation reactions in polymers, Polym. Rev. 44 (2015) 351–388.
[21] X. Hu, C.F.J. Pun, H.Y. Tam, P. Mégret, C. Caucheteur, Highly reflective bragg gratings in slightly etched step-index polymer optical fiber, Opt. Express 22 (2014) 18807–18817.
[22] K. Bhowmik, G.D. Peng, Y. Luo, E. Ambikairajah, V. Lovric, W.R. Walsh, G. Rajan, Etching process related changes and effects on solid-core single-mode polymer optical fibre, IEEE Photonics J. 8 (2016) 2500109.
[23] W. Blanc, B. Dussardier, Formation and applications of nanoparticles in silicaoptical fibers, J. Opt. 45 (3) (2016) 247–254.
[24] B. Faure, W. Blanc, B. Dussardier, G. Monnom, Improvement of the Tm^{3+}:$^3H_4$ level lifetime in silica optical fibers by lowering the local phonon energy, J. Non-Cryst. Solids 353 (29) (2007) 2767–2773.
[25] S. Girard, J. Kuhnhenn, A. Gusarov, B. Brichard, M.V. Uffelen, Y. Ouerdane, A. Boukenter, C. Marcandella, Radiation effects on silica-based optical fibers: recent advances and future challenges, IEEE Trans. Nucl. Sci. 60 (2013) 2015–2036.
[26] C. Schultz, Preparation of very low-loss optical waveguides, Am. Ceram. Soc. Bull. 52 (1973) 383.
[27] J.B. MacChesney, Preparation of low loss optical fibers using simultaneous vapor phase deposition and fusion, Proc. Int. Congress on Glass 6 (1974) 40–45.
[28] D.N. Payne, W.A. Gambling, New silica-based low-loss optical fibre, Electron. Lett. 10 (1974) 289–290.
[29] J.A. Arnaud, W. Mommel, Dispersion in optical fibres with stairlike refractive-index profiles, Electron. Lett. 12 (1976) 6–8.
[30] S.K. Shukla, G.K. Parashar, A.P. Mishra, P. Mishra, B.C. Yadav, R.K. Shukla, L.M. Bali, G.C. Dubey, Nano-like magnesium oxide films and its significance in optical fiber humidity sensor, Sens. Actuators B Chem. 98 (2004) 5–11.
[31] S.K. Shukla, G.K. Ashutosh Tiwari, A.P. Parashar, G.C. Dubey Mishra, Exploring fiber optic approach to sense humid environment over nano-crystalline zinc oxide film, Talanta 80 (2009) 565–571.
[32] M. Sedlar, L. Pust, Preparation of cobalt doped nickel ferrite thin films on optical fibers by dip-coating technique, Ceram. Int. 21 (1) (1995) 21–27.
[33] E. Boyacı, N. Horzum, A. Çağır, M.M. Demir, A.E. Eroğlu, Electrospun amino-functionalized PDMS as a novel SPME sorbent for the speciation of inorganic and organometallic arsenic species, RSC Adv. 3 (2013) 22261.
[34] R.K. Poduval, S. Noimark, R.J. Colchester, T.J. Macdonald, I.P. Parkin, A.E. Desjardins, I. Papakonstantinou, Optical fiber ultrasound transmitter with electrospun carbon nanotube-polymer composite, Appl. Phys. Lett. 110 (2017) 223701.
[35] J. Kirchhof, S. Unger, Thermodynamics of fluorine incorporation into silica glass, J Non-Crystal. Solids 354 (2008) 540–545.
[36] S. Yoo, U.C. Paek, W.T. Han, Development of a glass optical fiber containing ZnO–Al_2O_3–SiO_2 glass-ceramics doped with Co^{2+} and its optical absorption characteristics, J. Non-Cryst. Solids 315 (2003) 180–186.
[37] J.E. Townsend, S.B. Poole, D.N. Payne, Solution-doping technique for fabrication of rare earth doped optical fibres, Electron. Lett. 23 (1987) 329–331.
[38] P. Barua, E.H. Sekiya, K. Saito, A.J. Ikushima, Influences of Yb^{3+} ion concentration on the spectroscopic properties of silica glass, J. Non-Cryst. Solids 354 (2008) 4760–4764.
[39] A.S. Webb, A.J. Boyland, R.J. Standish, S. Yoo, J.K. Sahu, D.N. Payne, MCVD in-situ solution doping process for the fabrication of complex design large core rare-earth doped fibers, J. Non-Cryst. Solids 356 (2010) 848–851.
[40] A.J. Boyland, A.S. Webb, M.P. Kalita, S. Yoo, C.A. Codemard, R.J. Standish, J. Nilsson, J.K. Sahu, Rare-earth doped optical fiber fabrication using novel gas phase deposition technique, Optical Society of America, 2010.
[41] W. Blanc, V. Mauroy, L. Nguyen, B.N.S. Bhaktha, P. Sebbah, B.P. Pal, B. Dussardier, Fabrication of rare earth-doped transparent glass ceramic optical fibers by modified chemical vapor deposition, J. Am. Ceram. Soc. 94 (2010) 2315–2318.
[42] M.C. Paul, S. Bysakh, S. Das, M. Pal, S.K. Bhadra, S. Yoo, A.J. Boyland, J.K. Sahu, Nano-engineered Yb_2O_3 doped optical fiber: fabrication, material characterizations, spectroscopic properties and lasing characteristics: a review, Sci. Adv. Mater. 4 (2012) 292–321.
[43] A. Pastouret, C. Gonnet, C. Collet, O. Cavani, E. Burov, C. Chaneac, A. Carton, J.P. Jolivet, Nanoparticle doping process for improved fibre amplifiers and lasers, Proc. SPIE 7195 (2009) 71951X.
[44] C. Pedrido, (inventor) Dätwyler Fiber Optics SA, Optical fiber and its preform as well as method and apparatus for fabricating them, Patent Nr. WO /102947 (2005) A1.
[45] A. Langner, M. Such, G. Schötz, V. Reichel, S. Grimm, F. Just, M. Leich, J. Kirchhof, B. Wedel, G. Köhler, et al., Development, manufacturing and lasing behavior of Yb-doped ultra large mode area fibers based on Yb-doped fused bulk silica, Proc. SPIE 7580 (2010) 75802X.
[46] M. Leich, F. Just, A. Langner, M. Such, G. Schötz, T. Eschrich, S. Grimm, Highly efficient Yb-doped silica fibers prepared by powder sinter technology, Opt. Lett. 36 (2011) 1557–1559.
[47] K. Schuster, S. Unger, C. Aichele, F. Lindner, S. Grimm, D. Litzkendorf, J. Kobelke, J. Bierlich, K. Wondraczek, H. Bartelt, Material and technology trends in fiber optics, Adv. Opt. Technol. 3 (2014) 447–468.
[48] N.M.J. Hyatt, D.E. Day, Glass Properties in the Yttria-Alumina-Silica System, J. Am. Ceram. Soc. 70 (1987) 283–287.
[49] J.E. Shelby, Alkali and alkaline earth galliosilicate, Key Eng. Mater. 94–95 (1994) 279–316.
[50] M.J. Dejneka, B.Z. Hanson, S.G. Crigler, L.A. Zenteno, J.D. Minelly, La_2O_3-Al_2O_3-SiO_2 glasses for high-power, Yb^{3+}-doped, 980-nm fiber lasers, J. Am. Ceram. Soc. 85 (2002) 1100–1106.
[51] D. Litzkendorf, S. Grimm, K. Schuster, J. Kobelke, A. Schwuchow, Study of lanthanum aluminum silicate glasses for passive and active optical fibers, Int. J. Appl. Glass Sci. 3 (2012) 321–331.
[52] S. Kuhn, A. Herrmann, J. Hein, M.C. Kaluza, C. Russel, Sm^{3+}-doped La_2O_3–Al_2O_3–SiO_2-glasses: structure, fluorescence and thermal expansion, J. Mater. Sci. 48 (2013) 8014–8022.
[53] R.E. Jaeger, J.B. MacChesney, T.J. Miller, The preparation of optical waveguide preforms by plasma deposition, Bell Syst. Tech. J. 57 (1) (1978) 205–210.
[54] P. Geittner, D. Koppers, H. Lydtin, Low-loss optical fibers prepared by plasma-activated chemical vapor deposition (CVD), Appl. Phys. Lett. 28 (1976) 645–646.
[55] E.M. Dianov, K.M. Golant, V.I. Karpov, R.R. Khrapko, A.S. Kurkov, V.N. Protopopov, S.L. Semenov, A.G. Shebuniaev, Application of reduced-pressure plasma CVD technology to the fabrication of Er-doped optical fiber, Opt. Mater. 3 (1994) 181–185.
[56] I.A. Bufetov, K.M. Golant, S.V. Firstov, A.V. Kholodkov, A.V. Shubin, E.M. Dianov, Bismuth activated alumosilicate optical fibers fabricated by surface-plasma chemical vapor deposition technology, Appl. Opt. 47 (2008) 4940–4944.
[57] E.A. Savelev, K.M. Golant, Influence of fusing on the uniformity of the distribution of Yb3+ ions and the formation of clusters in silica with phosphorus admixture synthesized by SPCVD, Opt. Mater. Express 5 (2015) 2337–2346.
[58] I.P. Johnson, D.J. Webb, K. Kalli, Utilisation of thermal annealing to record multiplexed fig sensors in multimode microstructured polymer optical fibre, in: W. J. Bock, J. Albert, X. Bao (Eds.), 21st international conference on optical fiber sensors (OFS21), Proc. SPIE, 7753 (2011) 7327–7753.
[59] W. Yuan, A. Stefani, M. Bache, T. Jacobsen, B. Rose, N. Herholdt-Rasmussen, F.K. Nielsen, S. Andresen, O.B. Sorensen, K.S. Hansen, O. Bang, Improved thermal and strain performance of annealed polymer optical fiber bragg gratings, Opt. Commun. 284 (2011) 176–182.
[60] G. Woyessa, K. Nielsen, A. Stefani, C. Markos, O. Bang, Temperature insensitive hysteresis free highly sensitive polymer optical fiber bragg grating humidity sensor, Opt. Express 24 (2016) 1206–1213.
[61] J. Villatoro, O. Arrizabalaga, G. Durana, I.S.D. Ocáriz, E.A. Lopez, J. Zubia, A. Schülzgen, R.A. Correa, Accurate strain sensing based on super-mode interference in strongly coupled multi-core optical fibres, Sci. Rep. 7 (2017) 4451.
[62] A. Nadort, J. Zhao, E.M. Goldys, Lanthanide upconversion luminescence at the nanoscale: Fundamentals and optical properties, Nanoscale 8 (2016) 13099–13130.
[63] M.J. Dejneka, Transparent oxy-fluoride glass ceramics, MRS Bull. 23 (1998) 57–62.
[64] A. Herrmann, M. Tylkowski, C. Bocker, C. Rüssel, Cubic and hexagonal $NaGdF_4$ crystals precipitated from an aluminosilicate glass: preparation and luminescence properties, Chem. Mater. 25 (2013) 2878–2884.
[65] S. Xiaoying, C. Ping, C. Wenjing, Z. Kan, M. Jing, F. Donghai, Z. Shian, S. Zhenrong, Q. Jianrong, J. Tianqing, Fine tunable red-green upconversion luminescence from glass ceramic containing 5% Er^{3+}:$NaYF_4$ nanocrystals under excitation of two near infrared femtosecond lasers, J. Appl. Phys. 116 (2014) 063101.
[66] M. Mattarelli, G. Gasperi, M. Montagna, P. Verrocchio, Transparency and long-ranged fluctuations: the case of glass ceramics, Phys. Rev. B 82 (2010) 094204.
[67] Y. Ledemi, A.A. Trudel, V.A.G. Rivera, S. Chenu, E. Veron, L.A. Nunes, M. Allix, Y. Messaddeq, White light and multicolor emission tuning in triply doped Yb^{3+}/Tm^{3+}/Er^{3+} novel fluoro-phosphate transparent glass-ceramics, J. Mater. Chem. C 2 (2014) 5046–5056.
[68] D. Chen, Y. Wang, Y. Yu, P. Huang, F. Weng, Near-infrared quantum cutting in transparent nanostructured glass ceramics, Opt. Lett. 33 (2008) 1884–1886.
[69] C. Liu, J. Heo, Lead chalcogenide quantum dot-doped glasses for photonic devices, Int. J. Appl. Glass Sci. 4 (2013) 163–173.
[70] J. Zhao, Z. Lu, Y. Yin, C. McRae, J.A. Piper, J.M. Dawes, D. Jin, E.M. Goldys, Upconversion luminescence with tunable lifetime in $NaYF_4$:Yb Er nanocrystals: role of nanocrystal size, Nanoscale 5 (2013) 944–952.
[71] D.J. Gargas, E.M. Chan, A.D. Ostrowski, S. Aloni, M.V.P. Altoe, E.S. Barnard, B. Sanii, J.J. Urban, D.J. Milliron, B.E. Cohen, P.J. Schuck, Engineering bright sub-10-nm up converting nanocrystals for single-molecule imaging, Nat. Nanotechnol. 9 (2014) 300–305.
[72] D. Liu, X. Xu, Y. Du, X. Qin, Y. Zhang, C. Ma, S. Wen, W. Ren, E.M. Goldys, J.A. Piper, Three-dimensional controlled growth of monodisperse sub-50 nm heterogeneous nanocrystals, Nat. Commun. 7 (2016) 10254.
[73] A.M. Edmonds, M.A. Sobhan, V.K.A. Vasan, E.E.A. Grebenik, J.R. Rabeau, E.M. Goldys, A.V. Zvyagin, Nano-ruby, a promising fluorescent probe for background-free cellular imaging, Part. Part. Syst. Charact. 30 (2013) 506–513.
[74] P. Reineck, B.C. Gibson, Near-infrared fluorescent nanomaterials for bioimaging and sensing, Adv. Opt. Mater. 5 (2016) 1600446.
[75] P. Reineck, A. Francis, A. Orth, D.W.M. Lau, R.D.V. Nixon-Luke, I.D. Rastog, W.A.W. Razali, N.M. Cordina, L.M. Parker, V.K.A. Sreenivasan, brightness and photostability of emerging red and near-ir fluorescent nanomaterials for bioimaging, Adv. Opt. Mater. 4 (2016) 1549–1557.
[76] M.R. Henderson, B.C. Gibson, H.E. Heidepriem, K. Kuan, V.S. Afshar, J.O. Orwa, I. Aharonovich, S.T. Hanic, A.D. Greentree, S. Prawer, Diamond in tellurite glass: a new medium for quantum information, Adv. Mater. 23 (2011) 2806–2810.
[77] H.E. Heidepriem, Y. Ruan, H. Ji, A.D. Greentree, B.C. Gibson, T.M. Monro, Nanodiamond in tellurite glass part I: origin of loss in nanodiamond-doped glass, Opt. Mater. Express 4 (2014) 2608–2620.

[78] Y. Ruan, H. Ji, B.C. Johnson, T. Ohshima, A.D. Greentree, B.C. Gibson, T.M. Monro, H.E. Heidepriem, Nanodiamond in tellurite glass part II: practical nanodiamond-doped fibers, Opt. Mater. Express 5 (2015) 73–87.
[79] J. Zhao, X. Zheng, E.P. Schartner, P. Ionescu, R. Zhang, T.L. Nguyen, D. Jin, H.E. Heidepriem, Up-conversion nanocrystals doped glass: a new paradigm for photonic materials, Adv. Opt. Mater. 4 (2016) 1507–1517.
[80] K. Shimamura, S. Uda, T. Yamada, S. Sakaguchi, T. Fukuda, Silicon single crystal fiber growth by micro pulling down method, Jpn. J. Appl. Phys. 35 (1996) 793–795.
[81] P. Sazio, A.A. Correa, C. Finlayson, J. Hayes, T. Scheidemantel, N. Baril, B. Jackson, D. Won, F. Zhang, E. Margine, Microstructured optical fibers as high-pressure microfluidic reactors, Science 311 (2006) 1583–1586.
[82] J. Ballato, T. Hawkins, P. Foy, R. Stolen, B. Kokuoz, M. Ellison, C. McMillen, J. Reppert, A. Rao, M. Daw, Silicon optical fiber, Opt. Express 16 (2008) 18675–18683.
[83] B. Scott, W. Ke, G. Pickrell, Fabrication of n-type silicon optical fibers, Photon Technol. Lett. 21 (2009) 1798–1800.
[84] J. Ballato, T. Hawkins, P. Foy, S. Morris, N. Hon, B. Jalali, R. Rice, Silica-clad crystalline germanium core optical fiber, Opt. Lett. 36 (2011) 687–688.
[85] D. Deng, N. Orf, S. Danto, A. Abouraddy, J. Joannopoulos, Y. Fink, Processing and properties of centimeter-long, in-fiber, crystalline-selenium filaments, Appl. Phys. Lett. 96 (2010) 023102.
[86] G. Tang, Q. Qian, X. Wen, G. Zhou, X. Chen, M. Sun, D. Chen, Z. Yang, Phosphate glass-clad tellurium semiconductor core optical fibers, J. Alloys Compd. 633 (2015) 1–4.
[87] D. Coucheron, M. Fokine, N. Patel, D. Breiby, O. Tore Buset, T. Hawkins, M. Jones, J. Ballato, U. Gibson, Laser inscription of compositional microstructures in crystalline SiGe-core fibres, Nat. Commun. 7 (2016) 13265.
[88] G. Tang, Q. Qian, X. Wen, X. Chen, W. Liu, M. Sun, Z. Yang, Reactive molten core fabrication of glass-clad Se0.8Te0.2 semiconductor core optical fibers, Opt. Express 23 (2015) 624–633.
[89] J. Ballato, T. Hawkins, P. Foy, C. McMillen, L. Burka, J. Reppert, R. Podila, A. Rao, R. Rice, Binary III-V semiconductor core optical fiber, Opt. Express 18 (2010) 4972–4979.
[90] J. Sparks, R. He, N. Healy, M. Krishnamurthi, A. Peacock, P. Sazio, V. Gopalan, J. Badding, Zinc selenide optical fibers, Adv. Mater. 23 (2011) 1647–1651.
[91] J.P. Zimmer, S.W. Kim, S. Ohnishi, E. Tanaka, J.V. Frangioni, M.G. Bawendi, Size series of small indium arsenide− zinc selenide core− shell nanocrystals and their application to in vivo imaging, J. Am. Chem. Soc. 128 (2006) 2526–2527.
[92] C. Hou, X. Jia, L. Wei, A. Stolyarov, O. Shapira, J. Joannopoulos, Y. Fink, Direct atomic-level observation and chemical analysis of ZnSe synthesized by in situ high-throughput reactive fiber drawing, Nano Letters 13 (2013) 975–979.
[93] N.D. Orf, O. Shapira, F. Sorin, S. Danto, M.A. Baldo, J.D. Joannopoulos, Y. Fink, Fiber draw synthesis, Proc. Natl. Acad. Sci. USA 108 (2011) 4743–4747.
[94] C. Hou, X. Jia, L. Wei, S. Tan, X. Zhao, J. Joannopoulos, Y. Fink, Crystalline silicon core fibres from aluminium core preforms, Nat. Commun. 6 (2015) 6248.
[95] S. Morris, T. Hawkins, P. Foy, J. Hudson, L. Zhu, R. Stolen, J. Ballato, On loss in silicon core optical fibers, Opt. Mater. Express. 2 (2012) 1511–1519.
[96] S. Morris, C. McMillen, T. Hawkins, P. Foy, R. Stolen, R. Rice, J. Ballato, The influence of core geometry on the crystallography of silicon optical fiber, J. Cryst. Growth. 352 (2012) 53–58.
[97] C. McMillen, G. Brambilla, S. Morris, T. Hawkins, P. Foy, N. Broderick, R. Rice, J. Ballato, On crystallographic orientation in crystal core optical fibers II: effects of tapering, Opt. Mater. 35 (2012) 93–96.
[98] N. Healy, S. Mailis, N. Bulgakova, P. Sazio, T. Day, J. Sparks, H. Cheng, J. Badding, A. Peacock, Extreme electronic band gap modification in laser-crystallized silicon optical fibres, Nat. Mater. 13 (2014) 1122–1127.
[99] D. Coucheron, M. Fokine, N. Patil, D. Breiby, O. Buset, N. Healy, A. Peacock, T. Hawkins, M. Jones, J. Ballato, CO_2 Laser-induced directional recrystallization to produce single crystal silicon-core optical fibers with low loss, Adv. Opt. Mater. 4 (2016) 1004–1008.
[100] A. Gumennik, L. Wei, G. Lestoquoy, A. Stolyarov, P. Rekemeyer, M. Smith, X. Liang, B. Grena, S. Johnson, Silicon-in-silica spheres via axial thermal gradient in-fibre capillary instabilities, Nat. Commun. 4 (2013) 2216–2220.
[101] C. Lin, J. Chen, L. Wang, High-Q Si microsphere resonators fabricated from Si-cored fibers for WGMs excitation, IEEE Photonics Technol. Lett. 27 (2015) 1355–1358.
[102] N. Vukovic, N. Healy, F. Suhailin, P. Mehta, T. Day, J. Badding, A. Peacock, Ultrafast optical control using the Kerr nonlinearity in hydrogenated amorphous silicon microcylindrical resonators, Sci. Rep. 3 (2013) 2885.
[103] F. Suhailin, N. Healy, Y. Franz, M. Sumetsky, J. Ballato, A. Dibbs, U. Gibson, A. Peacock, Kerr nonlinear switching in a hybrid silica-silicon microspherical resonator, Opt. Express 23 (2015) 17263–17268.
[104] R. He, T. Day, M. Krishnamurthi, J. Sparks, P. Sazio, V. Gopalan, J. Badding, Silicon p-i-n junction fibers, Adv. Mater. 25 (2013) 1461–1467.
[105] D. Homa, A. Cito, G. Pickrell, C. Hill, B. Scott, Silicon fiber with p-n junction, Appl. Phys. Lett. 105 (2014) 122110.
[106] F. Martinsen, B. Smeltzer, M. Nord, T. Hawkins, J. Ballato, U. Gibson, Silicon-core glass fibres as microwire radial-junction solar cells, Sci. Rep. 4 (2014) 6283.
[107] F. Martinsen, B. Smeltzer, J. Ballato, T. Hawkins, M. Jones, U. Gibson, Light trapping in horizontally aligned silicon microwire solar cells, Opt. Express 23 (2015) 1463–1471.
[108] J.A. Savage, Optical properties of chalcogenide glasses, J. Non-Cryst. Solids 47 (1982) 101–116.
[109] G. Snopatin, V. Shiryaev, V. Plotnichenko, E. Dianov, M. Churbanov, High-purity chalcogenide glasses for fiber optics, Inorg. Mater. 25 (2009) 1439–1460.
[110] M.F. Churbanov, High-purity chalcogenide glasses as materials for fiber optics, J. Non Cryst. Solids 184 (1995) 25–29.
[111] M.F. Churbanov, V.S. Shiryaev, I.V. Scripachev, G.E. Snopatin, V.V. Gerasimenko, S.V. Smetanin, I.E. Fadin, V.G. Plotnichenko, Optical fibers based on As-S-Se glass system, J. Non-Cryst. Solids 284 (2001) 146–152.
[112] W.H. Kim, V.Q. Nguyen, L.B. Shaw, L.E. Busse, C. Florea, D.J. Gibson, R.R. Gattass, S.S. Bayya, F.H. Kung, G.D. Chin, Recent progress in chalcogenide fiber technology at NRL, J. Non-Cryst. Solids 431 (2016) 8–15.
[113] F. Chenard, O. Alvarez, H. Moawad, MIR chalcogenide fiber and devices: In proceedings of the SPIE BiOS, International society for optics and photonics, San Francisco, CA, USA, 2015, p. 93170.
[114] J. Troles, Y. Niu, C. Duverger-Arfuso, F. Smektala, L. Brilland, V. Nazabal, V. Moizan, F. Desevedavy, P. Houizot, Synthesis and characterization of chalcogenide glasses from the system Ga-Ge-Sb-S and preparation of a single-mode fiber at 1.55 μm, Mater. Res. Bull. 43 (2008) 976–982.
[115] C. Conseil, Q. Coulombier, C. Boussard-Pledel, J. Troles, L. Brilland, G. Renversez, D. Mechin, B. Bureau, J.L. Adam, J. Lucas, Chalcogenide step index and microstructured single mode fibers, J. Non-Cryst. Solids 357 (2011) 2480–2483.
[116] S.D. Savage, C.A. Miller, D. Furniss, A.B. Seddon, Extrusion of chalcogenide glass preforms and drawing to multimode optical fibers, J. Non-Cryst. Solids 354 (2008) 3418–3427.
[117] T.A. Birks, J.C. Knight, P.S. Russell, Endlessly single-mode photonic crystal fiber, Opt. Lett. 22 (1997) 961–963.
[118] G. Renversez, F. Bordas, B.T. Kuhlmey, Second mode transition in microstructured optical fibers: Determination of the critical geometrical parameter and study of the matrix refractive index and effects of cladding size, Opt. Lett. 30 (2005) 1264–1266.
[119] P. Toupin, L. Rilland, C.B. Pledel, B. Bureau, D. Mechin, J.L. Adam, J. Troles, Comparison between chalcogenide glass single index and microstructured exposed-core fibers for chemical sensing, J. Non-Cryst. Solids. 377 (2013) 217–219.
[120] R.R. Gattass, D. Rhonehouse, D. Gibson, C.C. McClain, R. Thapa, V.Q. Nguyen, S.S. Bayya, R.J. Weiblen, C.R. Menyuk, L.B. Shaw, Infrared glass-based negative-curvature anti-resonant fibers fabricated through extrusion, Opt. Express 24 (2016) 25697–25703.
[121] P. Russell, Photonic crystal fibers, Science 299 (2003) 358–362.
[122] M. El-Amraoui, G. Gadret, J.C. Jules, J. Fatome, C. Fortier, F. Désévédavy, L. Skripatchev, Y. Messaddeq, J. Troles, L. Brilland, L, Microstructured chalcogenide optical fibers from As_2S_3 glass: towards new infrared broadband sources, Opt. Express 18 (2010) 26655–26665.
[123] P. Zhang, J. Zhang, P. Yang, S. Dai, X. Wang, W. Zhang, Fabrication of chalcogenide glass photonic crystal fibers with mechanical drilling, Opt. Fiber Technol. 26B (2015) 176–179.
[124] J. Heo, M. Rodrigues, S.J. Saggese, G.H. Sigel, Remote fiber-optic chemical sensing using evanescent-wave interactions in chalcogenide glass fibers, Appl. Opt. 30 (1991) 3944–3951.
[125] B.J. Park, H.S. Seo, J.T. Ahn, Y.G. Choi, D.Y. Jeon, W.J. Chung, Mid-infrared (3.5–5.5 μm) spectroscopic properties of Pr^{3+}-doped Ge–Ga–Sb–Se glasses and optical fibers, J. Lumin. 128 (2008) 1617–1622.
[126] L.B. Shaw, B. Cole, P.A. Thielen, Z.S. Sanghera, I.D. Aggarwal, Mid-wave IR and long-wave IR laser potential of rare-earth doped chalcogenide glass fiber, IEEE J. Quantum Elect. 37 (2001) 1127–1137.
[127] T. Schweizer, D.W. Hewak, B.N. Samson, D.N. Payne, Spectroscopy of potential mid-infrared laser transitions in gallium lanthanum sulfide glass, J. Lumin. 72–74 (1997) 419–421.
[128] F. Prudenzano, L. Mescia, L.A. Allegretti, M. De Sario, T. Palmisano, F. Smektala, V. Moizan, V. Nazabal, J. Troles, Design of Er^{3+}-doped chalcogenide glass laser for mid-IR application, J. Non-Cryst. Solids 355 (2009) 1145–1148.
[129] F. Starecki, F. Charpentier, J.L. Doualan, L. Quetel, K. Michel, R. Chahal, J. Troles, B. Bureau, A. Braud, P. Camy, Mid-IR optical sensor for CO_2 detection based on fluorescence absorbance of Dy^{3+}: $Ga_5Ge_{20}Sb_{10}S_{65}$ fibers, Sens. Actuators B Chem. 207 (2015) 518–525.
[130] S. Binu, Calibration of accelerometers by using an extrinsic fiber optic Probe, Microw. Opt. Technol. Lett. 49 (2007) 2700.
[131] R.Y. Shah, Y.K. Agrawal, Introduction to fiber optics: sensors for biomedical applications, Indian J. Pharm. Sci. 73 (1) (2011) 17–22.
[132] S. Rizzolo, A. Boukenter, E. Marin, M. Cannas, J. Perisse, S. Bauer, J.-R. Mace, Y. Ouerdane, S. Girard, Vulnerability of OFDR-based distributed sensors to high γ-ray doses, Opt. Express 2 (2015) 18997.
[133] A. Méndez, A. Csipkes, Overview of fiber optic sensors for NDT applications, Nondestructive testing of materials and structures, Springer, Dordrecht, 2013, pp. 179–184.
[134] K.A. Fidanboylu, H.S. Efendioglu, Fiber optic sensors and their applications, 5th International Advanced Technologies Symposium (IATS-09), Turkey, Karabuk, 2009, pp. 1–6.
[135] B. Mac Craith, C. McDonagh, A. McEvoy, T. Butler, G. Okeeffe, Optical chemical sensors based on sol-gel materials: recent advances and critical issues, J. Sol-Gel Sci. Technol. 8 (1997) 1053–1061.
[136] P. Fabbri, F. Pilati, L. Rovati, R. McKenzie, J. Mijovic, Poly (ethylene oxide)–silica hybrids entrapping sensitive dyes for biomedical optical pH sensors: Molecular dynamics and optical response, Opt. Mater. 33 (2011) 1362–1369.
[137] B. Schyrr, S. Pasche, E. Scolan, R. Ischer, D. Ferrario, Development of a polymer optical fiber pH sensor for on-body monitoring application, Sens. Actua. B Chem. 194 (2014) 238–248.
[138] C.P. Chang, C.Y. Chao, J.H. Huang, A.K. Li, C.S. Hsu, Fluorescent conjugated polymer films as TNT chemosensors, Synth. Met. 144 (2004) 297–301.
[139] F. Chu, J. Yang, Coil-shaped plastic optical fiber sensor heads for fluorescence

quenching based TNT sensing, Sens. Actuators A Phys. 175 (2012) 43–46.
[140] D.E. Jiang, V.R. Cooper, S. Dai, Porous graphene as the ultimate membrane for gas separation, Nano Letters 9 (2009) 4019–4024.
[141] C. Lee, X. Wei, J.W. Kysar, J. Hone, Measurement of the elastic properties and intrinsic strength of monolayer graphene, Science 321 (2008) 385–388.
[142] J.A. Kim, T. Hwang, S.R. Dugasani, R. Amin, A. Kulkarni, Graphene based fiber optic surface plasmon resonance for bio-chemical sensor applications, Sens. Actuators. B Chem. 187 (2013) 426–433.
[143] H. Zhang, A. Kulkarni, H. Kim, D. Woo, Y.J. Kim, Detection of acetone vapor using graphene on polymer optical fiber, J. Nanosci. Nanotechnol. 11 (2011) 5939–5943.
[144] A. Kulkarni, H. Kim, R. Amin, S.H. Park, B.H. Hong, A novel method for large area graphene transfer on the polymer optical fiber, J. Nanosci. Nanotechnol. 12 (2012) 3918–3921.
[145] S. Some, Y. Xu, Y. Kim, Y. Yoon, H. Qin, Highly sensitive and selective gas sensor using hydrophilic and hydrophobic graphenes, Sci. Rep. 3 (2013) 1868.
[146] S.A. Kharitonov, P.J. Barnes, Biomarkers of some pulmonary diseases in exhaled breath, Biomarkers 7 (2002) 1–32.
[147] G. Peng, U. Tisch, O. Adams, M. Hakim, N. Shehada, Diagnosing lung cancer in exhaled breath using gold nanoparticles, Nat. Nanotechnol. 4 (2009) 669–673.
[148] A. Méndez, T.F. Morse, Specialty optical fibres handbook, Elsevier Inc., Burlington, USA, 2007.
[149] K.M. Mayer, J.H. Hafner, Localized surface plasmon resonance sensors, Chem. Rev. 111 (2011) 3828–3857.
[150] Y. Jin, A.M. Granville, Polymer Fiber Optic Sensors – A Mini Review of their Synthesis and Applications, J. Biosens. Bioelectron. 7 (2016) 194.
[151] C. Pulido, O. Esteban, Tapered polymer optical fiber oxygen sensor based on fluorescence-quenching of an embedded fluorophore, Sens. Actuators. B Chem. 184 (2013) 64–69.
[152] F. Chu, J. Yang, H. Cai, R. Qu, Z. Fang, Characterization of a dissolved oxygen sensor made of plastic optical fiber coated with ruthenium-incorporated solgel, Appl. Opt. 48 (2009) 338–342.
[153] E. Udd, W. Schulz, J. Seim, J. Corones, H.M. Laylor, Fiber optic sensors for infrastructure applications, Oregon Department of Transportation, Washington DC, 1998.
[154] R. Kashya, Fiber bragg gratings, Academic Press, Burlington, MA, 1999.
[155] P.M. Tracey, Intrinsic fiber-optic sensors, IEEE Trans. Ind. Appl. 27 (1) (1991) 96–98.
[156] F. Chiavaioli, C. Trono, A. Giannetti, M. Brenci, F. Baldini, Characterization of a label-free biosensor based on long period grating, J. Biophotonics 7 (2014) 312–322.
[157] Z. Xiong, G. Peng, B. Wu, P. Chu, Highly tunable Bragg gratings in single mode polymer optical fibers, IEEE Photonics Technol. Lett. 11 (1999) 352–354.
[158] A. Stefani, W. Yuan, C. Markos, O. Bang, Narrow bandwidth 850-nm fiber Bragg gratings in few-mode polymer optical fibers, IEEE Photonics Technol. Lett. 23 (2011) 660–662.
[159] G. Statkiewicz-Barabach, K. Tarnowski, D. Kowal, P. Mergo, W. Urbanczyk, Fabrication of multiple Bragg gratings in microstructured polymer fibers using a phase mask with several diffraction orders, Opt. Express. 21 (2013) 8521–8534.
[160] Y. Luo, B. Yan, M. Li, X. Zhang, W. Wu, Analysis of multimode POF gratings in stress and strain sensing applications, Opt. Fiber Technol. 17 (2011) 201–209.
[161] F. Gu, H. Yu, W. Fang, L. Tong, Nano imprinted polymer micro/nanofiber Bragg gratings for high-sensitive strain sensing, IEEE Photon. Technol. Lett. 25 (2013) 22–24.
[162] X. Chen, C. Zhang, D.J. Webb, G.D. Peng, K. Kalli, Bragg grating in a polymer optical fibre for strain, bend and temperature sensing, Meas. Sci. Technol. 21 (2010) 094005.
[163] P.S.J. Russell, Photonic-crystal fibers, J. Lightwave Technol. 24 (2006) 4729–4749.
[164] M.C. Large, D. Blacket, C.A. Bunge, Microstructured polymer optical fibers compared to conventional POF: novel properties and applications, IEEE Sens. J. 10 (2010) 1213–1217.
[165] D. Li, L. Wang, Fluorescence hydrogen peroxide probe based on a microstructured polymer optical fiber modified with a titanium dioxide film, Appl. Spectrosc. 64 (2010) 514–519.
[166] J. Wang, L. Wang, Carbon dioxide gas sensor derived from a 547-hole microstructured polymer optical fiber preform, Opt. Lett. 35 (2010) 3270–3272.
[167] X. Yang, L. Peng, L. Yuan, P. Teng, F. Tian, Oxygen gas optrode based on microstructured polymer optical fiber segment, Opt. Commun. 284 (2011) 3462–3466.
[168] D.P. O'Neal, M.A. Meledeo, J.R. Davis, B.L. Ibey, V.A. Gant, M.V. Pishko, G.L. Coté, Oxygen sensor based on the fluorescence quenching of a ruthenium complex immobilized in a biocompatible poly(ethylene glycol) hydrogel, IEEE Sens. J. 4 (6) (2004) 728–734.
[169] L. Peng, X. Yang, L. Yuan, L. Wang, E. Zhao, Gaseous ammonia fluorescence probe based on cellulose acetate modified microstructured optical fiber, Opt. Commun. 284 (2011) 4810–4814.
[170] R.B. Schasfoort, A.J. Tudos, Handbook of surface plasmon resonance, Royal Society of Chemistry, Cambridge, UK, 2008.
[171] K.A. Willets, R.P. Van Duyne, Localized surface plasmon resonance spectroscopy and sensing, Annu. Rev. Phys. Chem. 58 (2007) 267–297.
[172] I.C. Chen, S.S. Lin, T.J. Lin, J.K. Du, Detection of hydrofluoric acid by a SiO_2 sol-gel coating fiber-optic probe based on reflection-based localized surface plasmon resonance, Sensors 11 (2011) 1907–1923.
[173] N. Cennamo, A. Donà, P. Pallavicini, G. D'Agostino, G. Dacarro, Sensitive detection of, 4, 6-trinitrotoluene by tridimensional monitoring of molecularly imprinted polymer with optical fiber and five-branched gold nanostars, Sens. Actuators. B Chem. 208 (2015) 291–298.
[174] Y. Jin, K.H. Wong, A.M. Granville, Developing localized surface plasmon resonance biosensor chips and fiber optics via direct surface modification of PMMA optical waveguides, Coll. Surf. A 492 (5) (2016) 100–109.
[175] R. Verma, S.K. Srivastava, B.D. Gupta, Surface-plasmon-resonance-based fiber-optic sensor for the detection of low-density lipoprotein, IEEE Sens. J. 12 (12) (2012) 3460–3466.
[176] J. Homola, Surface plasmon resonance sensors for detection of chemical and biological species, Chem. Rev. 108 (2008) 462–493.
[177] A. Hassani, M. Skorobogatiy, Design criteria for microstructured-opticalfiber-based surface-plasmon-resonance sensor, J. Opt. Soc. Am. B 24 (2007) 1423–1429.
[178] N. Cennamo, D. Massarotti, L. Conte, L. Zeni, Low cost sensors based on SPR in a plastic optical fiber for biosensor implementation, Sensors 11 (2011) 11752–11760.
[179] Y. Lu, C.J. Hao, B.Q. Wu, M. Musideke, L.C. Duan, Surface plasmon resonance sensor based on polymer photonic crystal fibers with metal nanolayers, Sensors (Basel) 13 (2013) 956–965.
[180] A. Wang, A. Docherty, B.T. Kuhlmey, F.M. Cox, M.C. Large, Side-hole fiber sensor based on surface plasmon resonance, Opt. Lett. 34 (2009) 3890–3892.
[181] H. Lamela, D. Gallego, R. Gutierrez, A. Oraevsky, Interferometric fiber optic sensors for biomedical applications of optoacoustic imaging, J. Biophotonics 4 (2011) 184–192.
[182] B. Culshaw, G. Thursby, D. Betz, B. Sorazu, The detection of ultrasound using fiber-optic sensors, IEEE Sens. J. 8 (2008) 1360–1367.
[183] D. Gallego, H. Lamela, High-sensitivity ultrasound interferometric singlemode polymer optical fiber sensors for biomedical applications, Opt. Lett. 34 (2009) 1807–1809.
[184] J.W. Parker, O. Laksin, Y. Clement, M. Lau, S. Klima, R. Fisher, I. Scott, B.W. Atwater, Fiber-optic sensors for pH and carbon dioxide using a self-referencing dye, Anal. Chem. 65 (1993) 2329–2334.
[185] K. Buchholz, N. Buschmann, K. Cammann, A fibre-optical sensor for the determination of sodium with a reversible response, Sens. Actuators. B Chem. 9 (1992) 41–47.
[186] S.A. Grant, R.S. Glass, A sol–gel based fiber optic sensor for local blood pH measurements, Sens. Actuators. B chem. 45 (1997) 35–42.
[187] S. Singh, B.D. Gupta, Fabrication and characterization of a highly sensitive surface plasmon resonance based fiber optic pH sensor utilizing high index layer and smart hydrogel, Sens. Actuators. B Chem. 173 (2012) 268.
[188] C.C. Chiang, C.H. Hsu, C.H. Ou, pH Value Detection with CLPFG Sensor, Appl. Mech. Mater. 284–287 (2013) 2157–2161.
[189] B. Schyrr, S. Pasche, E. Scolan, R. Ischer, D. Ferrario, J.A. Porchet, G. Voirin, Development of a polymer optical fiber pH sensor for on-body monitoring application, Sens. Actuators. B Chem. 194 (2014) 238.
[190] S. Islam, R.A. Rahman, Z.B. Othaman, S. Riaz, S. Naseem, Synthesis and characterization of multilayered sol–gel based plastic-clad fiber optic pH sensor, J. Ind. Eng. Chem. 23 (2015) 140–144.
[191] Q. Zhao, M. Yin, A.P. Zhang, S. Prescher, M. Antonietti, J. Yuan, Hierarchically Structured nanoporous poly(ionic liquid) membranes: facile preparation and application in fiber-zptic pH sensing, J. Am. Chem. Soc. 135 (2013) 5549–5552.
[192] P.E. Henning, P. Geissinger, Application of time-correlated single photon counting and stroboscopic detection methods with an evanescent-wave fibre-optic sensor for fluorescence-lifetime-based pH measurements, Meas. Sci. Technol. 23 (2012) 045104.
[193] Q. Yang, H. Wang, X. Lan, B. Cheng, S. Chen, H. Shi, H. Xiao, Y. Ma, Reflection-mode micro-spherical fiber-optic probes for *in vitro* real-time and single-cell level pH sensing, Sens. Actuators. B Chem. 207 (2015) 571–580.
[194] D. Dey, T. Goswami, Optical biosensors: a revolution towards quantum nanoscale electronics device fabrication, J. Biomed. Biotechnol. 2011 (2011) 348218.
[195] M.E. Bosch, A.J.R. Sánchez, F.S. Rojas, C.B. Ojeda, Recent development in optical fiber biosensors, Sensors 7 (2007) 797–859.
[196] P. Damborsky, J. Svitel, J. Katrlık, Optical biosensors, Essays Biochem. 60 (2016) 91–100.
[197] T. Riedel, C. Rodriguez-Emmenegger, A. De los Santos Pereira, A. Bedajankova, P. Jinoch, P.M. Boltovets, Diagnosis of epstein–barr virus infection in clinical serum samples by an SPR biosensor assay, Biosens. Bioelectron. 55 (2014) 278–284.
[198] F. Fernandez, K. Hegnerova, M. Piliarik, F. Sanchez-Baeza, J. Homola, M.P. Marco, A label-free and portable multichannel surface plasmon resonance immune-sensor for on analysis of antibiotics in milk samples, Biosens. Bioelectron. 26 (2010) 1231–1238.
[199] A. Pennacchio, G. Ruggiero, M. Staiano, G. Piccialli, G. Oliviero, A. Lewkowicz, A surface plasmon resonance based biochip for the detection of patulin toxin, Opt. Mater. 36 (2014) 1670–1675.
[200] T. Endo, T. Kerman, K. Nagatani, N.M. Hiepa, D.K. Kim, Y. Yonezawa, Multiple label-free detection of antigen – antibody reaction using localized surface plasmon resonance-based core – shell structured nanoparticle layer nano chip, Anal. Chem. 78 (2006) 6465–6475.
[201] J. Yuan, R. Duan, H. Yang, X. Luo, M. Xi, Detection of serum human epididymis secretory protein 4 in patients with ovarian cancer using a label-free biosensor based on localized surface plasmon resonance, Int. J. Nanomedicine 7 (2012) 2921–2928.
[202] J.H. Lee, B.C. Kim, B.K. Oh, J.W. Choi, Highly sensitive localized surface plasmon resonance immunosensor for label-free detection of HIV-1, Nanomedicine 9 (2013) 1018–1026.
[203] C.R. Taitt, G.P. Anderson, F.S. Ligler, Evanescent wave fluorescence biosensors: advances of the last decade, Biosens. Bioelectron. 76 (2015) 103–111.

[204] M.J. Lochhead, K. Todorof, M. Delaney, J.T. Ives, C. Greef, K. Moll, Rapid multiplexed immunoassay for simultaneous serodiagnosis of HIV-1 and coinfections, J. Clin. Microbiol. 49 (2011) 3584–3590.
[205] N. Yildirim, F. Long, C. Gao, M. He, H.C. Shi, A.Z. Gu, Aptamer-based optical biosensor for rapid and sensitive detection of 17 beta-estradiol in water samples, Environ. Sci. Technol. 46 (2012) 3288–3294.
[206] K. Jia, E. Eltzov, T. Toury, R.S. Marks, R.E. Ionescu, A lower limit of detection for atrazine was obtained using bioluminescent reporter bacteria via a lower incubation temperature, Ecotoxicol. Environ. Saf. 84 (2012) 221–226.
[207] I. Biran, D.M. Rissin, E.Z. Ron, D.R. Walt, Optical imaging fiber-based live bacterial cell array biosensor, Anal. Biochem. 315 (2003) 106–113.
[208] S. Yu, D. Li, H. Chong, C. Sun, H. Yu, K. Xu, In vitro glucose measurement using tunable mid-infrared laser spectroscopy combined with fiber-optic sensor, Biomed. Opt. Express 5 (1) (2014) 275, https://doi.org/10.1364/BOE.5.000275.
[209] D. Li, S. Yu, C. Sun, C. Zou, H. Yu, K. Xu, U-shaped fiber-optic ATR sensor enhanced by silver nanoparticles for continuous glucose monitoring, Biosens. Bioelectron. 72 (2015) 370–375.
[210] D. Li, L. Wu, P. Wu, Y. Lin, Y. Sun, R. Zhu, J. Yang, K. Xu, Affinity based glucose measurement using fiber optic surface plasmon resonance sensor with surface modification by borate polymer, Sens. Actuators B Chem. 213 (2015) 295–304.
[211] S.K. Shukla, M.M. Demir, P.P. Govender, Ashutosh Tiwari, S.K. Shukla, Optical fibre based non-enzymatic glucose sensing over Cu^{2+}-doped polyaniline hybrid matrix, Sens. Actuators B Chem. 242 (2017) 522–528.
[212] S. Singh, B.D. Gupta, Fabrication and characterization of a surface plasmon resonance based fiber optic sensor using gel entrapment technique for the detection of low glucose concentration, Sens. Actuators. B Chem. 177 (2013) 589–595.
[213] P. Bhatia, B.D. Gupta, Fabrication and characterization of a surface plasmon resonance based fiber optic urea sensor for biomedical applications, Sens. Actuators B Chem. 161 (1) (2012) 434–438.
[214] A. Baliyan, P. Bhatia, B.D. Gupta, E.K. Sharma, A. Kumari, R. Gupta, Surface plasmon resonance based fiber optic sensor for the detection of triacylglycerides using gel entrapment technique, Sens. Actuators B Chem. 188 (2013) 917–922.
[215] M. Ye, P.J. Chien, K. Toma, T. Arakawa, K. Mitsubayashi, An acetone bio-sniffer (gas phase biosensor) enabling assessment of lipid metabolism from exhaled breath, Biosens. Bioelectron. 73 (2015) 208–213.
[216] H. Usman, M.H. Abu Bakar, A.S. Hamzah, A.B. Salleh, A tapered fibre optics biosensor for histamine detection, Sensor Rev. 36 (2016) 40–47.
[217] K. Knez, K.P.F. Janssen, J. Pollet, D. Spasic, J. Lammertyn, Fiber-optic high-resolution genetic screening using gold-labeled gene probes, Small. 8 (2012) 868–872.
[218] J. Albert, S. Lepinay, C. Caucheteur, M.C. Derosa, High resolution grating-assisted surface plasmon resonance fiber optic apta sensor, Methods 63 (2013) 239–254.
[219] R.B. Queiros, C. Gouveia, J.R.A. Fernandes, P.A.S. Jorge, Evanescent wave DNA-aptamer biosensor based on long period gratings for the specific recognition of *E. coli* outer membrane proteins, Biosens. Bioelectron. 62 (2014) 227.
[220] F. Long, A. Zhu, X. Zhou, H. Wang, Z. Zhao, L. Liu, H. Shi, Highly sensitive and selective optofluidics-based immunosensor for rapid assessment of bisphenol A leaching risk, Biosens. Bioelectron. 55 (2014) 19.
[221] E. Brzozowska, M. Smietana, M. Koba, S. Gorska, K. Pawlik, A. Gamian, W.J. Bock, Bacteriophage adhesin-coated long-period grating-based sensor: bacteria detection specificity, Biosens. Bioelectron. 67 (2015) 93.
[222] A.R. Camara, P.M. Gouvêa, A.C. Dias, A.M. Braga, R.F. Dutra, R.E. de Araujo, I.C. Carvalho, Dengue immunoassay with an LSPR fiber optic sensor, Opt. Express 21 (22) (2013) 27023–27031.
[223] H.H. Jeong, N. Erdene, J.H. Park, D.H. Jeong, H.Y. Lee, S.K. Lee, Real-time label-free immunoassay of interferon-gamma and prostate-specific antigen using a fiber-optic localized surface plasmon resonance sensor, Biosens. Bioelectron. 39 (1) (2013) 346–351.
[224] H.Y. Lin, C.H. Huang, S.H. Lu, I.T. Kuo, I.K. Chau, Direct detection of orchid viruses using nanorod-based fiber optic particle plasmon resonance immunosensors, Biosens. Bioelectron. 51 (2014) 371–378.
[225] S. Jitendra, J. Tharion, S. Mukherji, Facile synthesis of size and wavelength tunable hollow gold nanostructures for the development of a LSPR based label-free fiber-optic biosensor, RSC Adv. 5 (86) (2015) 69970–69979.
[226] F. Algaar, E. Eltzov, M.M. Vdovenko, I.Y. Sakharov, L. Fajs, M. Weidmann, A. Mirazimi, R.S. Marks, Fiber-optic immunosensor for detection of crimean-congo hemorrhagic fever igg antibodies in patients, Anal. Chem. 87 (16) (2015) 8394–8398.
[227] S.H. Ohk, A.K. Bhunia, Multiplex fiber optic biosensor for detection of Listeria monocytogenes, escherichia coli O157:H7 and Salmonella enterica from ready-to-eat meat samples, Food Microbiol. 33 (2013) 166.
[228] J. Hu, T. Lang, J. Jin, J. Chen, An optical fiber biosensor based on layer-by-layer electrostatic self-assembly for rapid detection of HIgG, In optical communications and networks (ICOCN), 2016 15th International Conference on IEEE, 2016, pp. 1–3.
[229] O. Tohyama, M. Kohashi, M. Sugihara, H. Itoh, A fiber-optic pressure micro-sensor for biomedical applications, Sens. Actuators. A Phys. 66 (1998) 150–154.
[230] R. Wolthuis, G. Mitchell, J. Hartl, E. Saaski, Development of dual function sensor system for measuring pressure and temperature at the tip of a single optical fiber, IEEE Trans. Biomed. Eng. BE-40 (1993) 298–302.
[231] L.H. Lindstrom, Miniaturized pressure transducer intended for intravascular use, IEEE Trans. Biomed. Eng. BE-17 (1970) 207–219.
[232] T.E. Hansen, A fiberoptic micro-tip pressure transducer for medical applications, Sens. Actuators 4 (1983) 545–554.
[233] D.A. Christensen, Fiberoptic temperature sensing for biomedical applications, Optical Fibers in Medicine. III (906) (1988) 108–114.
[234] Luxtron, 2775 Northwestern Parkway, Santa Clara, CA 95051-0941 (1995).
[235] N. Wu, X. Zou, J. Zhou, X. Wang, Fiber optic ultrasound transmitters and their applications, Measurement 79 (2016) 164–171.
[236] M. Kawasaki, B. Bouma, J. Bressner, S. Houser, S. Nadkarni, B. MacNeill, I. Jang, H. Fujiwara, G. Tearney, Diagnostic accuracy of optical coherence tomography and integrated backscatter intravascular ultrasound images for tissue characterization of human coronary plaques, J. Am. Coll. Cardiol. 48 (2006) 81–88.
[237] L.C.L. Chin, W.M. Whelan, I. Alex Vitkin, Optical fiber sensors for biomedical applications, Optical-thermal response of laser-irradiated tissue, Springer, Dordrecht, 2010, pp. 661–712.
[238] Y.J. Rao, D.J. Webb, D.A. Jackson, L. Zhang, I. Bennion, Optical in-fiber bragg grating sensor systems for medical applications, J. Biomed. Opt. 3 (1998) 38–44.
[239] F. Manns, P.J. Milne, X. Gonzalez-Cirre, D.B. Denham, J.M. Parel, D.S. Robinson, In situ temperature measurements with thermocouple probes during laser interstitial thermotherapy (LITT): Quantification and correction of a measurement artifact, Lasers Surg. Med. 23 (1998) 94–103.
[240] G. Wehrle, P. Nohama, H.J. Kalinowski, P.I. Torres, L.C.G. Valente, A fibre optic bragg grating strain sensor for monitoring ventilatory movements, Meas. Sci. Technol. 12 (2001) 805–809.
[241] P. Polygerinos, L.D. Seneviratne, R. Razavi, T. Schaeffter, K. Althoefer, Triaxial catheter-tip force sensor for MRI-guided cardiac procedures, IEEE/ASME Trans. Mechatron. 18 (2013) 386–396.
[242] J.C. Kennedy, R.H. Pottier, Endogenous protoporphyrin IX, a clinically useful photosensitizer for photodynamic therapy, J. Photochem. Photobiol. B 14 (1992) 275–292.
[243] A.C. Kubler, Photodynamic therapy, Med. Laser Appl. 20 (2005) 37–45.
[244] O. Yizhar, L.E. Fenno, T.J. Davidson, M. Mogri, K. Deisseroth, Optogenetics in neural systems, Neuron 71 (2011) 9–34.
[245] E.S. Boyden, F. Zhang, E. Bamberg, G. Nagel, K. Deisseroth, Millisecond time scale, genetically targeted optical control of neural activity, Nat. Neurosci. 8 (2005) 1263–1268.
[246] N. Stone, C.K. Endall, J. Smith, P. Crow, H. Barr, Raman spectroscopy for identification of epithelial cancers, Faraday Discuss. 126 (2004) 141–157.
[247] O. Stevens, I.E.I. Petterson, J.C.C. Day, N. Stone, Developing fibre optic raman probes for applications in clinical spectroscopy, Chem. Soc. Rev. 45 (2016) 1919–1934.
[248] A.G. Mignani, F. Baldini, Biomedical sensors using optical fibres, Rep. Prog. Phys. 59 (1996) 1–28.
[249] F. Baldini, A. Giannetti, A.A. Mencaglia, C. Trono, Fiber Optic sensors for biomedical applications, Curr. Anal. Chem. 4 (2008) 378390.
[250] I. Clausen, T. Glott, Development of clinically relevant implantable pressure sensors: perspectives and challenges, Sensors. 14 (2014) 17686–17702.
[251] J.T. Pollak, M. Neimark, J.T. Connor, G.W. Davila, Air-charged and micro-transducer urodynamic catheters in the evaluation of urethral function, Int. Urogynecol. J. 15 (2004) 124–128.
[252] G.A. Digesu, A. Derpapas, P. Robshaw, G. Vijaya, C. Hendricken, V. Khullar, Are the measurements of water-filled and air-charged catheters the same in urodynamics? Int. Urogynecol. J. 25 (2014) 123–130.
[253] Q. Wang, H.R. Brunner, M. Burnier, Determination of cardiac contractility in awake unsedated mice with a fluid-filled catheter, Am. J. Physiol. Heart Circ. Physiol. 286 (2004) 806–814.
[254] J.D. Zampi, J.C. Hirsch, B.H. Goldstein, A.K. Armstrong, Use of a pressure guidewire to assess pulmonary artery band adequacy in the hybrid stage I procedure for high-risk neonates with hypoplastic left heart syndrome and variants, Congenit. Heart Dis. 8 (2013) 149–158.
[255] C. Yang, C. Zhao, L. Wold, K.R. Kaufman, Biocompatibility of a physiological pressure sensor, Biosens. Bioelectron. 19 (2003) 51–58.
[256] P.R. Woldbaek, T.A. Strømme, J.B. Sande, G. Christensen, T. Tønnessen, A. Ilebekk, Evaluation of a new fiber-optic pressure recording system for cardiovascular measurements in mice, Am. J. Physiol. Heart Circ. Physiol. 285 (2003) 2233–2239.
[257] N. Wu, Y. Tian, X. Zou, Y. Zhai, K. Barringhaus, X. Wang, A miniature fiber optic blood pressure sensor and its application in in vivo blood pressure measurements of a swine model, Sens. Actuators B Chem. 181 (2013) 172–178.
[258] Q.Y. Yuan, L. Zhang, D. Xiao, K. Zhao, C. Lin, L.Y. Si, An accurate, flexible and small optical fiber sensor: a novel technological breakthrough for real-time analysis of dynamic blood flow data in vivo, PLoS ONE 9 (2014) 0114794.
[259] Y. Tian, N. Wu, X. Zou, Y. Zhang, K. Barringhaus, X. Wang, A Study on packaging of miniature fiber optic sensors for in-vivo blood pressure measurements in a swine model, IEEE Sensor J. 14 (2014) 629–635.
[260] E. Bakker, K. Visser, A. Van Der Wal, M. Kuiper, M. Koopmans, R. Breedveld, Inflation and deflation timing of the auto CAT 2 WAVE intra-aortic balloon pump using the auto pilot mode in a clinical setting, Perfusion 27 (2012) 393–398.
[261] D.A.A. Rodriguez, E. Durand, L. de Rochefort, Y. Boudjemline, E. Mousseaux, Simultaneous pressure-volume measurements using optical sensors and MRI for left ventricle function assessment during animal experiment, Med. Eng. Phys. 37 (2015) 100–108.
[262] M. Chavko, W.A. Koller, W.K. Prusaczyk, R.M. McCarron, Measurement of blast wave by a miniature fiber optic pressure transducer in the rat brain, J. Neurosci. Methods 277–281 (2007).
[263] S. Poeggel, D. Tosi, F. Fusco, J. Ippolito, L. Lupoli, V. Mirone, S. Sannino, G. Leen, E. Lewis, Fiber-optic efpi pressure sensors for in vivo urodynamic analysis, IEEE Sensor J. 14 (2014) 2335–2340.
[264] S. Poeggel, D. Duraibabu, D. Tosi, G. Leen, E. Lewis, D. McGrath, F. Fusco, S. Sannino, L. Lupoli, J. Ippolito, Differential in vivo urodynamic measurement in a single thin catheter based on two optical fiber pressure sensors, J. Biomed. Opt.

20 (2015) 037005.
[265] W. Inokuchi, B.S. Olsen, J.O. Sojbjerg, O. Sneppen, The relation between the position ofthe glenohumeral joint and the intra articular pressure: an experimental study, J. Shoulder Elbow Surg. 6 (1997) 144–149.
[266] P.S. Cottler, D. Blevins, J. Averett, T.A. Wavering, D.A. Morrow, A.Y. Shin, K.R. Kaufman, Miniature optical fiber pressure microsensors for in vivo measurement of intramuscular pressure, Proc. SPIE. 6433 (2007) 643304.
[267] A. Nilsson, Q. Zhang, J. Styf, The amplitude of pulse-synchronous oscillations varies with the level of intramuscular pressure in simulated compartment syndrome, J. Exp. Orthop. 2 (2015) 3.
[268] P. Roriz, J.M.C. Ferreira, J.C. Potes, M.T. Oliveira, O. Frazao, J.L. Santos, J.A.D.O. Simoes, In vivo measurement of the pressure signal in the intervertebral disc of an anaesthetized sheep, J. Biomed. Opt. 19 (2014) 037006.
[269] D. Kokkinos, S. Dehipawala, T. Holden, E. Cheung, M. Musa, G. Tremberger, P. Schneider, D. Lieberman, T. Cheung, Fiber optic based heart-rate and pulse pressure shape monitor, Proc. SPIE. 8218 (2012) 82180V.
[270] A. VanBrakel, P.L. Swart, A.A. Chtcherbakov, M.G. Shlyagin, Blood pressure manometer using a twin bragg grating fabry-perot interferometer, Proc. SPIE. 5634 (2005) 595–602.
[271] Z. Mo, W. Xu, N. Broderick, A Fabry-perot optical fiber force sensor based on intensity modulation for needle tip force sensing, in: Proceedings of the 2015 6th International Conference on Automation, Robotics and Applications (ICARA), Queenstown, New Zealand, 17–19 February, 2015, pp. 376–380.
[272] X. Zou, N. Wu, Y. Tian, X. Wang, Broadband miniature fiber optic ultrasound Generator, Opt. Express 22 (2014) 18119–181127.
[273] V. Kochergin, K. Flanagan, Z. Shi, M. Pedrick, B. Baldwin, T. Plaisted, B. Yellampelle, E. Kochergin, L. Vicari, All-fiber optic ultrasonic structural health monitoring system, Proc. SPIE. 7292 (2009) 72923D.
[274] J. Tian, Q. Zhang, M. Han, Distributed fiber-optic laser-ultrasound generation based on ghost-mode of tilted fiber bragg gratings, Opt. Express. 21 (5) (2013) 6109–6114.
[275] B.H. Lee, E.J. Min, Y.H. Kim, Fiber-based optical coherence tomography for biomedical imaging, sensing, and precision measurements, Opt. Fiber Technol. 19 (2013) 729–740.
[276] M. Lenz, C. Mazzon, C. Dillmann, N.C. Gerhardt, H. Welp, M. Prange, M.R. Hofmann, Spectral domain optical coherence tomography for non-destructive testing of protection coatings on metal substrates, Appl. Sci. 7 (2017) 364–375.
[277] D. Culemann, A. Knuettel, E. Voges, Integrated optical sensor in glass for optical coherence tomography (OCT), IEEE J. Sel. Top. Quantum Electron. 6 (5) (2000) 730–734.
[278] K. Iwai, H. Takaku, M. Miyagi, Y.W. Shi, Y. Matsuura, Fabrication of shatter-proof metal hollow-core optical fibers for endoscopic mid-infrared laser applications, Fibers 6 (2018) 24.
[279] J. Eom, J.G. Shin, S. Park, B.H. Lee, All optical fiber combined-imaging system of photoacoustic and optical coherence tomography, Proc. SPIE. 9708 (2016) 97084D.
[280] S.P. Chong, M.T. Bernucci, D. Borycki, H. Radhakrishnan, V.J. Srinivasan, Structural and functional human retinal imaging with a fiber-based visible light OCT ophthalmoscope, Biomed. Opt. Express 8 (1) (2017) 323–337.
[281] K.S. Lee, H. Hur, H.Y. Sung, I.J. Kim, G.H. Kim, Spectrally encoded common-path fiber-optic-based parallel optical coherence tomography, Opt. Lett. 41 (2016) 4241–4244.
[282] F. Taffoni, D. Formica, P. Saccomandi, G.D. Pino, E. Schena, Optical fiber-based MR-cozpatible sensors for medical applications: an overview, Sensors 13 (2013) 14105–14120.
[283] P. Saccomandi, E. Schena, F.M. Di Matteo, M. Pandolfi, M. Martino, R. Rea, S. Silvestri, Laser interstitial thermotherapy for pancreatic tumor ablation: theoretical model and experimental validation, In proceedings of annual international conference on the IEEE engineering in medicine and biology society, Boston, MA 2011 (2011) 5585–5588.
[284] R. Gassert, R. Moser, E. Burdet, H. Bleuler, MRI/fMRI-Compatible robotic system with force feedback for interaction with human motion, IEEE/ASME Trans. Mech. 11 (2006) 216–224.
[285] L. Dziuda, F.W. Skibniewski, M. Krej, P.M. Baran, Fiber Bragg grating-based sensor for monitoring respiration and heart activity during magnetic resonance imaging examination, J. Biomed. Opt. 18 (5) (2013) 057006.
[286] A. Kaźmierczak, S. StopińskI, A. Jusza, K. Anders, K. Markowski, T. Osuch, R. Piramidowicz, Development of photonic sensing system for patient condition monitoring during MRI diagnostics, In Proc, Eur. Conf. Integrated Optics (ECIO) (2016) 46.
[287] T. Bützer, M. Rinderknecht, G.H. Johannes, W.L. Popp, R. Lehner, O. Lambercy, R. Gassert, Design and evaluation of a fiber-optic grip force sensor with compliant 3D-printable structure for (f) MRI applications, J. Sensors (2016) 1–11.
[288] J.D. Shephard, A. Urich, R.M. Carter, P. Jaworski, R.R.J. Maier, W. Belardi, F. Yu, W.J. Wadsworth, J.C. Knight, D.P. Hand, Silica hollow core microstructured fibers for beam delivery in industrial and medical applications, Front. Phys. 3 (2015) 24.
[289] P. Jaworski, F. Yu, R.R.J. Maier, W.J. Wadsworth, J.C. Knight, J.D. Shephard, Picosecond and nanosecond pulse delivery through a hollow-core Negative Curvature Fiber for micro-machining applications, Opt. Express 21 (2013) 22742–22753.
[290] A. Urich, R.R.J. Maier, F. Yu, J.C. Knight, D.P. Hand, J.D. Shephard, Flexible delivery of Er: YAG radiation at 2.94 μm with negative curvature silica glass fibers: a new solution for minimally invasive surgical procedures, Biomed. Opt. Express 4 (2013) 193–205.
[291] Q. Wang, D. Yuan, W. Liu, J. Chen, X. Lin, S. Cheng, F. Li, X. Duan, Use of optical fiber imported intra-tissue photodynamic therapy for treatment of moderate to severe acne vulgaris, Med. Sci. Monit. 22 (2016) 362–366.
[292] J.C. Kennedy, R.H. Pottier, Endogenous protoporphyrin IX, a clinically useful photosensitizer for photodynamic therapy, J. Photochem. Photobiol. B 14 (4) (1992) 275–292.
[293] W. Hongcharu, C.R. Taylor, Y. Chang, Topical ALA-photodynamic therapy for the treatment of acne vulgaris, J. Invest. Dermatol. 115 (2) (2000) 183–192.
[294] I. Zalaudek, J. Giacomel, K. Schmid, S. Bondino, C. Rosendahl, S. Cavicchini, Dermatoscopy of facial actinic keratosis, intraepidermal carcinoma, and invasive squamous cell carcinoma: A progression model, J. Am. Acad. Dermatol. 66 (4) (2012) 589–597.
[295] M. Daniel, Light emitting fabric, U.S. Patent 4,234,907 (1980). (www.google.com/patents/US4234907).
[296] L. Meunier, F.M. Kell, C. Cochrane, V. Koncar, Flexible displays for smart clothing: part I-overview, Ind. J. Fibre Text. Res. 36 (2011) 422–428.
[297] Z. Huang, W. Gong, K. Yuan, J. Zou, Y. Wang, G. Shi, Optimizing light source and light delivery for photodynamic therapy of portwine stain birthmarks, Photodiagnosis Photodyn. Ther. 17 (2017) A4–A78.
[298] L.M. Costa, F. DeSouza Matos, A.M. de Oliveira Correia, N.C. Carvalho, A.L. Faria-e-Silva, L.R. Paranhos, M.A.G. Ribeiro, Tooth color change caused by photosensitizers after photodynamic therapy: An in vitro study, J. Photochem. Photobiol. B Biol. 160 (2016) 225–228.
[299] M.B. Fonseca, P.O. Tessare Júnior, R.C. Pallota, H. Ferreira Filho, O.V.P. Denardin, A. Rapoport, R.A. Dedivitis, J.F. Veronezi, W.J. Genovese, A.L.F. Ricardo, Photodynamic therapy for root canals infected with Enterococcus faecalis, Photomed. Laser Surg. 26 (2008) 209–213.
[300] S.I. Al-Juboori, A. Dondzillo, E.A. Stubblefield, G. Felsen, T.C. Lei, A. Klug, Light scattering properties vary across different regions of the adult mouse brain, PLoS ONE 8 (2013) e67626.
[301] Y. Shin, H.S. Kwon, Mesh-based Monte Carlo method for fibre-optic optogenetic neural stimulation with direct photon flux recording strategy, Phys. Med. Biol. 61 (2016) 2265–2282.
[302] L. Grosenick, J.H. Marshel, K. Deisseroth, Closed loop and activity-guided opto genetic control, Neuron 86 (2015) 106–139.
[303] F. Zhang, V. Gradinaru, A.R. Adamantidis, R. Durand, R.D. Airan, L. De Lecea, K. Deisseroth, Optogenetic interrogation of neural circuits: technology for probing mammalian brain structures, Nat. Protoc. 5 (3) (2010) 439–456.
[304] A.M. Aravanis, L.P. Wang, F. Zhang, L.A. Meltzer, M.Z. Mogri, M.B. Schneider, K. Deisseroth, An optical neural interface: in vivo control of rodent motor cortex with integrated fiberoptic and optogenetic technology, J. Neural. Eng. 4 (3) (2007) S143–S156.
[305] M.R. Warden, J.A. Cardin, K. Deisseroth, Optical neural interfaces, Annu. Rev. Biomed. Eng. 16 (2014) 103–129.
[306] K.L. Montgomery, A.J. Yeh, J.S. Ho, V. Tsao, S.M. Iyer, L. Grosenick, A.S. Poon, Wirelessly powered, fully internal optogenetics for brain, spinal and peripheral circuits in mice, Nat. methods 12 (10) (2015) 969–974.
[307] Y.G. Ermakova, A.A. Lanin, I.V. Fedotov, M. Roshchin, I.V. Kelmanson, D. Kulik, Y.A. Bogdanova, A.G. Shokhina, D.S. Bilan, D.B. Staroverov, P.M. Balaban, Thermogenetic neurostimulation with single-cell resolution, Nat. Commun. 8 (2017) 15362.
[308] M.A. Mackanos, C.H. Contag, Fiber-optic probes enable cancer detection with FTIR spectroscopy, Trends Biotechnol. 28 (2010) 317–323.
[309] H.M. Heise, L. Küpper, W. Pittermann, M. Stücker, Epidermal in vivo and in vitro studies by attenuated total reflection mid-infrared spectroscopy using flexible silver halide fibre-probes, J. Mol. Struct. 651–653 (2003) 127–132.
[310] U. Bindig, G. Müller, Fibre-optic laser-assisted infrared tumour diagnostics (FLAIR), J. Phys. D Appl. Phys. 38 (2005) 2716–2731.
[311] M.A. Mackanos, J. Hargrove, R. Wolters, C.B. Du, S. Friedland, R.M. Soetikno, C.H. Contag, M.R. Arroyo, J.M. Crawford, T.D. Wang, Use of an endoscope-compatible probe to detect colonic dysplasia with Fourier transform infrared spectroscopy, J. Biomed. Opt. 14 (2009) 044006.
[312] V.K. Katukuri, J. Hargrove, S.J. Miller, K. Rahal, J.Y. Kao, R. Wolters, E.M. Zimmermann, T.D. Wang, Detection of colonic inflammation with fourier transform infrared spectroscopy using a flexible silver halide fiber, Biomed. Opt. Express 1 (2010) 1014–1025.
[313] L. Dong, X. Sun, Z. Chao, S. Zhang, J. Zheng, R. Gurung, J. Du, J. Shi, Y. Xu, Y. Zhang, J. Wu, Evaluation of FTIR spectroscopy as diagnostic tool for colorectal cancer using spectral analysis, Spectrochim. Acta. A 122 (2014) 288–294.
[314] J. Ollesch, M. Zaczek, H.M. Heise, O. Theisen, F. Groberüschkamp, R. Schmidt, K. Morgenroth, S. Philippou, M. Kemen, K. Gerwert, Clinical application of infrared fibre-optic probes for the discrimination of colorectal cancer tissues and cancer grades, Vib. Spectrosc. 91 (2017) 99–110.
[315] C.K. Ho, A. Robinson, D.R. Miller, M.J. Davis, Overview of sensors and needs for environmental monitoring, Sensors 5 (1) (2005) 4–37.
[316] J. Hromadka, S. Korposh, M.C. Partridge, S.W. James, F. Davis, D. Crump, R.P. Tatam, Multi-parameter measurements using optical fibre long period gratings for indoor air quality monitoring, Sens. Actuators B Chem. 244 (2017) 217–225.
[317] T. Venugopalan, T. Sun, K.T.V. Grattan, Long period grating-based humidity sensor for potential structural health monitoring, Sens. Actuators A Phys. 148 (1) (2008) 57–62.
[318] S. Korposh, R. Selyanchyn, W. Yasukochi, S.-W. Lee, S.W. James, R.P. Tatam, Optical fibre long period grating with a nanoporous coating formed fromsilica nanoparticles for ammonia sensing in water, Mater. Chem. Phys. 173 (2–3) (2012) 784–792.
[319] S.M. Topliss, S.W. James, F. Davis, S.P.J. Higson, R.P. Tatam, Optical fibre long

period grating based selective vapour sensing of volatile organic compounds, Sens. Actuators B Chem. 143 (2) (2010) 629–634.
[320] F.J. Arregui, I.R. Matias, J.M. Corres, I. Del Villar, J. Goicoechea, C.R. Zamarrenoa, M. Hernáez, R.O. Claus, Optical fiber sensors based on layer-by-layer nanostructured films, Proc. Eng. 5 (2010) 1087–1090.
[321] C. Elosua, C. Bariain, I.R. Matias, Optical fiber sensors to detect volatile organic compound in sick building syndrome applications, Open Constr. Build. Technol. J. 4 (1) (2005) 113–120.
[322] J. Hromadka, S. Korposh, M. Partridge, S.W. James, F. Davis, D. Crump, R.P. Tatam, Volatile organic compounds sensing using optical fibre long period grating with mesoporous nano-scale coating, Sensors 17 (2) (2017) 205.
[323] C.M. Cordeiro, M.A. Franco, G. Chesini, E.C. Barretto, R. Lwin, C.B. Cruz, M.C. Large, Microstructured-core optical fibre for evanescent sensing applications, Opt. Express 14 (26) (2006) 13056–13066.
[324] Y.L. Hoo, W. Jin, C. Shi, H.L. Ho, D.N. Wang, S.C. Ruan, Design and modeling of a photonic crystal fiber gas sensor, Appl. Opt. 42 (18) (2003) 3509.
[325] M. Morshed, M.I. Hasan, S.M.A. Razzak, Enhancement of the sensitivity of gas sensor based on microstructure optical fiber, Photonic Sens. 5 (4) (2015) 312–320.
[326] S. Olyaee, A. Naraghi, Design and optimizationn of index-guiding photonic crystal fiber gas sensor, Photonic Sens. 3 (2) (2013) 131–136.
[327] M.I. Islam, K. Ahmed, S. Sen, S. Chowdhury, B.K. Paul, M.S. Islam, M.B.A. Miah, S. Asaduzzaman, Design and optimization of photonic crystal fiber based sensor for gas condensate and air pollution monitoring, Photonic Sens. 7 (2017) 234–245.
[328] S. Olyaee, A. Naraghi, V. Ahmadi, High sensitivity evanescent-field gas sensor based on modified photonic crystal fiber for gas condensate and air pollution monitoring, Optik 125 (1) (2014) 596–600.
[329] V. Bhatia, D.K. Campbell, D. Sherr, T.G. D'Alberto, N.A. Zabaronick, G.A. TenEyck, K.A. Murphy, R.O. Claus, Temperature-insensitive and strain-insensitivelong-period grating sensors for smart structures, Opt. Eng. 36 (7) (1997) 1872–1875.
[330] P. Zu, L.S. Ping, C.C. Chi, An ultrahigh sensitivity point temperature sensor based on fiber loop mirror, IEEE J. Sel. Top. Quantum Electron. 23 (2) (2017) 274–277.
[331] N. Van de Giesen, S.C. Steele-Dunne, J. Jansen, O. Hoes, M.B. Hausner, S. Tyler, J. Selker, Double-ended calibration of fiber-optic raman spectra distributed temperature sensing data, Sensors 12 (2012) 5471–5485.
[332] B.M. Freifeld, S. Finsterle, T.C. Onstott, P. Toole, L.M. Pratt, Ground surface temperature reconstructions: using in situ estimates for thermal conductivity acquired with a fiber-optic distributed thermal perturbation sensor, Geophys. Res. Lett. 35 (2008) L14309.
[333] F. Ciocca, I. Lunati, N. Van de Giesen, M.B. Parlange, Heated optical fiber for distributed soil-moisture measurements, A lysimeter experiment, Vadose Zone J. 11 (4) (2012) 1–10.
[334] J. Jansen, P. Stive, N. Van de Giesen, S. Tyler, S. Steele-Dunne, L. Williamson, Estimating soil heat flux using distributed temperature sensing, IAHS-AISH Publ. 343 (2011) 140–144.
[335] R.D. Henderson, F.D. Day-Lewis, C.F. Harvey, Investigation of aquifer-estuary interaction using wavelet analysis of fiber-optic temperature data, Geophys, Res. Lett. 36 (2009) 6403.
[336] E.A. Mamer, C.S. Lowry, Locating and quantifying spatially distributed groundwater-surface water interactions using temperature signals with paired fiber-optic cables, Water Resour. Res. 49 (2013) 7670–7680.
[337] F. Suárez, J.E. Aravena, M.B. Hausner, A.B. Childress, S.W. Tyler, Assessment of a vertical high-resolution distributed temperature sensing system in a shallow thermohaline environment, Hydrol. Earth Syst. Sci. 15 (2011) 1081–1093.
[338] M.C. Westhoff, M.N. Gooseff, T.A. Bogaard, H.H.G. Savenije, Quantifying hyporheic exchange at high spatial resolution using natural temperature variations along a first-order stream, Water Resour. Res. 47 (2011) W10508.
[339] T. Van Emmerik, A. Rimmer, Y. Lechinskya, K. Wenker, S. Nussboim, N. Van de Giesen, Measuring heat balance residual at lake surface using distributed temperature sensing, Limnol. Oceanogr. Meth. 11 (2013) 79–90.
[340] T. Read, O. Bour, V. Bense, T. Le Borgne, P. Goderniaux, M. Klepikova, R. Hochreutener, N. Lavenant, V. Boschero, Characterizing groundwater flow and heat transport in fractured rock using fiber-optic distributed temperature sensing, Geophys. Res. Lett. 40 (2013) 2055–2059.
[341] A. Curtis, P. Kyle, Geothermal point sources identified in a fumarolic ice cave on erebus volcano, antarctica using fiber optic distributed temperature sensing, Geophys. Res. Lett. 38 (2011) L16802.
[342] M. Dornstadter, D. Aufleger, Distributed temperature sensing in dams, The prospect for reservoirs in the 21st century, Thomas Telford Publishing, Thomas Telford Ltd., London, 1998, pp. 135–140.
[343] O. Hoes, R. Schilperoort, W. Luxemburg, F. Clemens, N.V. Giesen, Locating illicit connections in storm water sewers using fiber-optic distributed temperature sensing, Water Res. 43 (2009) 5187–5197.
[344] G. Yilmaz, S.E. Karlik, A distributed optical fiber sensor for temperature detection in power cables, Sens. Actuators A Phys. 125 (2006) 148–155.
[345] F. Tanimola, D. Hill, Distributed fibre optic sensors for pipeline protection, J. Nat. Gas Sci. Eng. 1 (2009) 134–143.
[346] S.A.P. De Jong, J.D. Slingerland, N.C. Van de Giesen, Fiber optic distributed temperature sensing for the determination of air temperature, Atmospheric Measur. Tech. 8 (2015) 335–339.
[347] K. Lee, J. Neff, Measurement of oil in produced water Ming Yang Produced Water, Environmental risks and advances in mitigation technologies, Springer, New York, 2011, pp. 57–88.
[348] J.M. López-Higuera, Handbook of optical fiber sensing technology, Published by Wiley, USA, 2002.
[349] A. MacLean, C. Moran, W. Johnstone, B. Culshaw, D. Marsh, P. Parker, Detection of hydrocarbon fuel spills using a distributed fiber optic sensor, Sens. Actuators A Phys. 109 (2003) 60–67.
[350] J. Barnes, M. Dreher, K. Plett, R.S. Brown, C.M. Crudden, H.P. Loock, Chemical sensor based on a long-period fiber grating modified by a functionalized poly dimethylsiloxane coating, Analyst 133 (2008) 1541–1548.
[351] S. Kopitzke, P. Geissinger, An optical fiber-based sensor array for the monitoring of zinc and copper ions in aqueous environments, Sensors 14 (2014) 3077.
[352] J. Buerck, S. Roth, K. Kraemer, S. Scholz, N. Klaas, Application of a fiber optic NIR-EFA sensor system for insitumonitoring of aromatic hydrocarbons in contaminated groundwater, J. Hazard. Mater. 83 (2001) 11–17.
[353] R.P. McCue, J.E. Walsh, F. Walsh, F. Regan, Modular fiber optic sensor for the detection of hydrocarbons in water, Sens. Actuators B Chem. 114 (2006) 438–444.
[354] T. Okazaki, T. Orii, A. Ueda, A. Ozawa, H. Kuramitz, Fiber optic sensor for real-time sensing of silica scale formation in geothermal water, Sci. Rep. 7 (2017) 3387.
[355] R.C. Jorgenson, S.S. Yee, Control of the dynamic range and sensitivity of a surface plasmon resonance based fiber optic sensor, Sens. Actuators A Phys. 43 (1994) 44–48.
[356] J. Homola, S.S. Yee, G. Gauglitz, Surface plasmon resonance sensors review, *Sens.* Actuators B Chem. 54 (1999) 3–12.
[357] M. Irigoyen, J.A. Sánchez-Martin, E. Bernabeu, A. Zamora, Tapered optical fiber sensor for chemical pollutants detection in seawater, Meas. Sci. Technol. 28 (2017) 045802.
[358] S. Kim, M. Kim, S.K. Lim, Y. Park, Titania-coated plastic optical fiber fabrics for remote photocatalytic degradation of aqueous pollutants, J. Environ. Chem. Eng. 5 (2017) 1899–1905.
[359] W.B. Jia, S.H.K. Yapa, N. Panwara, L.L. Zhanga, B. Linb, K.T. Yonga, S.C. Tjina, W.J. Ngc, M.B.A. Majid, Detection of low-concentration heavy metal ions using optical microfiber sensor, Sens. Actuators B Chem. 237 (2016) 142–149.
[360] J.A. García, D. Monzón-Hernández, O. Cuevas, B. Noriega-Lunaa, E. Bustos, Optical fiber detector for monitoring volatile hydrocarbons during electrokinetic treatment, J. Chem. Technol. Biotechnol. 91 (2016) 2162–2169.
[361] M. Hernandez, L. Moreno, M. Escobar, Fast response fiber optic hydrogen sensor based on palladium and gold nano-layers, Sens. Actuators B. Chem. 136 (2009) 562–566.
[362] A. Seki, H. Sasaki, K. Watanabe, Anionic surfactant sensor based on a hetero-core structured optical fiber, Microchim. Acta. 165 (2009) 335–339.
[363] J.A. Garcia, D. Monzon-Hernandez, A. Martinez, S. Pamukcu, R. Garcia, E. Bustos, Optical fibers to detect heavy metals in environment: generalities and case studies, in: Environmental risk assessment of soil contamination, IntechOpen, 2014, pp. 427–457.
[364] J.H. Chang, Z. Qiang, C.P. Huang, A.V. Ellis, Phenanthrene removal in unsaturated soils treated by electrokinetics with different surfactants–Triton X-100 and rhamnolipid, Colloid. Surface A. 348 (2009) 157–163.
[365] A.Z. Al-Hamdan, K.R. Reddy, Transient behavior of heavy metals in soils during electrokinetic remediation, Chemosphere 71 (2008) 860–871.
[366] V.A. Korolev, Electrochemical soil remediation from environmental toxicants: results and prospects, Moscow Uniy. Geol. Bull. 63 (2007) 11–18.
[367] K.R. Reddy, C. Camoselle, Electrochemical remediation technologies for polluted soils, sediments and groundwater, John Wiley & Sons Inc, Hoboken, New Jersey, USA, 2009.
[368] L. Alwis, T. Sun, K.T.V. Grattan, Optical fibre-based sensor technology for humidity and moisture measurement: Review of recent progress, Measurement 46 (2013) 4052–4074.
[369] J.S. Hallett, M. Partridge, S.W. James, D. Tiwari, T. Farewell, S.H. Hallett, R.P. Tatam, Soil moisture content measurement using optical fiber long period gratings, IEEE Optical Fiber Sensors Conference (OFS) (2017) 1–4.
[370] G. Woyessa, A. Fasano, C. Markos, H.K. Rasmussen, O. Bang, Low Loss Polycarbonate Polymer Optical Fiber for High Temperature FBG Humidity Sensing, IEEE Photonics Technol. Let. 29 (7) (2017) 575–578.
[371] L.S. Alwis, H. Bustamante, K. Bremer, B. Roth, T. Sun, K.T. Grattan, A pilot study: Evaluation of sensor system design for optical fibre humidity sensors subjected to aggressive air sewer environment, IEEE Sensors (2016) 1–3.
[372] F.U. Hernandez, R. Correia, S.P. Morgan, B. Hayes-Gill, D. Evans, R. Sinha, A. Norris, D. Harvey, J.D. Hardman, S. Korposh, Simultaneous temperature and humidity measurements in a mechanical ventilator using an optical fibre sensor, Proc. SPIE 9916 (2016) 99160C.
[373] X. Liu, M. Jiang, Q. Sui, X. Geng, Optical fibre fabry–perot relative humidity sensor based on HCPCF and chitosan film, J. Modern Opt. 63 (17) (2016) 1668–1674.
[374] P.J. Thomas, J.O. Hellevang, A fully distributed fibre optic sensor for relative humidity measurements, Sens. Actuators B Chem. 247 (2017) 284–289.
[375] S. Acikgoz, B. Bilen, M.M. Demir, Y.Z. Menceloglu, Y. Skarlatos, G. Aktas, M. Nacincl, Use of polyethylene glycol coatings for optical fibre humidity sensing, Opt. Rev. 15 (2008) 84–90.